THESIS FOR THE DEGREE OF LICENTIATE OF ENGINEERING

# Design of ground source heat pump systems

## Thermal modelling and evaluation of boreholes

SAQIB JAVED

Building Services Engineering
Department of Energy and Environment
CHALMERS UNIVERSITY OF TECHNOLOGY
Göteborg, Sweden 2010

Design of ground source heat pump systems
Thermal modelling and evaluation of boreholes
Saqib Javed



Licentiatuppsats vid Chalmers tekniska högskola
Ny serie nr 2706
ISSN 0346-718X

Technical report D2010:02
Building Services Engineering
Department of Energy and Environment
Chalmers University of Technology
SE-412 96 GÖTEBORG
Sweden
Telephone +46 (0)31 772 1000

Printed by
Chalmers Reproservice
Göteborg 2010

# Design of ground source heat pump systems

## Thermal modelling and evaluation of boreholes

SAQIB JAVED
Building Services Engineering
Chalmers University of Technology

# Abstract

Ground source heat pump systems are fast becoming state-of-the-art technology to meet the heating and cooling requirements of the buildings. These systems have high energy efficiency potential which results in environmental and economical advantages. The energy efficiency of the ground source heat pump systems can be further enhanced by optimized design of the borehole system.

In this thesis, various aspects of designing a borehole system are studied comprehensively. A detailed literature review, to determine the current status of analytical solutions to model the heat transfer in the borehole system, indicated a shortage of analytical solutions to model the short-term borehole response and the long-term response of the multiple borehole systems. To address the modelling issue of long-term response of multiple boreholes, new methods based on existing analytical solutions are presented. To model the short-term response of a borehole system, new analytical and numerical solutions have been developed. The new analytical method studies the heat transfer problem in the Laplace domain and provides an exact solution to the radial heat transfer problem in boreholes. The new numerical solution studies the one dimensional heat transfer problem using a coordinate transformation technique. The new solution can be easily implemented in any building energy simulation software to optimize the overall performance of ground source heat pump systems.

Another significant aspect analyzed in this thesis is the uncertainty of input parameters when studying the thermal response of a borehole system. These parameters are often determined using in-situ thermal response tests. This issue has been investigated by conducting thermal response tests on nine boreholes of a newly developed ground source heat pump laboratory. The data from thermal response tests have been used to evaluate undisturbed ground temperature, ground thermal conductivity and borehole thermal resistance values for all nine boreholes. The sensitivity analysis of estimated parameters suggested that the short duration of the test causes the largest uncertainty in the ground thermal conductivity estimations. For tests longer than 48 hours the ground thermal conductivity estimations for nine boreholes vary within ±7 % of the mean value. The effects of variations in the estimated parameters on the design of a borehole system are examined for single as well as multiple borehole applications. The results indicate that the variations in the estimated parameters do not significantly affect the borehole field design.

**Keywords:** Ground source heat pump, ground-coupled, ground heat exchanger, borehole, thermal response test, sensitivity analysis, fluid temperature, simulation, optimization.

This licentiate thesis has been funded by the Swedish Energy Agency through their national research program EFFSYS2 in corporation with our industrial partners Akademiska Hus, Carrier, CTC, Fastighetsägarna, Geotec, Grundfos, IVT, NCC, Nibe, Sweco, TAC, Thermia Värme, Wilo and ÅF-Infrastruktur.

# Foreword

Research can definitely not be performed in isolation. Any undertaking such as this is a result of a collective effort of many individuals and organizations. This thesis has been made possible through the support, enthusiasm and patience of my supervisors Professor Per Fahlén and Professor Johan Claesson. The knowledge and insight of Professor Per Fahlén are unparalleled. He took the research initiative and lent me all the support I needed. Professor Johan Claesson on the other hand is a true mathematician in love with his work. He provided me all the help and support to understand the mysteries of the mathematics world in general and the Laplace world in particular. I would like to express my sincere gratitude and thanks to both my supervisors.

I thank the Swedish Energy Agency for their financial support and all the members of the project group for their active participation in the project. I would also like to extend my utmost gratitude to Professor Jeffrey Spitler from Oklahoma State University for his guidance and contributions throughout this research.

I have been fortunate indeed to have colleagues like Caroline Markusson, Jessica Erlandsson, Professor Jan-Olof Dalenbäck, Ragib Kadribegovic, and Torbjörn Lindholm. They have been a source of continuous encouragement throughout this undertaking. I thank you all for your friendship, inspiration and support. Very special thanks to Katarina Bergkvist for her assistance not only with the administrative issues of Chalmers but more importantly with everyday life issues in Göteborg and Sweden. I am also grateful to my other colleagues at Building Services Engineering for the wonderful working environment.

I thank my parents who inspired and supported me to become the person I am today. Last but certainly not the least; I thank Mona and Baasil for their understanding, patience and unconditional love.

Göteborg, June 2010

Saqib Javed

# Contents

# 0 Symbols and abbreviations

## 0.1 Symbols

### Latin letters

| | | |
|---|---|---|
| $A$ | area | [m$^2$] |
| $a$ | thermal diffusivity; $a = \dfrac{\lambda}{\rho \cdot c}$ | [m$^2$/s] |
| $C$ | thermal capacity per unit length | [J/(m·K)] |
| $c$ | specific heat capacity | [J/(kg·K)] |
| $Fo$ | Fourier number i.e. dimensionless time; $Fo = \dfrac{a \cdot \tau}{r^2}$ | [-] |
| $g$ | geometry factor | [m] |
| $H$ | height | [m] |
| $h$ | convective heat transfer coefficient | [W/(m$^2$·K)] |
| $I_n$ | nth-order modified Bessel function of first kind | [-] |
| $J_n$ | nth-order Bessel function of first kind | [-] |
| $K$ | thermal conductance | [W/(m·K)] |
| $K_n$ | nth-order modified Bessel function of second kind | [-] |
| $\bar{K}(s)$ | thermal conductance in Laplace domain | [W/(m·K)] |
| $k$ | slope | [K/hour] |
| $l$ | load factor | [-] |
| $\dot{M}$ | mass flow rate | [kg/s] |
| $N$ | total number of cells for the numerical model | [-] |
| $Q$ | thermal capacity | [W] |
| $q$ | rate of heat transfer per unit length | [W/m] |
| $R$ | thermal resistance | [(m·K)/W] |
| $r$ | radius | [m] |
| $r_x^*$ | non-dimensional radius | [-] |
| $s$ | Laplace transform variable | [-] |
| $s_s$ | shank spacing of U-tube | [m] |
| $T$ | thermodynamic (absolute) temperature | [K] |
| $T_{pty}$ | temperature penalty | [K] |
| $\bar{T}(s)$ | Laplace transform of $T(t)$ | [K·s] |
| $t$ | Celsius temperature | [°C] |
| $V$ | volume | [m$^3$] |
| $Y_n$ | nth-order Bessel function of second kind | [-] |
| $z$ | axial coordinate | [m] |

### Greek letters

| | | |
|---|---|---|
| $\gamma$ | constant | [-] |
| $\lambda$ | thermal conductivity | [W/(m·K)] |
| $\rho$ | density | [kg/m$^3$] |
| $\tau$ | time | [s] |

### Subscripts

| | |
|---|---|
| b | borehole |
| f | fluid |
| g | grout |
| i | in / inner |
| o | out / outer |
| p | pipe |
| s | soil (ground) |
| u | U-tube |

## 0.2 Abbreviations

| | |
|---|---|
| ASHRAE | American Society of Heating, Refrigeration, and Air-Conditioning Engineers |
| BEC | Buried Electric Cable |
| BFTM | Borehole Fluid Thermal Mass |
| BH | Borehole |
| BTES | Borehole Thermal Energy Storage |
| CS | Cylindrical Source |
| GSHP | Ground Source Heat Pump |
| HVAC | Heating, Ventilation and Air-Conditioning |
| L&B | Lamarche and Beauchamp's |
| LS | Line Source |
| TRT | Thermal Response Test |
| VS | Virtual Solid |

# 1 Introduction

Ground Source Heat Pump (GSHP) systems are rapidly becoming state-of-the-art in the field of Heating, Ventilation and Air Conditioning (HVAC). The growth of the GSHP system is evident from the fact that the worldwide installed capacities of the GSHP systems have increased by 23.8 % between the years 2000 and 2005[44]. In Sweden, there are around 350,000 installations of GSHP systems, increasing at a steady rate of about 10 percent a year[2]. The tremendous growth of the GSHP systems is attributed to their high energy efficiency potential, which results in both environmental and economic advantages. The attraction of GSHP systems is that, below a certain depth, the ground temperature is not affected by seasonal changes. This enables ground to be used as a heat source or a heat sink in a dissipative system. Alternatively, ground can also be used for seasonal storage of heat. The dissipative GSHP systems are designed to maximize heat transfer between the borehole system and the neighbouring ground. Storage systems, on the other hand, are designed to store thermal energy in the ground at a time of energy surplus and extract it at a later time.

The design of a GSHP system requires knowledge of the heating and cooling requirements of the building, the operating characteristics of the heat pump and the thermal performance of the borehole system. The heating and cooling requirements of the building are often represented as hourly demands and can be estimated using the location, the intended occupancy and the planned operation of the building. The performance of the heat pump depends on factors like inlet fluid temperature and flow rate. The heat pump manufacturers provide data sheets to indicate the performance of the heat pump. Simple but reasonably accurate steady-state heat pump models can be developed by curve fitting of the provided data. Alternatively, parameter estimation models can be used to extrapolate beyond the manufacturer's data. The borehole system is typically designed using models which calculate the required borehole depth by predicting its long-term performance. The input parameters to these models are either measured experimentally, using in-situ thermal response tests, for large and commercial systems or estimated for small and residential systems. The design process of the GSHP system can be significantly improved by optimized design of the ground collector and storage system.

## 1.1 Research objective and perspective

There is a general inadequacy of non-commercial and easy-to-use calculation tools to design and optimize GSHP systems. Certain building energy simulation platforms like TRNSYS[52], EnergyPlus[21] and HVACSIM+[20] have implemented some borehole system solutions to simulate the whole GSHP system. The implemented borehole system solutions are typically in the form of numerically calculated response functions which are incorporated in the building energy simulation software as databases. However, at present these programs are not only abstruse and difficult to use but also they are better suited to modelling the long-term response of the GSHP system than studying the dynamic short-term response required to optimize the operation and performance of the system. There are also stand-alone commercial programs like Earth Energy Designer (EED)[15] and Ground Loop Heat Exchanger Pro (GLHEPRO)[59] but these programs are specifically developed to determine the required borehole length and the borehole field configuration for given heating and cooling requirements of the buildings and are not aimed at optimizing the operation and performance of the GSHP system. In addition, there are also numerous numerical algorithms and solutions developed to study and simulate different aspects of borehole heat transfer. Most of these solutions cannot be directly incorporated into building energy simulation software and hence have limited practical applications. Given this background one objective of the research is to develop simple and user-friendly calculation tools to facilitate the work of designers and researchers interested in GSHP system optimization. The focus, during the first phase of the research project, was primarily on the development of analytical solutions to model the long and the short term response of a borehole field. As reported later in this licentiate thesis, it was shown that the existing analytical models can be used to determine the long-term response of a multiple borehole field. In addition, a new analytical solution was developed and validated to model the dynamic short-term borehole response. The implementation of these analytical solutions to a comprehensive calculation tool to design and optimize GSHP systems will be carried out during the next phase of the project and will be reported in the PhD dissertation.

The second objective of the research is to identify key optimization factors for the GSHP systems by means of modelling and simulations, field studies and experiments. It is another long-term objective and the aim during the first half of the project was to carry out thermal modelling and experimental evaluation of the boreholes. This interim objective was successfully met and this licentiate thesis presents the long and the short term response evaluations of the studied borehole systems using modelling and simulations. The initial experimental investigations regarding the thermal response of the boreholes are also reported. Additionally, the uncertainties regarding the quality of input data when evaluating the thermal response of boreholes are studied. The foundation of the future experimental investigations is also laid down by presenting the development and the planned operation of a new GSHP test facility. In the next phase of the project, investigations regarding operation, control and optimization of simple and hybrid GSHP systems will be conducted and the results will be presented in the PhD thesis.

## 1.2 Research methodology

This work started with a comprehensive review of the literature, the purpose of which was to determine the state-of-the-art in modelling and simulation of GSHP systems in general and of borehole systems in particular. As the aim of the project is to develop new analytical solutions, these were the focus of the review.

The next step was to check the suitability of the existing analytical solutions to model the long and short term response of the borehole system. This task was accomplished by modelling and simulation of borehole system response using existing analytical solutions and comparing the results with those from exact solutions.

The observed shortcomings of the existing analytical solutions were addressed by developing new solutions to design and model borehole systems. In addition to analytical solutions, a flexible and easy-to-implement numerical solution was also developed.

When designing and modelling GSHP systems, the uncertainties regarding the quality of input data can be more significant than the model uncertainties. The input data are often derived from in-situ measurements using thermal response tests. An experimental setup was built and experimental investigations were conducted to study the effects of the ensuing input data uncertainties on the design of borehole systems.

## 1.3 Thesis outline

This thesis is made up of eight chapters that cover important details regarding this research. The current chapter describes background, motivation and the perspective of the research.

Chapter 2 is a literature review of the existing solutions to determine the borehole response. It mainly focuses on analytical solutions; however references are also made to state-of-the-art numerical solutions. This chapter is mainly based on the following paper.

- Javed, S, Fahlén, P and Claesson, J, 2009. Vertical ground heat exchangers: A review of heat flow models. *11th international conference on thermal energy storage; Effstock 2009*, June 14-17, Stockholm, Sweden.

In chapter 3, an analysis of the existing analytical solutions to determine the long and the short term response of the borehole system is presented. This chapter provides comparisons of existing solutions to determine their suitability to predict long and short term response of the borehole system. This chapter is based on the following two papers.

- Javed, S, Fahlén, P and Holmberg, H, 2009. Modelling for optimization of brine temperature in ground source heat pump systems. *8th international conference on sustainable energy technologies; SET2009*, August 31- September 3, Aachen, Germany.

- Javed, S, Claesson, J and Fahlén, P, 2010. Analytical modelling of short-term response of ground heat exchangers in ground source heat pump systems. *10th REHVA world congress; Clima 2010*, May 9-12, Antalya, Turkey.

Chapter 4 presents the new solutions developed through this research to model short-term response of a borehole. The new solutions include an analytical and a numerical solution and the chapter presents background, mathematical formulation and validation of the two solutions.

In chapter 5, development and planned operation of a new GSHP test facility is described. This chapter is based on the following paper.

- Javed, S and Fahlén, P, 2010. Development and planned operation of a ground source heat pump test facility. *Newsletter IEA heat pump centre*, vol. 28, no. 1/2010, pp. 32-35.

Chapter 6 provides the details of the thermal response tests conducted to estimate the thermal properties of the borehole system at the new laboratory. The estimated thermal properties include undisturbed ground temperature, ground thermal conductivity and borehole thermal resistance.

In chapter 7, an analysis of the results of the thermal response tests is presented. The analysis includes a sensitivity study of different parameters on the estimated result values and a comparison of experimental and simulated results.

Finally, chapter 8 is a discussion of the overall results, conclusions and recommendations for future work.

# 2 Literature review

Over the years various analytical and numerical solutions of varying complexity have been developed and used as design and research tools to predict, among others, the heat transfer mechanism inside a borehole, the conductive heat transfer from a borehole and the thermal interactions between boreholes. This chapter is based on reviews of scientific work and provides a state-of-the-art review of analytical solutions for the borehole heat transfer. Noteworthy analytical models to determine short and long term response are described and discussed. In addition various methods to analyze the borehole thermal resistance are also discussed.

## 2.1 Long-term response

The modelling of a borehole heat exchanger is an intricate procedure and so far determination of the long-term temperature response has been the predominant modelling application. In the following section, three types of solutions, the infinite and the finite length line sources and the cylindrical source are discussed.

### 2.1.1 Infinite length line source – Analytical solution

The very first significant contribution to modelling of borehole systems came from Ingersoll et al.[36] who developed the line source theory of Kelvin[41] and implemented it to model the borehole heat transfer. In this solution, the borehole is assumed to be a line source of constant heat output and of infinite length surrounded by an infinite homogeneous medium. The classical solution to this problem, as proposed by Ingersoll et al. is:

$$T_b - T_0 = \frac{q}{4\pi\lambda_s} \int_{1/4Fo}^{\infty} \frac{e^{-u}}{u} du = \frac{q}{4\pi\lambda_s} \cdot E_1\left(\frac{1}{4Fo}\right), \qquad Fo = \frac{a_s\tau}{r_b^2}. \tag{2.1}$$

Equation 2.1 is an exact solution to the radial heat transfer in a plane perpendicular to the line source. As the temperature response at the wall of the borehole is sought, the dimensionless time, i.e. Fourier number (*Fo*), is based on the borehole radius ($r_b$). Many researchers have approximated the exact integral of Equation 2.1 using simpler algebraic expressions. Ingersoll et al.[36], for instance, presented the approximations in tabulated form. Hart and Couvillion[32], on the other hand, approximated the integral by assuming that only a certain radius of the surrounding ground would absorb the heat rejected by the line source. Various other algebraic approximations of the exact integral of Equation 2.1 can be found in ‘Handbook of mathematical functions’[1] and similar mathematical handbooks.

The line source solution can be used with reasonable accuracy to predict the response of a borehole for medium to long term ranges. Ingersoll and Plass[35] have recommended using line source solution only for applications with $Fo > 20$. The solution cannot be used for smaller Fourier numbers as the solution gets distorted for the shorter time scales because of its line source assumption. The classical line source solution also ignores the end effects of the heat source as it assumes the heat source to have infinite length.

To counter the constant heat flow assumption of the infinite length line source solution, Ingersoll et al.[36] proposed using multiple time intervals with each interval having a constant heat flow rate. The ground thermal response can then be calculated using the superposition principle shown in Equation 2.2. This approach has been adopted by a number of researchers to predict the long-term response and to perform the annual hourly simulations of the GSHP systems.

$$T_b - T_0 = \sum_{i=1}^{n} \frac{q_i - q_{i-1}}{4\pi\lambda_s} \cdot E_1 \left( \frac{r_b^2}{4a_s \cdot (\tau_n - \tau_{i-1})} \right) \tag{2.2}$$

### 2.1.2 Cylindrical source – Analytical solution

The cylindrical source solution is another established analytical way of modelling heat transfer in boreholes. This method provides a classical solution for the radial transient heat transfer from a cylinder surrounded by an infinite homogeneous medium. The cylinder, which usually represents the borehole outer boundary in this approach, is assumed to have a constant heat flux across its outer surface. The solution has the following general form.

$$T_b - T_0 = \frac{q}{\lambda_s} G(Fo, r_b^*) \tag{2.3}$$

where

$$G(Fo, r_b^*) = \frac{1}{\pi^2} \int_0^\infty \frac{e^{-u^2 Fo} - 1}{\left(J_1^2(u) + Y_1^2(u)\right)} \cdot [J_0(r_b^* u) Y_1(u) - J_1(u) Y_0(r_b^* u)] \frac{du}{u^2} . \tag{2.4}$$

The integral in Equation 2.4 is often referred to as the *G-factor* in literature. As with the exact integral in the line source solution, the *G-factor* has also been approximated using various tabular and algebraic expressions. Ingersoll et al.[36], Kavanaugh[40] and more recently Bernier[10] have all made important contributions.

Like the line source solution, the cylindrical source solution also ignores the end effects of its heat source. It also overlooks the thermal capacities of the fluid and the grout in the borehole. However, the issue of having a constant heat flux across the borehole boundary has been tackled by some researchers by superimposing time-variable loads. The systematic approach of Bernier et al.[12] deserves a special mention. Based on the cylindrical source method, they have modelled the annual hourly variations of a borehole by categorizing the thermal history of the ground into 'immediate' and 'past' time scales in their so-called Multiple Load Aggregation Algorithm. Mean aggregated loads are used for the 'past' period and are divided into daily mean (*dm*), weekly mean (*wm*), monthly mean (*mm*) and yearly mean (*ym*) aggregated loads. The loads in the 'immediate' time period $N_h$ remain non-aggregated. The ground thermal response at time $\tau_h$ can then be calculated as:

$$T_b - T_0 = \frac{1}{\lambda_s}\left(q_{ym}[A - B] + q_{mm}[B - C] + q_{wm}[C - D] + q_{dm}[D - E] + q_{\tau_h - N_h + 1}[E - F_1] + q_{\tau_h - N_h + 2} [F_1 - F_2] + \ldots + q_{\tau_h - 1}\left[F_{N_h - 1} - F_{N_h}\right] + q_{\tau_h}\left[F_{N_h}\right]\right), \quad (2.5)$$

where:

$q_{im} = mean\ aggregated\ ground\ loads\ with\ i = y, m, w\ \&\ d,$

$q_j = non - aggregated\ ground\ load\ with\ j = \tau_h - N_h + 1, \ldots \tau_h,$

$A = G\left(Fo_{\tau=\tau_h}\right),$

$B = G\left(Fo_{\tau=\tau_h - N_y}\right),$

$C = G\left(Fo_{\tau=\tau_h - N_y - N_m}\right),$

$D = G\left(Fo_{\tau=\tau_h - N_y - N_{m - N_w}}\right),$

$E = G\left(Fo_{\tau=N_h}\right),$

$F_1 = G\left(Fo_{\tau=N_h - 1}\right),$

$F_2 = G\left(Fo_{\tau=N_h - 2}\right),$

$F_{N_h} = G(Fo_{\tau=1}).$

Similar cylindrical source based approaches have also been used by Forsén and Lundqvist[26] and Nagano et al.[47], among others.

### 2.1.3 Finite length line source – Numerical solution

Eskilson[24] numerically modelled the thermal response of the borehole using non-dimensional thermal response functions, better known as *g-functions*. The temperature response to a unit step heat pulse is calculated using the finite difference approach. Eskilson's solution, which is referred to as the Superposition Borehole Model (SBM) in literature, accounts for the influence between boreholes by an intricate superposition of numerical solutions with transient radial-axial heat conduction, one for each borehole. This solution is the only one that accounts for the long-term influence between boreholes in a very exact way. The thermal capacities of the borehole elements, however, are neglected.

The response to any heat input can be calculated by devolving the continuous heat injection to a series of step functions. The temperature response of the boreholes is obtained from a sum of step responses. A representation of *g-functions* plotted for various borehole configurations is shown in Figure 2.1. The temperature response for any piecewise-constant heat extraction is calculated using Equation 2.6.

$$T_b - T_0 = \sum_i \frac{\Delta q_i}{2\pi\lambda_s} \cdot g\left(\frac{\tau - \tau_i}{\tau_s}, r_H^*, \ldots.\right), \qquad \tau_s = \frac{H^2}{9a_s}. \tag{2.6}$$

Here, the change in heat extraction at time $\tau_i$ is $\Delta q_i$. The dots in the argument of the g-function refer to dimensionless parameters that specify the position of boreholes relative to each other. The limitation of the numerically calculated *g-functions* lies in the fact that they are only valid for times greater than ($5r_b^2 /a_s$), as estimated by Eskilson. This implies times of 3-6 hours for typical boreholes as noted by Yavuzturk[65]. Another practical aspect of the *g-functions* is that these functions have to be pre-computed for various borehole geometries and configurations and then have to be stored as databases in the building energy analysis software. The SBM has been has been implemented in many software including EED[15], TRNSYS[52], Energy Plus[21] and GLHEPRO[59].

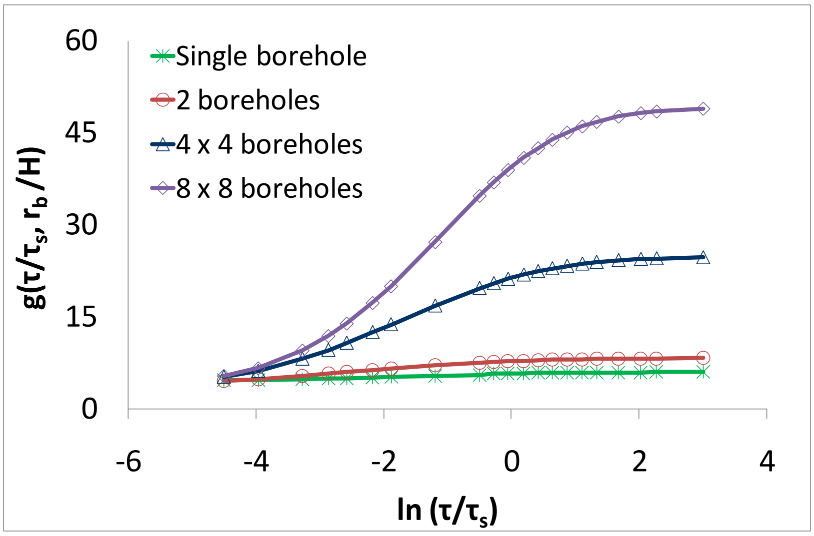


**Figure 2.1** Eskilson's g-functions for various borehole configurations.

## 2.1.4 Finite length line source – Analytical solution

Many researchers have tried to determine analytical *g-functions* to address the flexibility issue of numerically computed *g-functions*. Eskilson[24] himself developed an analytical *g-function* expression, which was later adopted by Zeng et al.[68] The explicit analytical *g-function* is determined using a line heat source with finite length. The temperature at the middle of the borehole of the length $H$ is taken as the representative temperature when calculating the heat transfer between the borehole and the fluid. The mathematical expression for this analytical *g-function* is:

$$g(Fo, r_H^*) = \frac{1}{2}\int_0^1 \left\{ \frac{erfc\left[\frac{\sqrt{r_H^{*2} + \left[0.5 - \frac{z}{H}\right]^2}}{2\sqrt{Fo}}\right]}{\sqrt{r_H^{*2} + \left[0.5 - \frac{z}{H}\right]^2}} - \frac{erfc\left[\frac{\sqrt{r_H^{*2} + \left[0.5 + \frac{z}{H}\right]^2}}{2\sqrt{Fo}}\right]}{\sqrt{r_H^{*2} + \left[0.5 + \frac{z}{H}\right]^2}} \right\} \mathrm{d}\left[\frac{z}{H}\right]. \tag{2.7}$$

Lamarche and Beauchamp[42] used a similar approach to calculate their analytical *g-function*. However, they used the integral mean temperature along the borehole depth *z*, instead of considering the middle point temperature. Their approach provided a better match to the numerically calculated *g-functions* than that proposed by Zeng et al.[68]

$$g(\mathrm{Fo}, \mathrm{r}_\mathrm{H}^*) = \int_{\mathrm{r}_\mathrm{H}^*}^{\sqrt{\mathrm{r}_\mathrm{H}^{*\,2}+1}} \frac{\mathrm{erfc}\,(\gamma z)}{\sqrt{z^2 - \mathrm{r}_\mathrm{H}^{*\,2}}} dz - D_A - \int_{\sqrt{\mathrm{r}_\mathrm{H}^{*\,2}+1}}^{\sqrt{\mathrm{r}_\mathrm{H}^{*\,2}+4}} \frac{\mathrm{erfc}\,(\gamma z)}{\sqrt{z^2 - \mathrm{r}_\mathrm{H}^{*\,2}}} dz - D_B, \qquad (2.8)$$

where:

$$\gamma = \frac{3}{2\sqrt{Fo}},$$

$$D_A = \int_{r_H^*}^{\sqrt{r_H^{*\,2}+1}} erfc(\gamma z)\, dz,$$

$$D_B = \frac{1}{2}\left(\int_{r_H^*}^{\sqrt{r_H^{*\,2}+1}} erfc(\gamma z)\, dz + \int_{\sqrt{r_H^{*\,2}+1}}^{\sqrt{r_H^{*\,2}+4}} erfc\,(\gamma z)\, dz\right).$$

More recently Bandos et al.[6] developed new analytical solutions for intermediate and long time scales taking the effects of geothermal gradient and temperature variations at the ground surface into account. The solutions include an exact solution at the middle of the borehole and an average solution along the borehole depth. The use of only one integral, in Equation 2.9, with mean integral temperature along the borehole depth, reduces the computational requirements significantly compared with the solution developed by Lamarche and Beauchamp[42]. Moreover, Bandos et al. also developed algebraic approximations (i.e. Equation 2.10) for their integral solutions. The two expressions in Equation 2.10 are valid for times $5r_b^2/a_s \le \tau \le H^2/ma_s$ and $\tau > H^2/ma_s$ respectively. The value of the constant *m* is determined at the intersection point of the two approximations. The developed algebraic approximations are quite simple and are reasonably precise; hence these approximations are good alternatives for simulations where better computational efficiencies are desired.

$$g(Fo, r_H^*) = \frac{1}{2}\int_{\frac{1}{\sqrt{4Fo}}}^{\infty} \left[4\, erf\left(\frac{u}{r_H^*}\right) - 2\, erf\left(\frac{2u}{r_H^*}\right) - \left(3 + e^{\frac{-4u^2}{r_H^{*\,2}}} - 4e^{\frac{-u^2}{r_H^{*\,2}}}\right)\frac{r_H^*}{u\sqrt{\pi}}\right] \frac{e^{-u^2}}{u} du \qquad (2.9)$$

$$g(Fo, r_H^*) = \frac{1}{2}\begin{cases} -\gamma + \ln 4Fo - \dfrac{3}{\sqrt{\pi}}\dfrac{\sqrt{4\tau}}{\sqrt{H^2/a_s}} + 3\, r_H^* - \dfrac{3\, \mathrm{r}_\mathrm{H}^{*\,2}}{\sqrt{\pi}}\dfrac{\sqrt{H^2/a_s}}{\sqrt{4\tau}} \\ -2 - 2\ln r_H^* + 3\, r_H^* - \dfrac{(H^2/a_s)^{3/2}}{12\sqrt{\pi}\,\tau^{3/2}} \end{cases} \qquad (2.10)$$

## 2.2 Short-term response

Until very recently, most of the solutions for the GSHP system analysis overlook the short-term response of the boreholes. The solutions either completely ignored it or used oversimplified assumptions. In reality, however, the short-term variations have significant effects on the performance of the heat pump and the overall system. Short-term response of the ground is also critical during heat-flux build-up stages and for cases with both heating and cooling demands. Studies regarding hourly or sub-hourly thermal energy use and the electrical demands of the ground source heat pump system also require the short-term response of the ground to be considered. In the following the analytical solutions of Young[67], Lamarche and Beauchamp[43] and Bandyopadhyay et al.[7] and the numerical solution of Yavuzturk[65] are discussed.

### 2.2.1 Numerical solution

The first major contribution to analyze the short-term response of a borehole came from Yavuzturk[65]. He extended Eskilson's concept of non-dimensional temperature response functions[24] to include the short-term analysis using a two dimensional implicit finite volume numerical approach. His solution approximated the cross section of the two legs of the U-tube as pie-sectors with constant flux entering the numerical domain for each time step. The solution accounted for pipe, grout and flow-related convective resistances.

Yavuzturk noted that the short-term *g-functions* are typically applicable for times in-between 2.5 min and 200 hours while the long term g-functions are applicable for times longer than 200 hours. As with Eskilson's *g-functions*[24] the short time-step *g-functions* of Yavuzturk lack in flexibility and inherit the disadvantages associated with most of the numerically obtained solutions. Due to these reasons, the analytical solutions to predict the short-term response of the boreholes have generated a lot of interest from the researchers.

### 2.2.2 Analytical Buried Electrical Cable analogy

Young[67] modified the classical Buried Electrical Cable (BEC) solution[18], which was developed to study the heating of the core of an electrical cable by steady current. Young, however, used the analogy between a buried electric cable and a vertical borehole by considering the core, the insulation and the sheath of the cable to represent respectively the equivalent-diameter fluid pipe, the resistance and the grout of the borehole. A grout allocation factor (*f*) allocating a portion of the thermal capacity of the grout to the core, was also introduced to provide a better fit for borehole modelling. The classical solution to the BEC problem has the following general form as proposed by Carslaw and Jaeger[17].

$$T_b - T_0 = \frac{q}{\lambda_s} \cdot \frac{2 \cdot \alpha_1^2 \cdot \alpha_2^2}{\pi^3} \int_0^\infty \frac{1 - e^{-u^2 \cdot Fo}}{u^3 \cdot \Delta(u)} du, \tag{2.11}$$

where:

$$\alpha_1 = \frac{2 \cdot \pi \cdot r_b^2 \cdot \rho_s \cdot c_s}{C_f} \qquad \text{with } C_f = \rho_f \cdot c_f \cdot A_f = \rho_f \cdot c_f \cdot \pi r_p^2 \, ,$$

$$\alpha_2 = \frac{2 \cdot \pi \cdot r_b^2 \cdot \rho_s \cdot c_s}{C_g} \qquad \text{with } C_g = \rho_g \cdot c_g \cdot A_{grout} = \rho_g \cdot c_g \cdot (\pi r_b^2 - \pi r_p^2),$$

$$h = 2 \cdot \pi \cdot \lambda_s \cdot R_b,$$

$$\Delta(u) = \left(u(\alpha_1 + \alpha_2 - hu^2)\, J_0(u) - \alpha_2(\alpha_1 - hu^2)\, J_1(u)\right)^2 + \left(u(\alpha_1 + \alpha_2 - hu^2)\, Y_0(u) - \alpha_2(\alpha_1 - hu^2)\, Y_1(u)\right)^2.$$

Young improved the original BEC method by introducing grout allocation (*f*) and fluid multiplication ($F_{fluid}$) factors. Using the grout allocation factor permits a better account for the borehole geometry as it assigns a part of grout's thermal capacity to the fluid. The fluid multiplication factor, on the other hand, accounts for the thermal capacity of the fluid outside the borehole loop.

$$S_{f'} = S_f \cdot F_{fluid} + S_g f \quad \text{and} \quad S_{g'} = S_g(1 - f)$$

### 2.2.3 Analytical solutions for composite media

Lamarche and Beauchamp[43] developed analytical solutions for short-term analysis of vertical boreholes by considering a hollow cylinder of radius $r_p$ inside the grout which is surrounded by infinite homogeneous ground. The cylinder, the grout and the surrounding ground all represent different media and have different thermal properties. Assuming that the cylinder reaches a steady flux condition much earlier than the adjacent grout, the following analytical solutions for short-term response of the borehole was developed.

$$T_b - T_0 = \frac{q}{\lambda_s} \cdot \frac{8\,\tilde{\lambda}}{\pi^5 \cdot \delta^2} \int_0^{\infty} \frac{(1 - e^{-u^2 \cdot Fo})}{u^5(\phi^2 + \psi^2)}\, du \qquad (2.12)$$

where:

$$\delta = r_b / r_p,$$

$$\tilde{\lambda} = \lambda_s / \lambda_g,$$

$$\phi(u) = Y_1(u)\left[Y_0(u\delta\gamma)J_1(u\delta) - Y_1(u\delta\gamma)J_0(u\delta)\tilde{\lambda}\gamma\right] - J_1(u)\left[Y_0(u\delta\gamma)Y_1(u\delta) - Y_1(u\delta\gamma)Y_0(u\delta)\tilde{\lambda}\gamma\right],$$

$$\psi(u) = J_1(u)\left[J_0(u\delta\gamma)Y_1(u\delta) - J_1(u\delta\gamma)Y_0(u\delta)\tilde{\lambda}\gamma\right] - Y_1(u)\left[J_0(u\delta\gamma)J_1(u\delta) - J_1(u\delta\gamma)J_0(u\delta)\tilde{\lambda}\gamma\right].$$

### 2.2.4 Analytical Virtual Solid Model

More recently Bandyopadhyay et al.[7] have modelled the short-term response of a borehole in a non-steady-state situation. The solution takes the thermal capacity of the circulating fluid into account by the $C/C_p$ ratio, which is the ratio of the unit length thermal capacity of an equivalent volume to the unit length thermal capacity of the pipe. The solution also considers the flow related convective heat transfer using the Biot number *Bi*. The circulating fluid in the borehole is modelled as a ‘virtual solid’ surrounded by an infinite homogeneous medium. The heat transferred to the ‘virtual solid’ is assumed to be generated uniformly over its length. The following classical solution proposed by Blackwell[14] is applicable under these conditions.

$$T_b - T_0 = \frac{\mathrm{q}}{\lambda_s}\frac{8}{\pi^3}\left(\frac{C}{\mathrm{C_p}}\right)^2 \int_0^\infty \frac{1 - e^{-u^2 \cdot Fo}}{u^3(O^2 + P^2)} du \tag{2.13}$$

where:

$$O = u\,Y_0(u) + 2\left(\frac{u^2}{Bi} - \frac{C}{\mathrm{C_p}}\right) Y_1(u),$$

$$P = u\,J_0(u) + 2\left(\frac{u^2}{Bi} - \frac{C}{\mathrm{C_p}}\right) J_1(u).$$

## 2.3 Borehole resistance

The internal heat transfer of a borehole is characterized by its thermal resistance. The borehole thermal resistance depends on the thermal properties of the borehole elements including U-tube and grouting and also on the physical arrangement of the U-tubes in the borehole. Several methods have been proposed to evaluate the thermal resistance of a borehole. Some of the noteworthy methods are discussed in the following.

The total borehole resistance includes the conductive resistances from U-tube ($R_u$) and the grout ($R_g$) and the convective resistance from the fluid ($R_f$) in the U-tube. However, in literature the term borehole resistance is often used only for the resistance of the grout region. This is because the U-tube wall resistance is fixed whereas the fluid resistance can be easily ignored for turbulent flows in the U-tube.

$$R_t = R_g + \frac{R_u + R_f}{2} \tag{2.14}$$

The thermal resistance of the U-tube can be found using the well known formula from Drake and Eckert[23] for steady state heat conduction through an annular region.

$$R_u = \frac{1}{2\pi \cdot \lambda_u} \cdot ln\left(\frac{r_{u,o}}{r_{u,i}}\right) \tag{2.15}$$

The fluid resistance can also be calculated according to Drake and Eckert[23]. The fluid resistance can be ignored in case of a turbulent flow in the pipe. For the laminar flow, it can be determined as:

$$R_f = \frac{1}{2\pi \cdot r_{u,i} \cdot h} \tag{2.16}$$

where $h$ (W/(m$^2$·K)) is the convective heat transfer coefficient of the fluid.

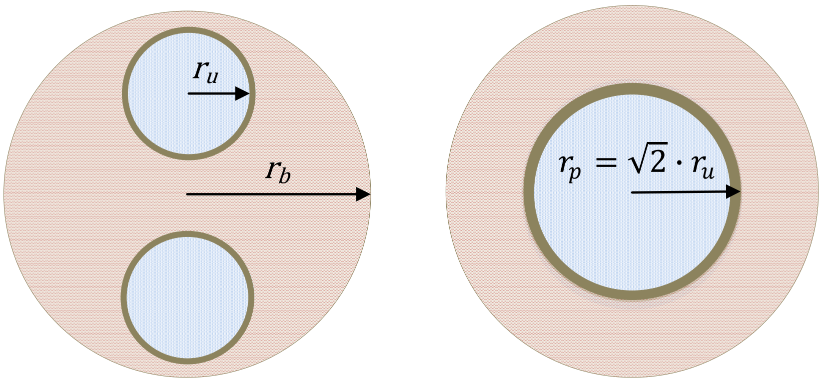


**Figure 2.2** Actual and simplified borehole geometries.

Assuming the U-tube as an equivalent-diameter pipe as shown in Figure 2.2, the grout resistance can be calculated using an expression similar to Equation 2.15.

$$R_b = R_g = \frac{1}{2\,\pi\,\lambda_g} \cdot ln\left(\frac{r_b}{r_p}\right) \tag{2.17}$$

As Equation 2.17 is based on the equivalent-pipe approximation, it does not account for thermal short-circuiting between the two legs of the U-tube. This was addressed by Gu and O'Neal[31] who modified Equation 2.17 to include the effects of shank spacing $s_s$.

$$R_b = \frac{1}{2\pi \cdot \lambda_g} \cdot ln\left(\frac{r_b}{r_p}\sqrt{\frac{2 \cdot r_p}{s_s}}\right) \tag{2.18}$$

Paul[49] studied three borehole configurations shown in Figure 2.3. Based on his experimental investigations on different grout materials, he proposed the following empirical relation to determine the borehole resistance.

$$R_b = \frac{1}{\beta_0 \cdot (r_b/r_u)^{\beta_1} \cdot \lambda_g} \tag{2.19}$$

The values of coefficient $\beta_0$ and $\beta_1$ of Equation 2.19 are given in the Table 2.1 for three different configurations of Figure 2.3.

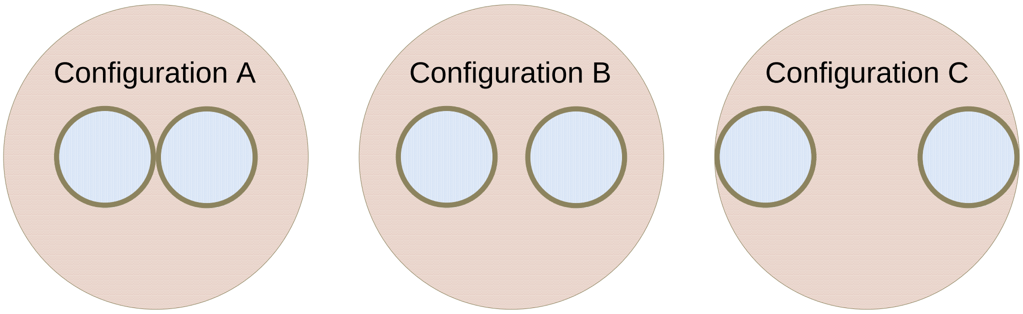


**Figure 2.3** Borehole configurations studied by Paul[49].

**Table 2.1** Values of coefficients used in Equation 2.19.

| ***Configuration*** | $\beta_0$ | $\beta_1$ |
|---|---|---|
| A | 20.10 | -0.9447 |
| B | 17.44 | -0.6052 |
| C | 21.91 | -0.3796 |

Another empirical relation was recently proposed by Sharqawy [53] et al.

$$R_b = \frac{1}{2\pi \cdot \lambda_g}\left[-1.49\left(\frac{s_s}{2r_b}\right) + 0.656 \ln\left(\frac{r_b}{r_u}\right) + 0.436\right]. \qquad (2.20)$$

Hellström[33] used the so-called line source thermal resistances to derive an analytical expression for the borehole resistance. His model assumes uniform borehole wall temperature along the borehole depth and treats the two legs of the U-tube as two separate pipes having similar fluid temperatures and heat fluxes. Under these conditions, the total borehole resistance as determined by Hellström is:

$$R_t = \frac{1}{4\pi\lambda_g}\left[\beta + \ln\left(\frac{r_b}{r_u}\right) + \ln\left(\frac{r_b}{s_s}\right) + \frac{\lambda_g - \lambda_s}{\lambda_g + \lambda_s}\ln\left(\frac{r_b^4}{r_b^4 - \left(\frac{s_s}{2}\right)^4}\right)\right], \qquad (2.21)$$

where:

$$\beta = \frac{\lambda_g}{\lambda_u} \cdot ln\left(\frac{r_{u,o}}{r_{u,i}}\right).$$

An alternate approach to determine the total borehole resistance is using the multipole method[33]. The multipole method solves the steady state heat transfer problem in the ground using a combination of a line heat source and multipoles. The line heat source represents the influence of a particular U-tube pipe on the temperature distribution while the multipoles account for the influence of other neighbouring pipes. Equation 2.22 gives the total borehole resistance using a first order multipole approximation.

$$R_t = \frac{1}{4\pi\lambda_g}\left[\beta + \ln\left(\frac{r_b}{r_u}\right) + \ln\left(\frac{r_b}{s_s}\right) + \frac{\lambda_g - \lambda_s}{\lambda_g + \lambda_s}\ln\left(\frac{r_b^4}{r_b^4 - \left(\frac{s_s}{2}\right)^4}\right)\right]$$
$$- \frac{1}{2\pi\lambda_g}\,\frac{\left(\frac{r_u}{s_s}\right)^2 \cdot \left[1 - \frac{\lambda_g - \lambda_s}{\lambda_g + \lambda_s}\cdot\frac{4{s_s}^4}{(16r_b^4 - {s_s}^4)}\right]^2}{\left\{\frac{1+\beta}{1-\beta} + \left(\frac{r_u}{s_s}\right)^2\left[1 + \frac{\lambda_g - \lambda_s}{\lambda_g + \lambda_s}\cdot\frac{{s_s}^4 \cdot r_b^4}{(r_b^4 - (0.5s_s)^4)^2}\right]\right\}} - \cdots \qquad (2.22)$$

Hellström[33] and Zeng et al.[69] have presented borehole resistance expressions which also account for the fluid temperature variations along the borehole depth. The expression developed by Zeng et al. for borehole resistance using a quasi-three-dimensional method is:

$$R_b = \frac{H}{\dot{M} \cdot c_f} \cdot \left(\frac{1}{\varepsilon} - \frac{1}{2}\right), \qquad \varepsilon = \frac{T_{f,i}(\tau) - T_{f,o}(\tau)}{T_{f,i}(\tau) - T_b(\tau)}. \qquad (2.23)$$

## 2.4 Discussion

In this chapter, various methods to determine the long and the short term borehole response and the borehole thermal resistance were described and discussed. When determining the long-term response the geometry of the borehole is often neglected and the borehole is modelled either as a line or as a cylindrical source with finite or infinite length. Due to these unrealistic assumptions regarding the geometry of the borehole, the thermal capacities of the borehole elements and the flow-related convective heat transfer inside the borehole are also ignored when analyzing the long-term response of the borehole. Bernier et al.[11] and Nagano et al.[47] have developed calculation tools using classical cylindrical source and line source methods. However, Eskilson's *g-function* approach[24], based on the finite line source assumption, is considered as the state-of-the-art and has been implemented in software like EED[15], TRNSYS[52], HVACSIM+[20] and GLHEPRO[59].

Short-term response of a borehole, on the other hand, requires more stringent assumptions and the borehole cannot be simply modelled as a line or a cylindrical source. The actual geometry of the borehole is therefore usually retained when determining its short-term response. An equivalent-diameter is often used for simplifications instead of considering a U-tube with two legs. The equivalent-diameter assumption allows taking the thermal mass of the borehole elements and the flow-related convective resistances into account. The short-term *g-functions* developed by Yavuzturk[65] are regarded as the-state-of-the-art in determining the short-term response of the borehole. Like the *g-function* approach of Eskilson[24], the short-term *g-function* approach has also been implemented in various building simulation and ground loop design software including HVACSIM+[20] and Energy Plus[21].

Like the short-term response calculations, the borehole thermal resistance is also often determined by approximating the two legs of the U-tube as an equivalent-diameter pipe and calculating the resistance of the annular region between the pipe and the borehole diameters. Empirical solutions based on experimental results have also been developed and used by researchers like Paul[49] and Sharqawy et al.[53] However, the multipole method[33] remains the state-of-the art solution to determine the borehole thermal resistance. The multipole method has been implemented in ground system design software EED[15].

## 2.5 Conclusions

A review of existing solutions to calculate long and short term response and the thermal resistance of the borehole was carried out. The simple analytical solutions described in this paper can be used with reasonable accuracy to predict the response of single borehole systems. However, there is a shortage of such solutions when it comes to multiple borehole systems. The use of existing analytical solutions to determine the long-term response of the multiple borehole systems should be investigated further. The existing short-term response solutions are based on many assumptions regarding the geometry and the heat transfer of the borehole. The existing short-term response solutions should also be checked for consistency and accuracy.

# 3 Analytical modelling and simulation

Lately, the high energy efficiency potential of Ground Source Heat Pump systems (GSHP) has resulted in rapidly growing numbers and sizes of such installations. Single borehole systems, which are mostly used in residential applications, can be designed by considering only the long-term thermal response of the borehole. The two most critical design criteria for these systems, the appropriate design length of the borehole and the need for balancing of the ground loads, can both be determined using the long-term response of the borehole. Multiple borehole systems, on the other hand, are generally used for energy storage and are more common for commercial applications. For multiple borehole systems, the short-term response of the borehole has significant impact on the efficiency of the whole GSHP system. Hence, for these systems short-term response of the borehole is equally important as the long-term response.

## 3.1 Introduction

In this chapter, the long and the short term response of the borehole system are studied in terms of mean fluid temperatures. The reason for studying the long and the short term effects in terms of fluid temperatures, instead of the more conventional borehole temperatures, is the fact that the actual design process of a GSHP system uses input values of inlet and outlet fluid temperatures. The borehole design method by ASHRAE[3] and software programs like EED[15] and GLHEPRO[59] also use fluid temperatures as an input. Moreover, the design of the borehole system and the capacity of the heat pump are decided based on the desired fluid temperatures. As the designers and practitioners are used to design GSHP systems using fluid temperatures rather than borehole temperatures, the variation in the fluid temperature is used as a measure to study the long and short term response of the borehole systems.

The fluid temperature leaving a borehole heat exchanger depends on various factors including heat flux, ground and grout properties and conductive heat transfer outside the borehole boundary etc. A common approach to model the heat transfer mechanism of a borehole is by assuming a mean borehole wall temperature ($T_b$) and a mean fluid temperature ($T_f$). Heat transfer inside the borehole is generally considered as quasi-steady-state. Under these conditions the mean fluid temperature can be calculated as:

$$T_f(\tau) = T_b(\tau) + q(\tau) \cdot R_b + T_{pty}(\tau) \tag{3.1}$$

where $q$ is the heat flow per unit length of the borehole, $R_b$ is the thermal resistance of the borehole and $T_{pty}$ is the temperature penalty because of temperature influence from the surrounding boreholes.

## 3.2 Long-term response

Determining the long-term response of a borehole system has traditionally been the major focus of the borehole response modelling. Several analytical and numerical solutions have been developed to model the thermal response of borehole systems after 10-25 years of their operation. The long-term thermal response is imperative to calculate the required length of the borehole system and to determine the performance deterioration of the borehole system over time.

### 3.2.1 Existing long-term response solutions

The long term response of a borehole depends on its mean wall temperature (i.e. $T_b$) and the influence from the surrounding boreholes (i.e. $T_{pty}$) as indicated by Equation 3.1. Calculation of $T_b$ and $T_{pty}$ is quite a challenge. Various analytic and numerical solutions have been developed over the years to determine $T_b$ and $T_{pty}$. The simplicity and flexibility of analytical solutions, like the line source and the cylindrical source, have prompted many researchers to use these solutions to calculate $T_b$, particularly for single boreholes. These two analytical solutions can be applied, with few limitations, to calculate $T_b$ for a single borehole. These models have also been used[37, 39] to calculate $T_{pty}$ for multiple borehole systems by applying the superposition principle. However, there is still scepticism among researchers regarding the application of these models for multiple boreholes.

Numerical solutions of varying complexity have also been developed and employed to determine for instance $T_b$ and $T_{pty}$. The work of Eskilson[24] is regarded as state-of-the-art and is the only method which accounts for the long-term influence between boreholes in a very exact way. The method, called the Superposition Borehole Model (SBM), numerically models the thermal response of the borehole using non-dimensional *g-functions*.

Lately, the classical line source theory has been extended and incorporation of the finite-length heat source has considerably enhanced the accuracy of the method to calculate $T_b$. Some researchers[22, 42] have used the finite-length line source to investigate $T_b$ and $T_{pty}$ for single and multiple borehole configurations. For multiple borehole configurations, analytical *g-functions* are derived using the finite-length line source and the superposition principle is applied to account for thermal interaction between boreholes. Two different approaches have been used. Lamarche and Beauchamp[42] have used the integral mean temperature along the borehole depth as the representative temperature when calculating heat transfer between the borehole and the fluid. For the same calculation, Diao et al.[22] instead propose the middle point temperature of the borehole. The first method, due to its superior approach, provides a better match to the numerically calculated *g-functions*. Both these approaches have been used[42, 50] to determine the thermal response of multiple borehole systems but the applications have mostly been limited to relatively simple configurations.

To summarize, various analytical and numerical solutions can be used to determine $T_b$ and correspondingly $T_f$ for single boreholes. However, the SBM is the only method which can determine these for multiple boreholes in a precise way. Other methods must be further tested and validated before they can be used to model multiple boreholes. In the following sections we will calculate fluid temperatures for a case study using a few of the above-mentioned solutions. The objective is to compare the existing analytical methods in order to evaluate their fitness for use in multiple borehole system design calculations.

### 3.2.2 Comparison of existing analytical solutions for long-term response modelling

In order to provide a comparison of existing analytical solutions to model the long-term response, the Astronomy-House building at Lund University in Sweden was selected as a case study. The building has a gross floor area of around

5,300 $m^2$. The borehole system, consisting of twenty 200 m deep boreholes in rectangular configuration, provides about 475 MWh of heating and 155 MWh of cooling. The monthly heating ($Q_h$) and cooling ($Q_c$) demands of the building are given in Table 3.1.

**Table 3.1** Monthly heating and cooling demands of the case study building.

| ***Month*** | ***$Q_h$* [MWh]** | ***$Q_c$* [MWh]** |
|---|---|---|
| January | 97.9 | - |
| February | 89.3 | - |
| March | 69.8 | 3.4 |
| April | 40.9 | 7.3 |
| May | 20.9 | 15.0 |
| June | - | 25.7 |
| July | - | 33.2 |
| August | - | 31.3 |
| September | - | 19.2 |
| October | 31.4 | 13.3 |
| November | 47.5 | 6.4 |
| December | 77 | - |
| Year | 475 | 155 |

The fluid temperatures have been simulated using five different approaches to evaluate the long-term response of the borehole system. The first two approaches use the cylindrical source solution to evaluate $T_b$. In the first approach $T_{pty}$ from surrounding boreholes is calculated using the infinite-length line source solution. In the second approach, however, the finite-length line source solution is used. The third and fourth approaches use the infinite-length line source and the finite-length line source respectively to calculate both $T_b$ and $T_{pty}$. The fifth and final approach calculates fluid temperature using the state-of-the-art SBM.

Figure 3.1 shows results of the simulations in terms of minimum and maximum mean fluid temperature. Taking state-of-the-art SBM simulation results as the reference indicates that all five approaches provide reasonably close results. The biggest deviation for maximum as well as minimum temperature for the 15$^{th}$ year is less than 1 ºC. The SBM simulations were conducted using a commercial software which uses highly accurate multipole method to determine $R_b$. In contrast, all other approaches used a simple analytical method[69] to calculate $R_b$. Approaches 2 and 4, both of which involve the finite-length line source, gave more accurate results than approaches 1 and 3, which involve the infinite-length line source.

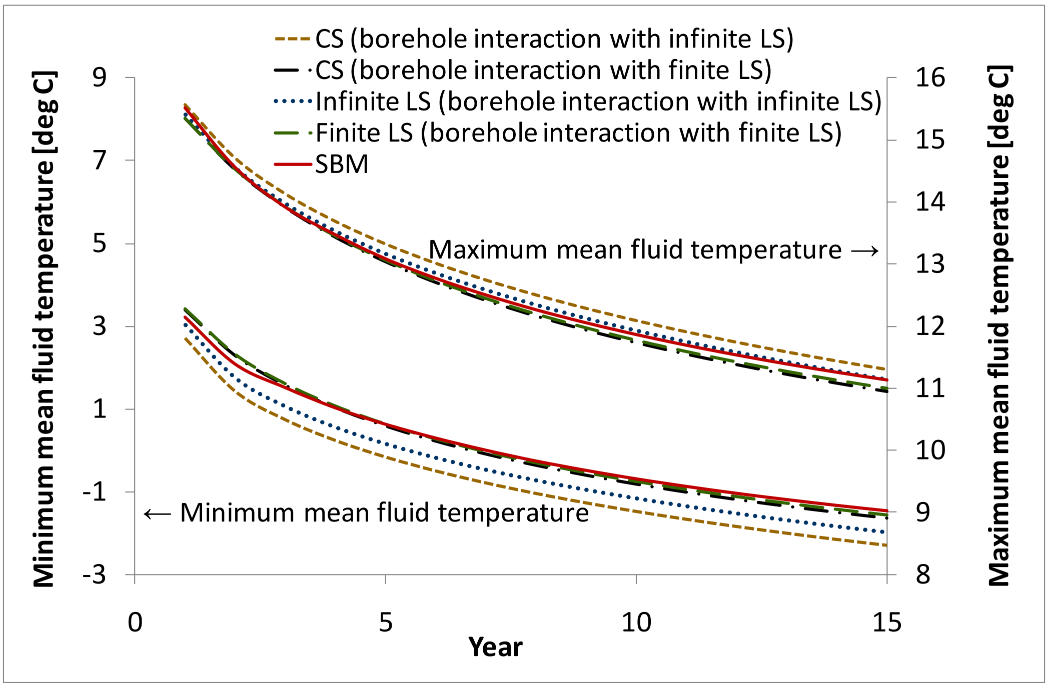


**Figure 3.1** Mean fluid temperatures using different approaches.

(Note: The y-axes in Figure 3.1 are arbitrarily offset to clarify the patterns of minimum and maximum mean fluid temperatures.)

### 3.2.3 Effects of building load pattern and borehole geometry on long-term response modelling

The building load pattern and the choice of borehole field geometry significantly influence the long-term response of a borehole system. The building load can be expressed as a ratio of net heating and cooling demands of the building using a load factor $l$ [48]. The concept of load factor is useful to characterize buildings based on their heating and cooling demands. Its value lies between -1 and +1. The two values indicate the extreme conditions of cooling only and heating only requirements respectively.

$$l = \frac{Q_h + Q_c}{|Q_h| + |Q_c|} \quad [-] \tag{3.2}$$

The Astronomy-House has a load factor of $l$=0.5, which indicates that it is a heating dominated building. In Figure 3.2, the actual situation in the building is compared with two scenarios of $l$=0.75 and $l$=0.25. These scenarios are developed by varying values of heating and cooling demands while keeping the sum of their net absolute values equal to the original case.

For $l$=0.25, both maximum and minimum mean fluid temperatures remain unchanged throughout the simulation time period. This is because, for values of $l$ around zero, the rectangular configuration ground system, if designed appropriately, acts like a heat storage system and fluid temperatures do not deteriorate over time. However, for $l$=0.75, there is a sharp decline in both maximum and minimum mean fluid temperatures with time. This is due to a decrease in the ground temperature because of consistent unbalanced heat extraction from the ground.

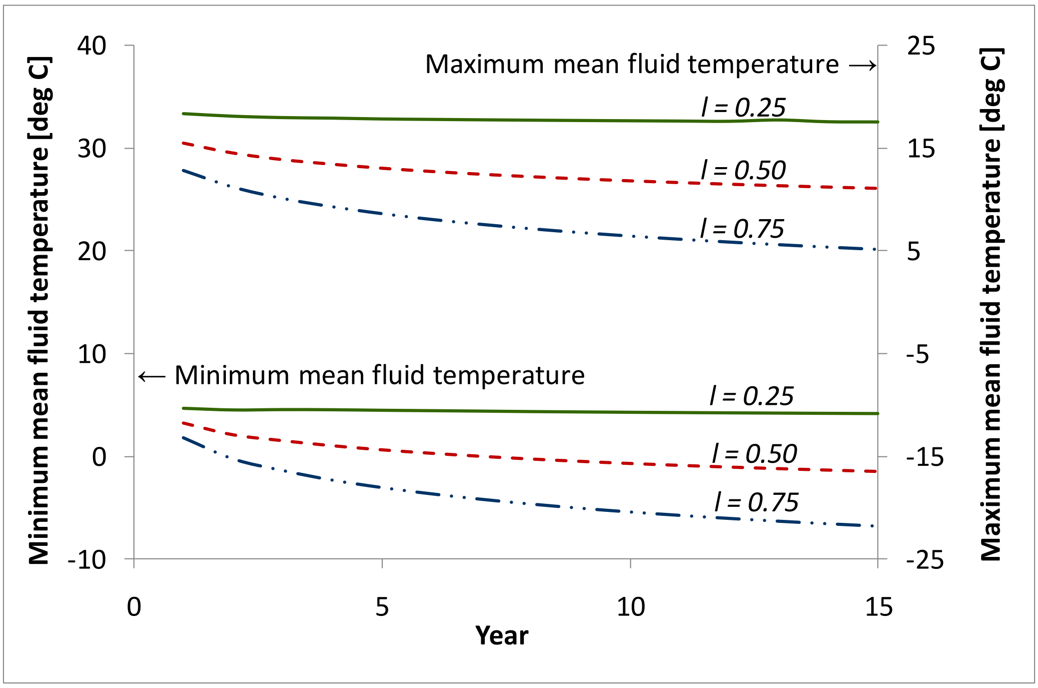


**Figure 3.2** Mean fluid temperatures for different load factors.

(Note: The y-axes in Figure 3.2 are arbitrarily offset to clarify the patterns of minimum and maximum mean fluid temperatures.)

The borehole field geometry can be expressed as the ratio of the volume $V$ of the ground system and its heat exchange area $A$ using a geometry factor $g$[48]. The significance of $g$ is illustrated in Figure 3.3, where $g$ is plotted for the two contrasting cases of line and square configurations. For the line configuration $g$ remains almost constant while for the square configuration $g$ increases linearly with an increasing number of boreholes.

$$g = \frac{V}{A}\ [\mathrm{m}] \tag{3.3}$$

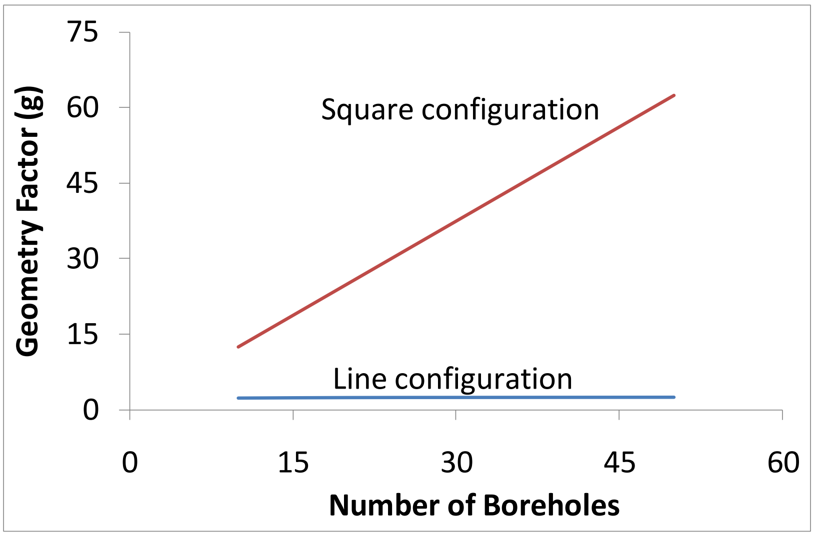


**Figure 3.3** Geometry factor for line and square configurations.

For predominant heating or cooling loads, the performance of the GSHP system will deteriorate significantly if a rectangular borehole configuration is selected. In such cases, a dissipative system with more open ground configuration will result in more desirable fluid temperatures. This can be seen from Figure 3.4 which presents fluid temperatures for various geometry factors (*g*). As seen, a line configuration has the lowest *g* value. This represents the most open configuration and will ensure maximum heat transfer with the ground. It will result in a minimum decline of the fluid temperature. This, however, is undesirable in the Astronomy-House case as the objective of this system is to exploit the ground's heat storage ability and hence a rectangular configuration was chosen. The selected system was designed to take care of the expected decline in borehole temperature with time.

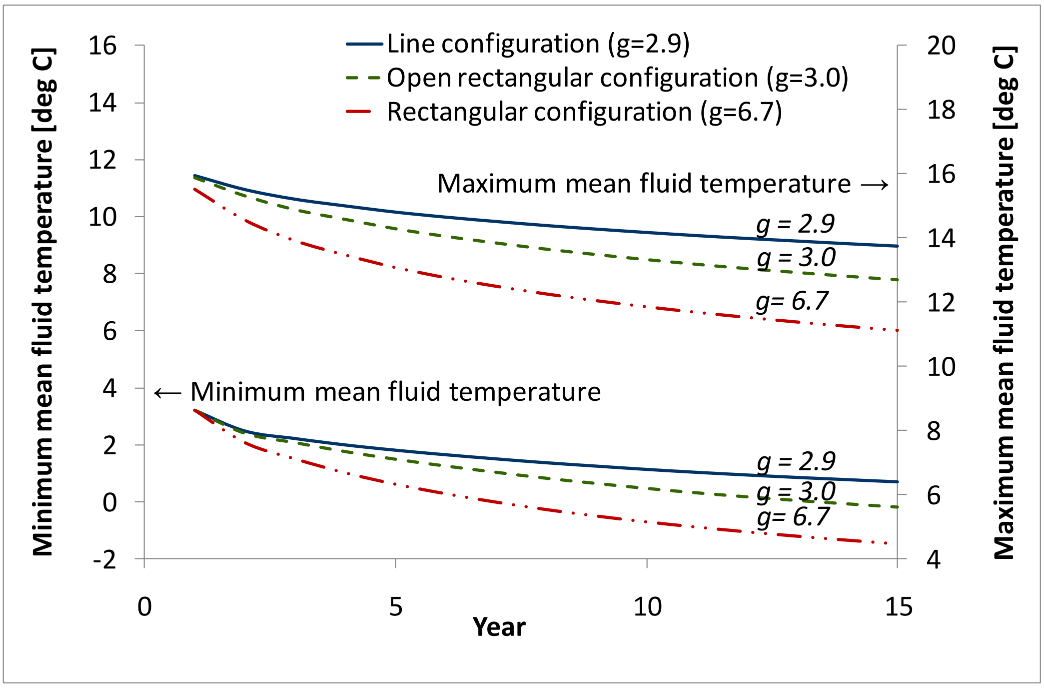


**Figure 3.4** Mean fluid temperatures for different geometry factors.

(Note: The y-axes in Figure 3.4 are arbitrarily offset to clarify the patterns of minimum and maximum mean fluid temperatures.)

To conclude, existing analytical solutions were used to simulate the response of a multiple borehole system. The simulation results indicate that the existing analytical models can be used with reasonable accuracy to determine the long-term response of multiple borehole systems. However, the computational efficiency of the long-term response calculations decreases with increasing number of boreholes. For reasonably large systems (i.e. > 50 boreholes), the use of existing analytical methods to evaluate long-term response is not recommended due to computational time constraints.

## 3.3 Short-term response

Nowadays, short-term response of the borehole system has also become a key input parameter when optimizing the overall performance of the GSHP systems. One of the major reasons behind this development is the fact that heating and cooling demands of buildings have changed considerably. Today, many commercial and office buildings have a cooling demand during the day, even in a climate as cold as Sweden's, and a heating demand during the night. Other commercial buildings, like shopping centres and supermarkets, have simultaneous heating and cooling demands. The changing heating and cooling demands of the buildings have shifted the optimization focus of the GSHP systems from long-term seasonal storage to hourly, daily and weekly balancing of the borehole system loads. The short-term response of a borehole is also significant when conducting thermal response tests (TRTs) to estimate the ground thermal properties. A typical TRT measures the response of the ground during flux build-up stages. The measured response is then analyzed using a heat transfer model to estimate properties like ground thermal conductivity and thermal resistance of the borehole. The long-term response solutions have often been utilized to analyze TRTs but using these solutions result in longer and more expensive tests as these solutions require steady flux situation. The short-term response solutions are much better suited to evaluate TRTs because of their inherent ability to model the transient heat transfer during the flux build-up stages.

### 3.3.1 Existing short-term response solutions

The classical methods to determine the thermal response of a borehole include the line source and the cylindrical source solutions. Both the line and the cylindrical source solutions are inaccurate for times smaller than 10-15 hours as both these solutions oversimplify the geometry of the borehole and disregard its internal heat transfer. Nevertheless, these solutions have been extensively used to determine the short-term response of boreholes, in particular when evaluating thermal response tests.

A number of numerical solutions have been developed to overcome the shortcomings of the line and cylindrical solutions when evaluating TRTs. Among others, Shonder and Beck[55] and Austin[4] have developed solutions which numerically solve the heat transfer in a borehole. Shonder and Beck solve the 1-D radial heat transfer problem using a finite difference approach. They model the U-tube as an equivalent-diameter pipe surrounded by a thin film layer in the grout. The film layer accounts for the thermal capacity and the convective heat transfer of the fluid, the thermal capacity of the pipe and the thermal resistance of the grout. Austin, on the other hand, uses a 2D finite volume approach. His solution approximates the cross-sections of the two legs of the U-tube as pie-sectors with constant heat-flux entering the numerical domain for each time step. Yavuzturk and Spitler[66] extended Austin's work and developed the so-called short time-step *g-functions*, which are essentially an extension to Eskilsons' *g-functions*[24] from the Superposition Borehole Model. These two numerical solutions are very attractive for parametric analysis and to obtain precise solutions, but as all other numerical solutions, they too have limited flexibility. The fact that these and other similar numerical solutions cannot be directly incorporated into building energy simulation software has vastly limited their use for optimization of GSHP systems.

The need for robust, yet rapid, solutions for parameterized design and optimization of GSHP systems has resulted in the development of various analytical and semi-analytical solutions. Gu and O'Neal[29] developed an analytical solution assuming a cylindrical source in an infinite composite region. They solve the borehole transient heat transfer problem using the generalized orthogonal expansion technique which requires calculation of multiple eigenvalues. Young[67] modified the classical Buried Electric Cable solution[18] to develop his Borehole Fluid Thermal Mass solution. Lamarche and Beauchamp[43] extended the classical cylindrical source solution[36] and developed short-term solutions for two cases of constant heat transfer rate and constant fluid temperature. More recently, Bandyopadhyay et al.[7] adapted the classical solution from Blackwell[14] in their 'Virtual Solid' model. They also developed a semi-analytical solution in which they first solve the borehole heat transfer problem in the Laplace domain and then use a numerical inversion[60] to obtain the time domain solution. Beier and Smith[9] also developed a semi-analytical solution using Laplace transformations.

### 3.3.2 Short-term response modelling challenges

All the short-term response solutions make simplifying assumptions regarding the geometry and the heat transfer problem of the borehole. Figure 3.5 illustrates the actual borehole geometry and also shows the thermal interactions of a borehole. The heat transfer inside the borehole depends on the thermal properties and interactions of its elements (i.e. the circulating fluid, the U-tube pipe and the grouting material). However, the conductive heat transfer across the borehole boundary also involves the thermal properties of the neighbouring ground. Assumptions regarding the borehole geometry and the thermal properties and the interactions of the borehole elements can significantly affect the short-term response calculations.

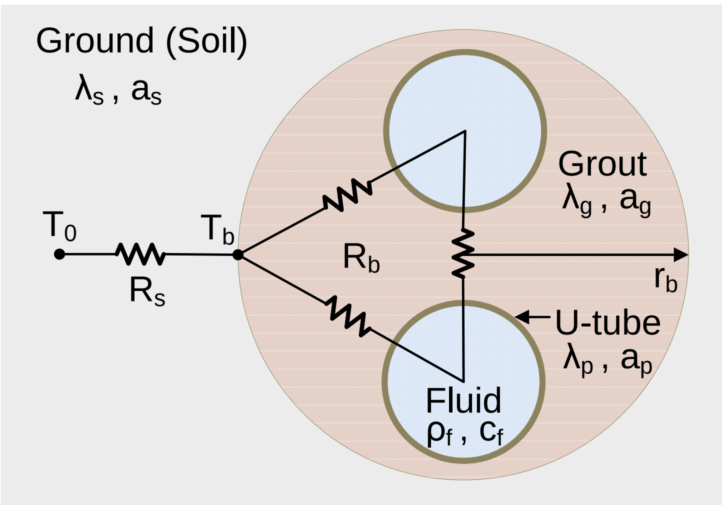


**Figure 3.5** The actual geometry and the thermal interactions of a borehole.

In most existing solutions, the borehole heat transfer is assumed to be radial only. This requires the U-tube to be approximated as a single equivalent-diameter pipe. Various methods[16, 30, 39, 61] have been suggested to approximate the radius ($r_p$) of the equivalent-diameter pipe. The resulting radial heat transfer problem is shown in Figure 3.6a. Some researchers have also developed solutions which eliminate the grout and study the heat transfer from the equivalent-diameter pipe directly to the surrounding ground (Figure 3.6b). Such solutions are useful for cases when the borehole has been backfilled with its cuttings.

### 3.3.3 Critical analysis of three existing analytical solutions

In this section, the strengths and limitations of the analytical solutions from Young[67], Lamarche and Beauchamp[43] and Bandyopadhyay[7] are highlighted and the transient heat transfer considered by these solutions is critically analyzed.

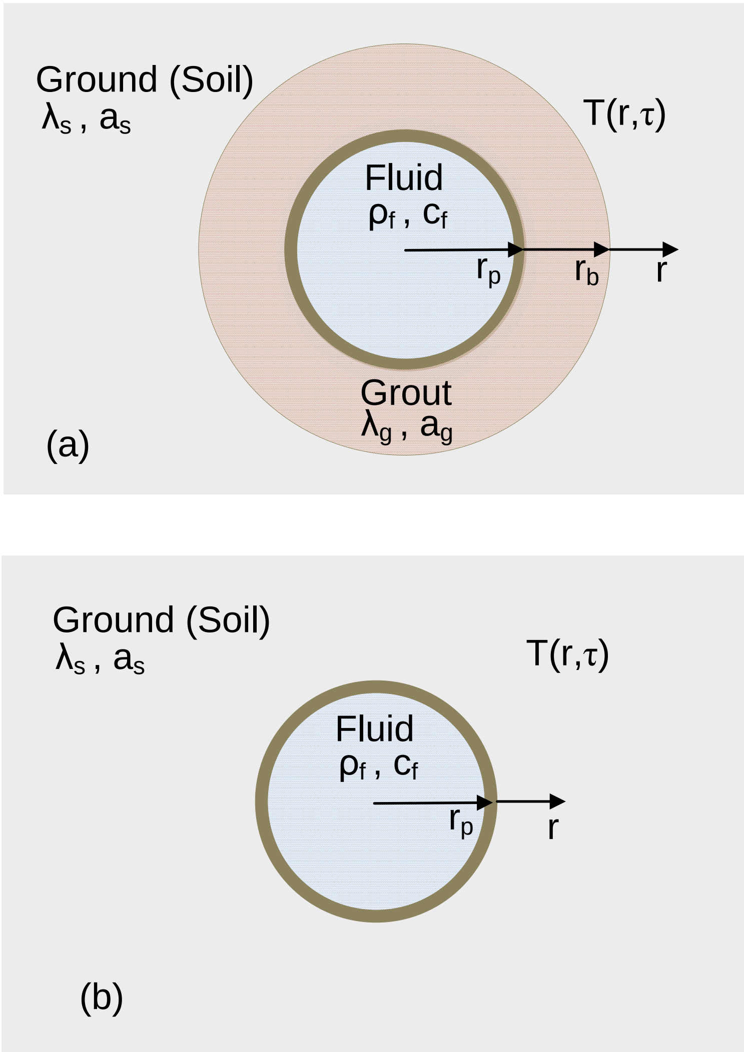


**Figure 3.6** Simplified borehole geometries.

#### 3.3.3.1 Borehole Fluid Thermal Mass (BFTM) and Buried Electric Cable (BEC) solutions

The BFTM solution developed by Young[67] is primarily a variation of the grouted borehole case shown in Figure 3.6a. In the actual BEC solution[18], the core and the sheath of the electric cable are both assumed to be metallic conductors and thus have lumped thermal capacities and temperatures. However, this assumption is not very accurate for vertical boreholes. Therefore, Young uses a grout allocation factor to assign a portion of the thermal capacity of the grout to the equivalent-diameter pipe. This improves the accuracy of the BFTM solution. Additionally, Young also suggests using a logarithmic extrapolation to get better precision and using multipole method to calculate the borehole resistance. In reality, the grout allocation factor varies from case to case and is extremely ambiguous to calculate. This makes the practical implementation of the BFTM solution quite challenging. Hence, the BFTM solution has rarely been implemented in its true essence.

#### 3.3.3.2 Lamarche and Beauchamp's (L&B) solution

Lamarche and Beauchamp[43] also solved the radial heat transfer problem for grouted boreholes. In their solution, they assumed the equivalent-diameter pipe of Figure 3.6a as a hollow cylinder with no thermal capacity. This solution is essentially an extension of the classical cylindrical source solution as it solves the heat transfer problem assuming a steady heat-flux condition across the hollow cylinder boundary. However, unlike the cylindrical source solution, this solution incorporates the thermal properties of the grout. This is done by taking the steady heat-flux condition across the hollow cylinder instead of the GHE boundary as considered by the cylindrical source solution. The heat transfer from the equivalent-diameter pipe to the grout depends on the thermal heat capacity and the convective heat transfer of the fluid and the physical and the thermal properties of the pipe. The temperature increase of the fluid is dampened by the presence of the fluid thermal capacity. In its absence, the fluid temperature will rapidly increase for short times before converging to the long-term response. Hence, the response calculated using the L&B solution is not accurate for short times.

#### 3.3.3.3 Virtual Solid (VS) solution

Bandyopadhyay et al.[7] recently presented their VS solution to determine the short-term response of the boreholes backfilled with their cuttings (Figure 3.6b). The solution, which was originally developed by Blackwell[14], models the circulating fluid as a virtual solid whereas the injected heat is assumed to be generated uniformly over the length of the virtual solid. The solution accounts for the thermal capacity of the circulating fluid and also considers the flow related convective heat transfer. However, the VS solution also has limited practical application as most of the boreholes are backfilled with a material quite different from their cuttings.

### 3.3.4 Comparison of existing analytical solutions for short-term response modelling

A comparison of the analytical solutions analyzed in the previous section was made to investigate the short-term response estimations by these solutions. The solutions are also compared to a newly developed exact and validated analytical solution[19]. Further details and descriptions of the new analytical solution are provided in Chapter 4. The comparison is done for three cases of borehole filled with groundwater, borehole backfilled with Thermally Enhanced Grout (TEG) and borehole backfilled with its own cuttings. For all three cases, the increase in the fluid temperature for a unit heat injection is simulated for a GHE of 110 mm diameter. The details of the considered grout and ground (i.e. soil) properties are given in Table 3.2.

**Table 3.2** Grout and ground properties of three simulated cases.

| Case | Grout properties | Ground properties |
|---|---|---|
| 1. GHE filled with groundwater | $\lambda_g$ = 0.57 W/(m·K)<br>$\rho_g$ = 1000 kg/m$^3$<br>$c_g$ = 4180 J/(kg·K) | $\lambda_s$ = 3 W/(m·K)<br>$\rho_s$ = 2500 kg/m$^3$<br>$c_s$ = 750 J/(kg·K) |
| 2. GHE backfilled with TEG (Thermally enhanced grout) | $\lambda_g$ = 1.5 W/(m·K)<br>$\rho_g$ = 1550 kg/m$^3$<br>$c_g$ = 2000 J/(kg·K) | |
| 3. GHE backfilled with borehole cuttings | $\lambda_g$ = 3 W/(m·K)<br>$\rho_g$ = 2500 kg/m$^3$<br>$c_g$ = 750 J/(kg·K) | |

The comparison of the analytical solutions for a groundwater-filled borehole is presented in Figure 3.7. Such installations are common in all Scandinavian countries and particularly in Sweden. In this study, effects of the convective heat transfer in the groundwater were not considered. As seen, the BFTM and VS solutions both underestimate the short-term fluid temperature increase when compared to the exact analytical solution. This is because both these solutions do not consider the actual thermal properties of the groundwater. The VS solution takes the thermal properties of the groundwater as those of the surrounding ground while the BFTM solution uses a lumped capacity and temperature for the groundwater. On the other hand, the L&B solution initially overestimates the short-term increase of the fluid temperature because it ignores the thermal capacity of the fluid. Hence, the predicted increase in the fluid temperature by L&B solution is higher than that predicted by the new analytical solution. However, the increase in the fluid temperature predicted by these two solutions converges with time.

The different predictions of the increase in the fluid temperature deviate less for a borehole backfilled with TEG (Figure 3.8) than a groundwater-filled borehole. This is because the thermal properties of the TEG are closer to the thermal properties of the ground than are those of water. Consequently, the short-term fluid temperature increase of the borehole backfilled with TEG, as predicted by the new analytical and the L&B solutions, is lower than that of a groundwater-filled borehole. This reduces the differences between the solutions in general as the fluid temperature predicted by the VS and the BFTM solutions remain virtually unchanged.

For the GHE backfilled with borehole cuttings (Figure 3.9), the VS and the new analytical solutions predict the same short-time fluid temperature increase. Like the first two cases, the L&B solution overestimates the increase in the fluid temperature for short times but converge to the results from the new analytical and VS solutions in the long run.

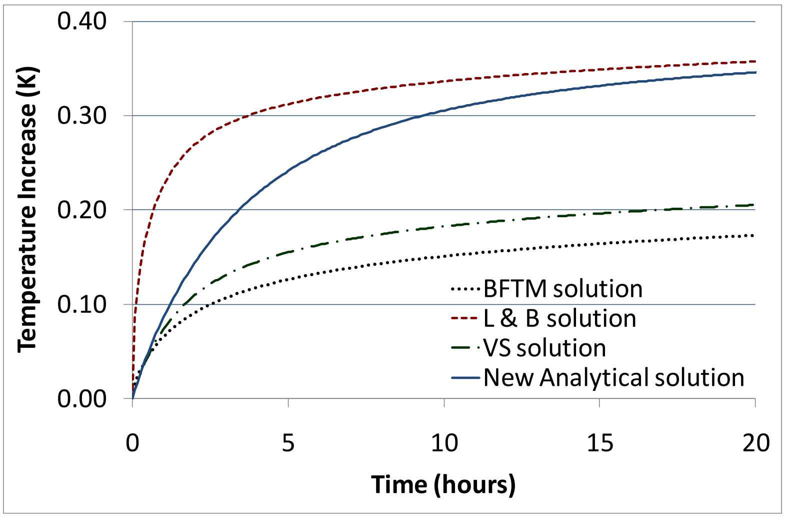


**Figure 3.7** Predicted fluid temperatures for a groundwater filled borehole.

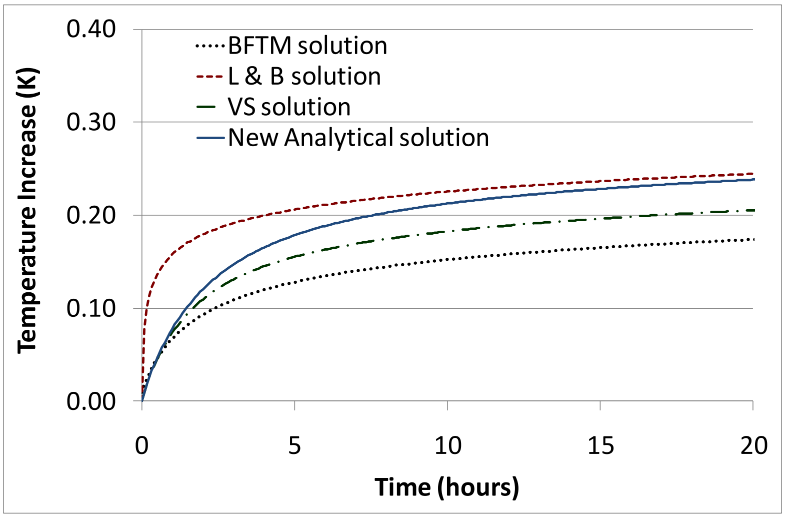


**Figure 3.8** Predicted fluid temperatures for a borehole backfilled with TEG.

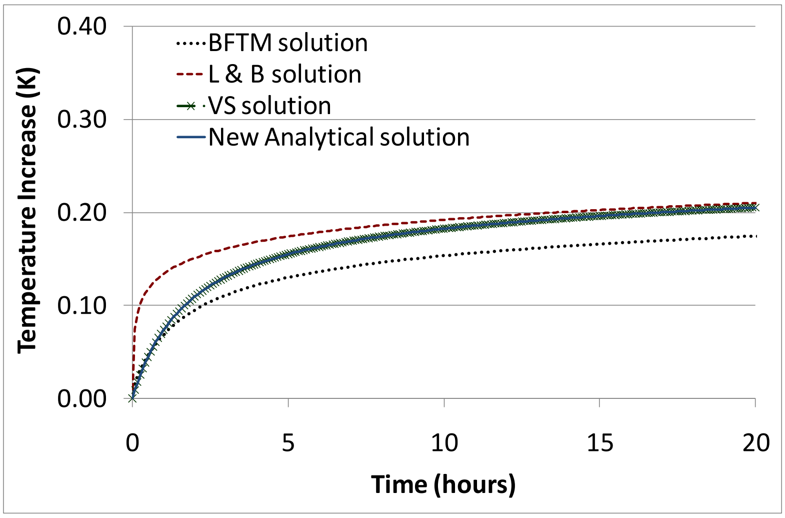


**Figure 3.9** Predicted fluid temperatures for a borehole backfilled with its cuttings.

The results clearly indicate the variations among different analytical solutions and highlight the significance of unrealistic assumptions regarding the geometry and the elements of the borehole. Thermal properties of the fluid and the grout are both critical to the short-term response modelling. Unreasonable assumptions, like not accounting for the fluid thermal capacity or not considering the actual grout properties, lead to unrealistic results. It is also interesting to see the influence of different grout properties on the predicted fluid temperature. Increase in the thermal conductivity of the grout and decrease in its thermal capacity have considerable influence on the short-term response of the GHE as indicated by the results of the new analytical solution for the three cases. The predicted increase in the fluid temperature varies around 75 % between the groundwater-filled borehole (i.e. the lowest grout thermal conductivity and the highest grout thermal capacity) and the borehole backfilled with borehole cuttings (i.e. the highest grout thermal conductivity and the lowest grout thermal capacity). For all the three cases, the BFTM solution tends to be the most inaccurate. To improve the BFTM-solution accuracy, Young[67] suggests calculating the borehole resistance using multipole method[33] and also recommends using a grout allocation factor and a logarithmic extrapolation procedure. These, however, were not done in this implementation of the BFTM solution.

## 3.4 Conclusions

In this chapter, the long and short term analytical solutions were studied in detail. It was shown that even simple analytical methods can be used with reasonable accuracy to evaluate long-term response both for multiple borehole systems. On the other hand, the existing analytical solutions provide inaccurate evaluations of the short-term borehole response. This is because the existing solutions overlook the thermal properties of some borehole elements or oversimplify the borehole geometry and the thermal interaction between borehole elements.

# 4 Development of new solutions

It was shown in chapter 3 that there exists a genuine need of a new analytical approach capable of simulating short-term response of a borehole considering all the significant heat transfer processes and without distorting the geometry of the borehole. This chapter reports on the development of a new analytical solution which was developed to overcome the limitations of existing short-term response solutions. The new analytical solution considers the thermal capacities, the thermal resistances and the thermal properties of all the borehole elements and provides an exact solution to the radial heat transfer problem in vertical boreholes. A new numerical solution was also developed primarily to validate the analytical model. The new numerical solution studies the one-dimensional heat conduction problem using a coordinate transformation technique.

## 4.1 Introduction

To address the fundamental deficiencies and shortcomings of existing analytical solutions, new analytical and numerical solutions were developed[19]. The new analytical solution studies the heat transfer and the related boundary conditions in the Laplace domain. The new numerical solution studies the one-dimensional heat conduction problem with a transformation of the radial coordinate to a conformal one for which the heat flux has the simplest possible form. The new solutions assume radial heat transfer in the borehole. To meet this requirement, the U-tube in the borehole is approximated as a single equivalent-diameter pipe of radius $r_p = \sqrt{2} \cdot r_u$. This equivalent pipe radius estimates the pipe cross sectional area equivalent to the sum of the cross sectional area of the two legs of the U-tube. As the new models explicitly consider the pipe and the fluid resistances, it is not required to implicitly include these resistances when calculating the equivalent pipe radius. The resulting problem is shown in Figure 4.1. The heat flux $q_{inj}$ is injected at a constant rate to the fluid at temperature $T_f(\tau)$. The fluid has a thermal capacity of $C_p$. The pipe thermal resistance is $R_p$, and the pipe outer boundary temperature is $T_p(\tau)$. The heat flux $q_p(\tau)$ is transferred from the pipe outer surface to the grout. The thermal conductivity and the thermal diffusivity of the grout are $\lambda_g$ and $a_g$ respectively. The heat flux $q_b(\tau)$ is transferred across the borehole boundary to the surrounding ground (soil). The borehole outer boundary temperature is $T_b(\tau)$. The thermal conductivity and the thermal diffusivity of the ground (soil) are $\lambda_s$ and $a_s$ respectively.

## 4.2 New analytical solution

In the new analytical solution, a set of equations for the Laplace transforms of the boundary temperatures and heat-fluxes are obtained. These equations are represented by a thermal network. The use of the thermal network enables swift and precise evaluation of any thermal or physical setting of the borehole. Finally, very concise formulas of the inversion integrals are developed to obtain the time dependent solutions. Thermal capacities, thermal resistances and thermal properties of all the borehole elements are considered. More details and the mathematical formulation of the new analytical solution are given in the following sections.

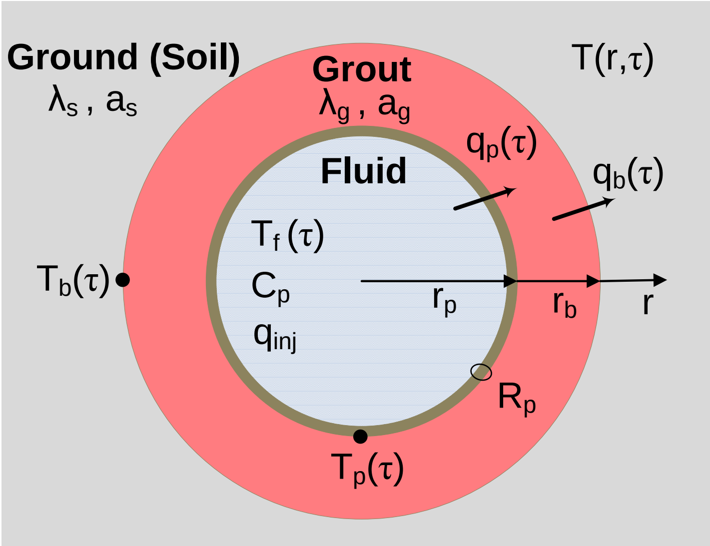


**Figure 4.1** The geometry and the thermal properties of the borehole.

### 4.2.1 Mathematical model

The heat transfer problem in a borehole with an equivalent-diameter pipe is shown in Figure 4.1. For this problem, the temperature distribution $T(r, \tau)$ must satisfy the following radial heat conduction equation both in the grout and the ground (soil) regions.

$$\frac{1}{a(r)} \cdot \frac{\partial T}{\partial \tau} = \frac{\partial^2 T}{\partial r^2} + \frac{1}{r} \cdot \frac{\partial T}{\partial r}, \qquad a(r) = \begin{cases} a_g, & r_p < r < r_b \\ a_s, & r > r_b \end{cases}. \tag{4.1}$$

The radial heat flux in the grout and the soil regions is:

$$q(r,\tau) = 2\pi r[-\lambda(r)] \cdot \frac{\partial T}{\partial r}, \qquad \lambda(r) = \begin{cases} \lambda_g, & r_p < r < r_b \\ \lambda_s, & r > r_b \end{cases}. \tag{4.2}$$

The heat flux at the grout-soil interface is continuous and hence the boundary condition from the Equation 4.2 at $r$=$r_b$ is:

$$\lambda_g \cdot \left.\frac{\partial T}{\partial r}\right|_{r=r_b-0} = \lambda_s \cdot \left.\frac{\partial T}{\partial r}\right|_{r=r_b+0}. \tag{4.3}$$

The pipe is filled with a heat transfer fluid at temperature $T_f(\tau)$. There is a thermal resistance $R_p$ over the pipe periphery between the fluid in the pipe to the grout just outside the pipe. This resistance accounts for the pipe wall and the fluid boundary layer. The heat flux over this thermal resistance is equal to the radial heat flux in the grout just outside the pipe. The boundary condition at the pipe-grout interface is then:

$$T_f(\tau) - T(r_p, \tau) = R_p \cdot q(r_p, \tau). \tag{4.4}$$

Here, the thermal resistance $R_p$ is defined as:

$$R_p = \frac{1}{K_p} = \frac{1}{2\,\pi \cdot \lambda_p} \cdot ln\left(\frac{r_{p,o}}{r_{p,i}}\right) + \frac{1}{2\,r_p \cdot h_p}. \qquad (4.5)$$

The first part of Equation 4.5 refers to the pipe conductive resistance and the second part refers to the fluid convective resistance.

The heat balance of the fluid in the pipe with the injected heat $q_{inj}$ is:

$$q_{inj} = C_p \cdot \frac{dT_f}{d\tau} + q\left(r_p, \tau\right). \qquad (4.6)$$

The initial temperatures in the pipe, the grout and the ground (soil) are all taken as zero.

$$T_f(0) = 0, \qquad T(r,0) = 0, \qquad r > r_p. \qquad (4.7)$$

### 4.2.2 Laplace transform for the pipe region

Taking Laplace transforms of Equations 4.4 and 4.6 give:

$$\bar{T}_f(s) - \bar{T}_p(s) = R_p \cdot \bar{q}_p(s) \qquad (4.8)$$

and

$$\frac{q_{inj}}{s} = C_p \cdot s \cdot \left[\bar{T}_f(s) - 0\right] + \bar{q}_p(s). \qquad (4.9)$$

Here, $\bar{T}_{\mathrm{p}}(s)$ and $\bar{q}_{\mathrm{p}}(s)$ are temperature and heat flux in the borehole at the pipe wall and $s$ is the complex-valued argument of the Laplace transform.

### 4.2.3 Laplace transform for the annular region

The Laplace transform of the radial heat equation for the annular region gives:

$$\frac{\partial^2 \bar{T}}{\partial r^2} + \frac{1}{r} \cdot \frac{\partial \bar{T}}{\partial r} = \frac{s}{a_g} \cdot \bar{T}(r,s) = \left(\sqrt{\frac{s}{a_g}}\right)^2 \cdot \bar{T}(r,s). \qquad (4.10)$$

We can scale $r$ with $\sqrt{(s/a_g)}$ together to have:

$$z = r\sqrt{\frac{s}{a_g}}\,, \qquad \bar{T}(r,s) = g(z). \qquad (4.11)$$

Now Equation 4.10 can be written as an ordinary differential equation as:

$$\frac{d^2 g}{dz^2} + \frac{1}{z} \cdot \frac{dg}{dz} - g(z) = 0. \qquad (4.12)$$

The solutions of Equation 4.12 are $I_0(z)$ and $K_0(z)$ which are modified Bessel functions of zero order[1]. Using these functions to get a general solution of Equation 4.10 gives:

$$\bar{T}(r,s) = A(s) \cdot I_0\left(r\sqrt{\frac{s}{a_g}}\right) + B(s) \cdot K_0\left(r\sqrt{\frac{s}{a_g}}\right), \quad r_p \le r \le r_b. \qquad (4.13)$$

Let us define:

$$\sigma_p = r_p\sqrt{\frac{s}{a_g}}, \qquad \sigma_b = r_b\sqrt{\frac{s}{a_g}}. \qquad (4.14)$$

Now Equation 4.13 can be written as the following two equations for the temperatures at the two boundaries (i.e. $r_p$ and $r_b$) of annular region,

$$\bar{T}_p(s) = A(s) \cdot I_0(\sigma_p) + B(s) \cdot K_0(\sigma_p) \qquad (4.15)$$

and

$$\bar{T}_b(s) = A(s) \cdot I_0(\sigma_b) + B(s) \cdot K_0(\sigma_b). \qquad (4.16)$$

Another set of equations can be obtained for the boundary fluxes by taking the Laplace transform of the radial heat flux (Equation 4.2) and inserting the Laplace transforms from Equation 4.13 and taking $r = r_p$ and $r = r_b$.

$$\bar{q}_p(s) = 2\pi \cdot \lambda_g \cdot \sigma_p\left[-A(s) \cdot I_1(\sigma_p) + B(s) \cdot K_1(\sigma_p)\right] \qquad (4.17)$$

and

$$\bar{q}_b(s) = 2\pi \cdot \lambda_g \cdot \sigma_b[-A(s) \cdot I_1(\sigma_b) + B(s) \cdot K_1(\sigma_b)]. \qquad (4.18)$$

$A(s)$ and $B(s)$ may be eliminated from Equations 4.15 to 4.18 and two equations between the Laplace transforms of the boundary temperatures and boundary fluxes are obtained. These equations may be written in the following way.

$$\bar{q}_p(s) = \bar{K}_p(s) \cdot \left(\bar{T}_p(s) - 0\right) + \bar{K}_t(s) \cdot \left(\bar{T}_p(s) - \bar{T}_b(s)\right) \qquad (4.19)$$

and

$$-\bar{q}_b(s) = \bar{K}_b(s) \cdot (\bar{T}_b(s) - 0) + \bar{K}_t(s) \cdot \left(\bar{T}_b(s) - \bar{T}_p(s)\right). \qquad (4.20)$$

Equations 4.19 and 4.20 can be represented in the form of a thermal network for the borehole annulus as shown in Figure 4.2.

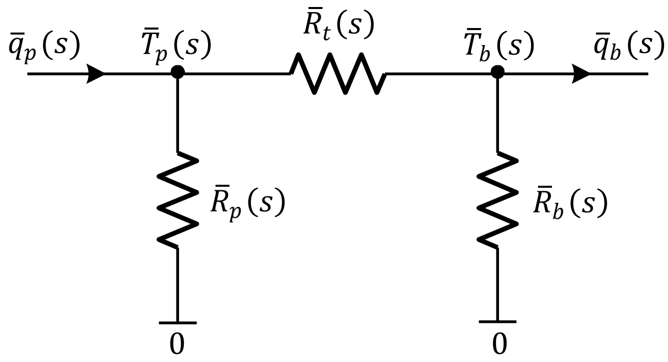


**Figure 4.2** Thermal network for the borehole annular region.

The values of one transmittive and two absorptive conductances (and their inverse, the resistances) used in Equations 4.19 and 4.20 and also in the thermal network for the annular region are:

$$\bar{K}_t(s) = \frac{1}{\bar{R}_t(s)} = \frac{2\pi\lambda_g}{K_0(\sigma_p)\cdot I_0(\sigma_b) - I_0(\sigma_p)\cdot K_0(\sigma_b)}, \tag{4.21}$$

$$\bar{K}_p(s) = \frac{1}{\bar{R}_p(s)} = \frac{\sigma_p\left[I_1(\sigma_p)\cdot K_0(\sigma_b) + K_1(\sigma_p)\cdot I_0(\sigma_b)\right] - 1}{\bar{R}_t(s)} \tag{4.22}$$

and

$$\bar{K}_b(s) = \frac{1}{\bar{R}_b(s)} = \frac{\sigma_b\left[I_1(\sigma_b)\cdot K_0(\sigma_p) + K_1(\sigma_b)\cdot I_0(\sigma_p)\right] - 1}{\bar{R}_t(s)}. \tag{4.23}$$

Further details and background of the Equations 4.19 to 4.23 can be found in the mathematical background report[19].

### 4.2.4 The soil region

For the soil region outside the borehole radius, there is a solution similar to the one given by Equation 4.13,

$$\bar{T}(r,s) = A(s)\cdot I_0\left(r\sqrt{\frac{s}{a_s}}\right) + B(s)\cdot K_0\left(r\sqrt{\frac{s}{a_s}}\right). \tag{4.24}$$

The function $I_0$ in Equation 4.24 increases exponentially with $r$ and is finite at $r = 0$. On the other hand the function $K_0$ decreases exponentially with $r$ and is infinite at $r = 0$. As the radius outside the borehole tends to infinity the value of coefficient $A(s)$ must be zero. This gives:

$$\bar{T}(r,s) = B(s)\cdot K_0\left(r\sqrt{\frac{s}{a_s}}\right), \qquad r \geq r_b. \tag{4.25}$$

The coefficient $B(s)$ can be eliminated if the temperature in the ground outside the borehole is expressed in the following form:

$$\bar{T}(r,s) = \frac{K_0\left(r\sqrt{\frac{s}{a_s}}\right)}{K_0\left(r_b\sqrt{\frac{s}{a_s}}\right)} \cdot \bar{T}_b(s). \tag{4.26}$$

For the soil region, we define:

$$\sigma_s = r_b\sqrt{\frac{s}{a_s}}. \tag{4.27}$$

Equation 4.26 can now be written as:

$$\bar{T}(r,s) = \frac{K_0\left(r\sqrt{\frac{s}{a_s}}\right)}{K_0(\sigma_s)} \cdot \bar{T}_b(s). \tag{4.28}$$

Taking the Laplace transform of radial heat flux (i.e. Equation 4.2) for the soil region (at $r = r_b$) and using Equations 4.3 and 4.28, we get:

$$\bar{q}_b(s) = 2\pi r_b(-\lambda_s) \cdot \frac{\sqrt{\frac{s}{a_s}} \cdot K_0'(\sigma_s)}{K_0(\sigma_s)} \cdot \bar{T}_b(s). \tag{4.29}$$

We get the following relations between the Laplace transforms of temperature and heat flux at boundary $r = r_b$.

$$\bar{T}_b(s) - 0 = \bar{R}_s(s) \cdot \bar{q}_b(s). \tag{4.30}$$

The following relation for the ground thermal resistance (and its inverse, the ground thermal conductance) is obtained from Equations 4.29 and 4.30.

$$\bar{R}_s(s) = \frac{1}{\bar{K}_s(s)} = \frac{1}{2\pi\lambda_s} \cdot \frac{K_0(\sigma_s)}{\rho_s \cdot K_1(\sigma_s)}. \tag{4.31}$$

### 4.2.5 The whole thermal network

The whole network (Figure 4.3) for the equivalent-diameter pipe, the circulating fluid, the borehole annulus region and the infinite ground outside the borehole can now be drawn using the Equations 4.8 and 4.9 for the pipe region, Equations 4.19 and 4.20 for the annular region and Equation 4.30 for the soil region.

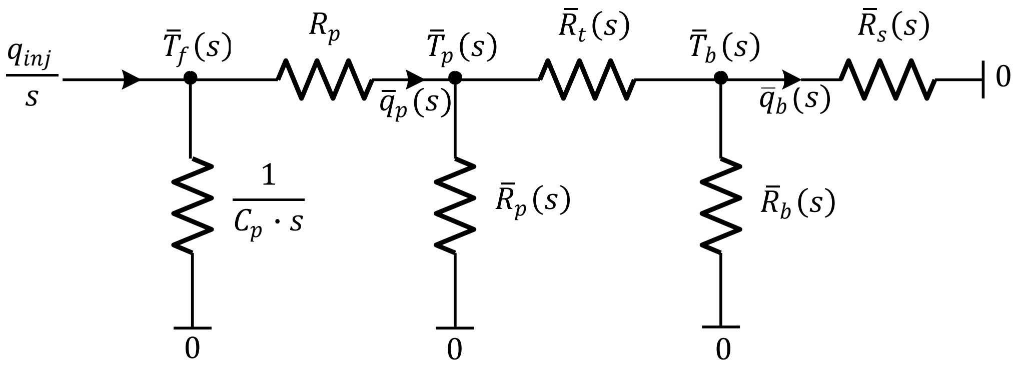


**Figure 4.3** The whole thermal network for a borehole in ground.

The Laplace transform for the fluid temperature can be readily obtained from the thermal network.

$$\bar{T}_f(s) = \frac{q_{inj}}{s} \cdot \cfrac{1}{C_p \cdot s + \cfrac{1}{R_p + \cfrac{1}{\bar{K}_p(s) + \cfrac{1}{\bar{R}_t(s) + \cfrac{1}{\bar{K}_b(s) + \bar{K}_s(s)}}}}}. \tag{4.32}$$

The network involves a sequence of composite resistances. We start from the right in Figure 4.3. The conductances $\bar{K}_b(s)$ and $\bar{K}_s(s)$ lie in parallel and are added. The inverse of this composite conductance is added to the resistance $\bar{R}_t(s)$. This composite resistance lies in parallel with $\bar{R}_p(s) = 1/\bar{K}_p(s)$ and their inverses are added. This composite resistance lies in series with the resistance of the pipe wall $R_p$. The total composite resistance from $R_p$ and rightwards lies in parallel with the thermal conductance $C_p \cdot s$.

### 4.2.6 Fluid temperature

In the type of problems considered here, the inversion formula to get $f(\tau)$ from $\bar{f}(s)$ is given by integral:

$$f(\tau) = \frac{2}{\pi} \cdot \int_0^\infty \frac{1 - e^{-u^2 \cdot \frac{\tau}{\tau_0}}}{u} \cdot L(u) du. \tag{4.33}$$

The function $L(u)$ in the above equations is given by:

$$L(u) = Im\left[-s \cdot \bar{f}(s)\right]_\Gamma, \qquad \Gamma: \ \tau_0 \cdot s = -u^2 + i \cdot 0,$$
$$\sqrt{\tau_0 \cdot s} = i \cdot u, \qquad 0 < u < \infty. \tag{4.34}$$

Here, $\tau_0$ (in seconds) is an arbitrary time constant, and $Im[...]$ denotes the imaginary part. The first factor in the integral depends on the dimensionless time $\tau/\tau_0$, and it is independent of the particular Laplace transform $\bar{f}(s)$. The second factor, the function $L(u)$, is independent of $\tau$ and represents the particular Laplace transform for the considered case.

The inversion integral in the Equation 4.33 is obtained by considering a closed loop in the complex $s$-plane, as indicated in Figure 4.4. The original integral along the vertical line $\Gamma_0$ is replaced by an integral along the negative real axis $\Gamma$. The following conditions have to be fulfilled:

$$f(0) = 0, \qquad \frac{df}{d\tau} \to 0, \qquad \tau \to \infty. \tag{4.35}$$

There is a pole at $s = 0$ and a cut in the complex s-plane along the negative real axis to account for $\sqrt{s}$. A final requirement, which is fulfilled in our applications, is that there must not be any other poles.

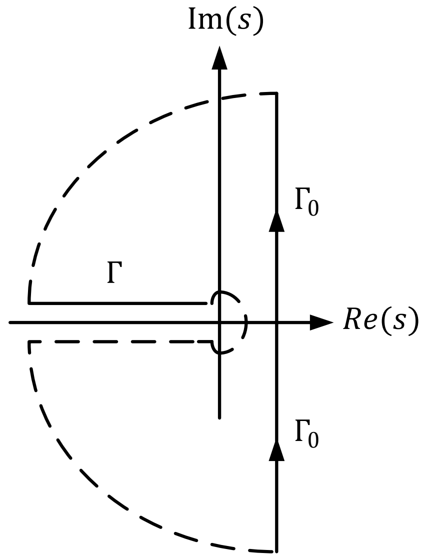


**Figure 4.4** Considered closed path for the inversion integral to get Equations 4.33 and 4.34.

Using Equation 4.33, we can now write the fluid temperature $T_f(\tau)$ as:

$$T_f(\tau) = \frac{2}{\pi} \cdot \int_0^\infty \frac{1 - e^{-u^2 \cdot \frac{\tau}{\tau_0}}}{u} \cdot L(u) du \,. \tag{4.36}$$

The Laplace transform for the fluid temperature is given by Equation 4.32. When taken for $s$ on the negative real axis $\Gamma$, we get:

$$L(u) = \mathrm{Im} \frac{-q_{inj}}{C_p \cdot \frac{-u^2}{\tau_0} + \cfrac{1}{R_p + \cfrac{1}{\bar{K}_p(u) + \cfrac{1}{\bar{R}_t(u) + \cfrac{1}{\bar{K}_b(u) + \bar{K}_s(u)}}}}} \,. \tag{4.37}$$

The four thermal resistances (and the corresponding conductances) for the Laplace transforms, are given by Equations 4.21 to 4.23 and Equation 4.31. On the negative real axis $\Gamma$, these become functions of the real variable $u$. From Equations 4.14, 4.27 and 4.34, we get:

$$\sigma_p = i \cdot p_p \cdot u, \qquad \sigma_b = i \cdot p_b \cdot u, \qquad \sigma_s = i \cdot p_s \cdot u \,, \tag{4.38}$$

and

$$p_p = \frac{r_p}{\sqrt{a_g \cdot \tau_0}}, \qquad p_b = \frac{r_b}{\sqrt{a_g \cdot \tau_0}}, \qquad p_s = \frac{r_b}{\sqrt{a_s \cdot \tau_0}} \,. \tag{4.39}$$

The arguments in the formulas for the resistances are now imaginary numbers. In this case, the modified Bessel functions may be expressed as ordinary Bessel functions. The final formulas for the thermal resistances taken on the negative real axis $\Gamma$ become:

$$\bar{R}_s(u) = \frac{1}{2\pi\lambda_s} \cdot \frac{J_0(p_s u) - i \cdot Y_0(p_s u)}{p_s u \cdot [J_1(p_s u) - i \cdot Y_1(p_s u)]}, \qquad 0 < u < \infty \tag{4.40}$$

$$\bar{R}_t(u) = \frac{J_0(p_p u) \cdot Y_0(p_b u) - Y_0(p_p u) \cdot J_0(p_b u)}{4\lambda_g}, \tag{4.41}$$

$$\bar{R}_p(u) = \frac{\bar{R}_t(u)}{0.5\,\pi\, p_p u \cdot \left[J_1(p_p u)\, Y_0(p_b u) - Y_1(p_p u)\, J_0(p_b u)\right] - 1} \tag{4.42}$$

and

$$\bar{R}_b(u) = \frac{\bar{R}_t(u)}{0.5\,\pi\, p_b u \cdot \left[J_1(p_b u)\, Y_0(p_p u) - Y_1(p_b u)\, J_0(p_p u)\right] - 1}. \tag{4.43}$$

Further details of the equations of this section can be found in the mathematical background report[19].

## 4.3 New numerical solution

The radial heat equation in its general form is:

$$\rho(r) \cdot c(r) \cdot \frac{\partial T}{\partial \tau} = \frac{1}{r} \cdot \frac{\partial}{\partial r}\left[r \cdot \lambda(r) \cdot \frac{\partial T}{\partial r}\right], \quad r \geq r_p. \tag{4.44}$$

The heat equation can also be rewritten as:

$$\begin{gathered} \rho \cdot c \cdot 2\pi \cdot r \cdot \frac{\partial T}{\partial \tau} = -\frac{\partial q}{\partial r}, \qquad r \geq r_p. \\ q(r,\tau) = -2\pi \cdot r \cdot \lambda \cdot \frac{\partial T}{\partial r}. \end{gathered} \tag{4.45}$$

The transient heat conduction for variable thermal conductivity *λ(r)* may be simplified by using the steady-state thermal resistance of an annular region as a new coordinate *u*:

$$\begin{gathered} u(r) = \int_{r_p}^{r} \frac{\lambda_g}{\lambda(r') \cdot r'}\, dr', \\ u(r_p) = 0, \qquad u_b = u(r_b) = ln\left(\frac{r_b}{r_p}\right). \end{gathered} \tag{4.46}$$

With the new coordinate, the heat equation behaves as a case with constant thermal conductivity.

$$q(r,\tau) = 2\pi \cdot r[-\lambda(r)] \cdot \frac{\partial T}{\partial u} \cdot \frac{du}{dr} = -2\pi \cdot \lambda_g \cdot \frac{\partial T}{\partial u}. \qquad (4.47)$$

The heat equation for $T(u,\tau)$ becomes:

$$\rho(r) \cdot c(r) \cdot 2\pi \cdot r \cdot \frac{\partial T}{\partial \tau} = 2\pi \cdot \lambda_g \cdot \frac{\partial^2 T}{\partial u^2}, \qquad r = r(u). \qquad (4.48)$$

The radius as function of $u$ becomes:

$$r(u) = \begin{cases} r_p \cdot \exp(\mathrm{u}), & 0 \le u \le u_b \\ \mathrm{r_b} \cdot \exp[(\mathrm{u} - \mathrm{u_b}) \cdot \lambda_s/\lambda_g], & u \ge u_b \end{cases}. \qquad (4.49)$$

The borehole region and the soil outside the borehole are divided into $N_b$ and $N_s$ cells, respectively. The total number of cells is $N = N_b + N_s$. A constant cell width $\Delta u$ and a time step of $\Delta\tau$ are used.

$$\Delta u = \frac{u_b}{N_b}, \qquad N_s = 1 + int\left[\frac{\lambda_s}{\Delta u \cdot \lambda_g} \cdot ln\left(\frac{\sqrt{p_{max} \cdot 4 a_s \tau_{max}}}{r_b}\right)\right]. \qquad (4.50)$$

Here, $\tau_{max}$ is the end time for the computations, and *int[...]* denotes the integer part. The number $N_s$ is chosen so that the heat flux at the outer boundary is negligible for $\tau \le \tau_{max}$. The particular expression is obtained from the line source solution in soil. The criterion is that the heat flux at the outer boundary is smaller than $(e^{-p_{max}} \cdot q_{inj})$ up to the maximum time $\tau_{max}$. The choice $p_{max}=4$ should be sufficient $(e^{-4}=0.02)$.

Figure 4.5 shows the notations that are used. The temperature at the midpoint of cell $n$ at time step $v$ is $T_{n,v}$ and the heat flux from cell $n$ to $n+1$ is $q_{n,v}$. The initial temperatures for $v = 0$ are zero: $T_{n,0} = 0, n = 0, 1, 2, \ldots N$.

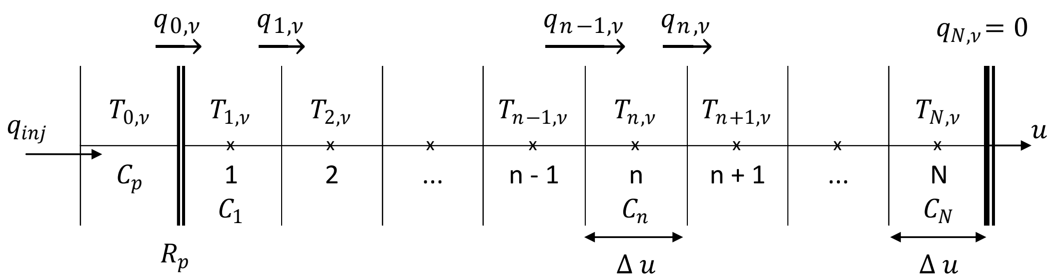


**Figure 4.5** Notations for the numerical solution.

The heat fluxes are given by:

$$q_{0,\nu} = K_0 \cdot \left(T_{0,\nu} - T_{1,\nu}\right), \qquad q_{N,\nu} = 0,$$
$$q_{n,\nu} = K_u \cdot \left(T_{n,\nu} - T_{n+1,\nu}\right), \qquad n = 1, 2, \dots, N-1. \tag{4.51}$$

The temperatures at the new time step, $\tau = (\nu + 1) \cdot \Delta\tau$, are given by:

$$T_{0,\nu+1} = T_{0,\nu} + \frac{q_{inj} - q_{0,\nu}}{C_p} \cdot \Delta\tau,$$
$$T_{n,\nu+1} = T_{n,\nu} + \frac{q_{n-1,\nu} - q_{n,\nu}}{C_n} \cdot \Delta\tau, \qquad n = 1, 2, \dots, N. \tag{4.52}$$

The above set of Equations 4.51 – 4.52 gives the iterative numerical calculation procedure. The conductances $K_0$ and $K_u$, the heat capacities $C_n$ of all cells and the time step $\Delta\tau$ must be specified. The thermal conductances are:

$$K_0 = \frac{1}{R_p + 0.5\,\Delta u\,/(2\pi \cdot \lambda_g)}, \qquad K_u = \frac{2\pi \cdot \lambda_g}{\Delta u}. \tag{4.53}$$

The heat capacity of cell $n$ is equal to the area of the annular cell times the volumetric heat capacity:

$$C_n = \pi\{[r(n \cdot \Delta u)]^2 - [r(n \cdot \Delta u - \Delta u]^2\} \cdot \begin{cases} \rho_g c_g & n = 1, \dots, N_b \\ \rho_s c_s & n = N_b + 1, \dots N \end{cases} \tag{4.54}$$

To ensure numerical stability, the time step must satisfy the inequalities:

$$\Delta t \leq min\left(\frac{C_{min}}{2K_u}, \frac{C_p}{K_0}\right), \qquad C_{min} = \underbrace{min}_{1 \leq n \leq N}(C_n) \tag{4.55}$$

Further details of the equations of this section can be found in the mathematical background report[19].

## 4.4 Testing and validation of new solutions

The new solutions were tested under various conditions and validated using different approaches. The first approach was the comparison of the results from the analytical and the numerical solutions. Next, the new solutions were compared to a semi-analytical solution by Beier and Smith[9]. The reasons for comparison with this particular solution are discussed in Section 4.4.2. Finally, the solutions were validated using experimental results from a medium-scale laboratory setup which simulates the physical and the thermal characteristics of a borehole in controlled laboratory conditions.

### 4.4.1 Validation by inter-model comparison of analytical and numerical solutions

A series of simulations were done to compare the new analytical and the numerical solutions. Such comparisons showed that the new solutions agree to an accuracy of higher than 0.01 K for all the simulated cases. As an illustration, the results from one of the comparisons using typical conditions are presented here. For the comparison, a heat injection rate of 50 W/m to an equivalent diameter pipe of radius 17.7 mm was considered. The considered thermal properties for the fluid-pipe, grout and soil regions are given in Table 4.1.

**Table 4.1** Thermal properties of the fluid, grout and soil considered for the comparison of the new models.

| Element | Fluid + Pipe | Grout | Soil |
|---|---|---|---|
| Thermal conductivity (W/(m·K)) | 0.47 (pipe) | 1.5 | 3.0 |
| Heat capacity (J/(kg·K)) | 4182 (fluid) | 2000 | 2500 |
| Density (kg/m$^3$) | 1000 (fluid) | 1550 | 750 |

Under these conditions, the increase in the fluid temperatures for the first 100 hours as predicted by the analytical and the numerical methods is shown in Figure 4.6. The difference in the predicted temperatures is remarkably small. It can be observed from Figure 4.7 that the difference in fluid temperatures predicted by two very different approaches lies between 0.002 and 0.004 K under the specified conditions.

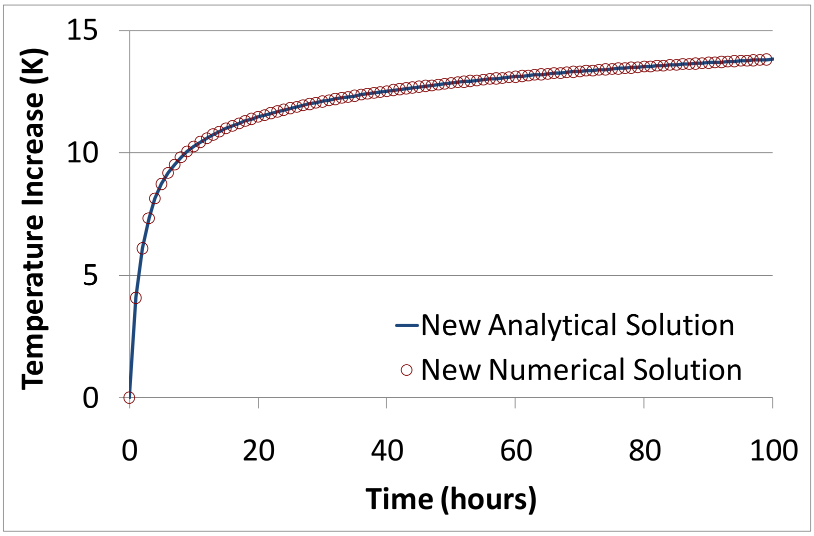


**Figure 4.6** Fluid temperature predicted by new analytical and numerical solutions for a test simulation.

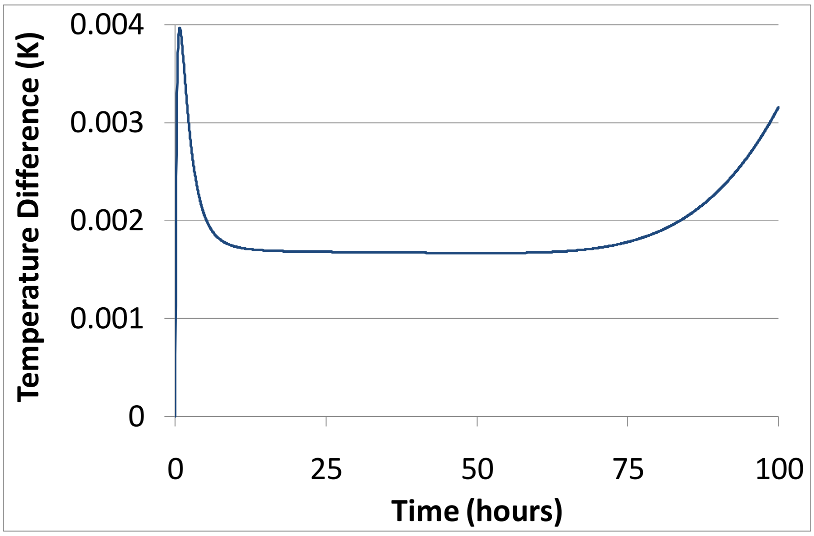


**Figure 4.7** Difference in fluid temperature predicted from the new solutions.

### 4.4.2 Validation against a semi-analytical model

Beier and Smith[9] have also used the Laplace transformation approach to develop their 'Composite model'. However, there are two fundamental differences between their model and the new analytical solution. First, that Beier and Smith used a numerical inversion algorithm[60] to invert the Laplace transforms in the real time. Using numerical methods for the inversion of the Laplace transforms complicates the solution and makes its implementation in building energy simulation software increasingly difficult. The second issue with the Composite model is that it assumes the fluid temperature to be the same as the pipe boundary temperature. In other words, the solution does not account for the fluid and the pipe resistances (i.e. $R_p=0$). These can, however, be implicitly added by adjusting the radius of the equivalent diameter pipe accordingly or by adding the fluid temperature increase because of the pipe and fluid resistance to the predicted fluid temperatures.

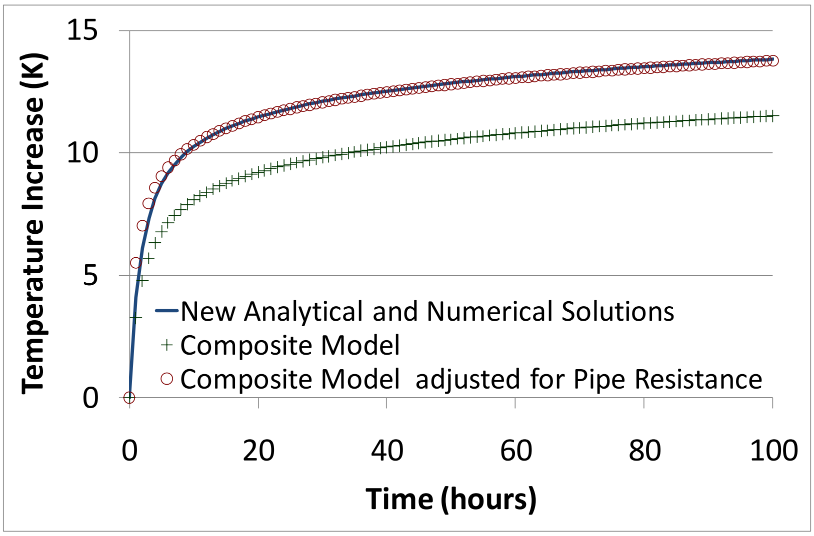


**Figure 4.8** Fluid temperatures from new solutions and the Composite model.

The comparison of the new analytical and numerical solutions with the Composite model, for the test case from the last section, is shown in Figure 4.8. As the fluid and the pipe resistances are ignored by the Composite model, the model under-predicts the increase in the fluid temperatures. However, the results from the Composite model become similar to the results from the analytical and numerical solutions if the effects of the pipe and the resistances are implicitly added (i.e. by adding $R_p \cdot q_{inj}$) to the predicted fluid temperatures.

### 4.4.3 Validation using experimental data

The new solutions have also been validated using data from a medium-scale laboratory setup. The setup is shown in Figure 4.9. The setup has been used by various Oklahoma State University researchers[5, 9, 65] to simulate and validate their models under controlled conditions. The setup consists of a wooden box of dimensions 1.8 m x 1.8 m x 18 m. An aluminium pipe of diameter 133 mm is centred along the length of the wooden box. The thermal resistance of the aluminium pipe is negligible. The aluminium pipe has a U-tube inserted in it. The U-tube is surrounded by bentonite-based grout and is kept centred in the aluminium pipe by means of spacers. The wooden box is filled with homogeneous sand and the whole setup is hence called a sandbox.

**Figure 4.9** The sandbox setup used to validate the new solutions (Spitler[58]).

Thermal conductivity and the volumetric heat capacity values for the grout and the soil in the sandbox are measured independently. These independently measured values, which have been used as input parameters to the new solutions, are given in Table 4.2.

**Table 4.2** Independently measured thermal properties of the sandbox elements.

| Element | Grout | Soil |
|---|---|---|
| Thermal conductivity (W/(m·K)) | 0.73 | 2.82 |
| Volumetric Heat Capacity (MJ/(m$^3$·K)) | 3.84 | 1.92 |

The comparison of the new analytical and numerical solutions with the experimental data from a sandbox test of 50 hours is shown in Figure 4.10. The length of the sandbox tests was kept to 50 hours to avoid any edge effects. As seen the results from the new solutions and the sandbox tests overlap each other. The difference between the temperatures predicted by the new solutions and the experimentally measured temperature is shown in Figure 4.11. The maximum absolute difference between the predicted and the measured temperatures is around 0.2 K while the average absolute difference between the two data sets is less than 0.1 K.

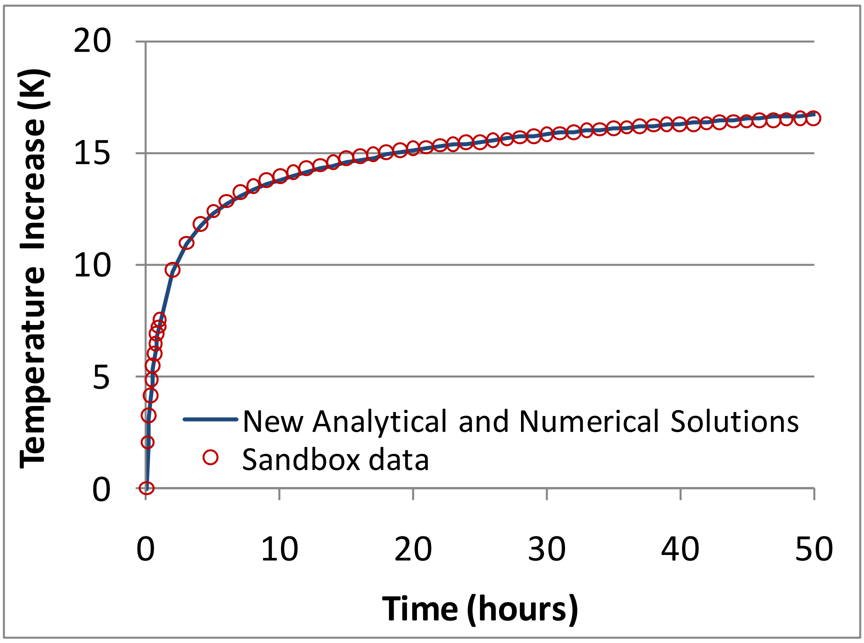


**Figure 4.10** Comparison of fluid temperatures from the new solutions and the experimental data from sandbox setup.

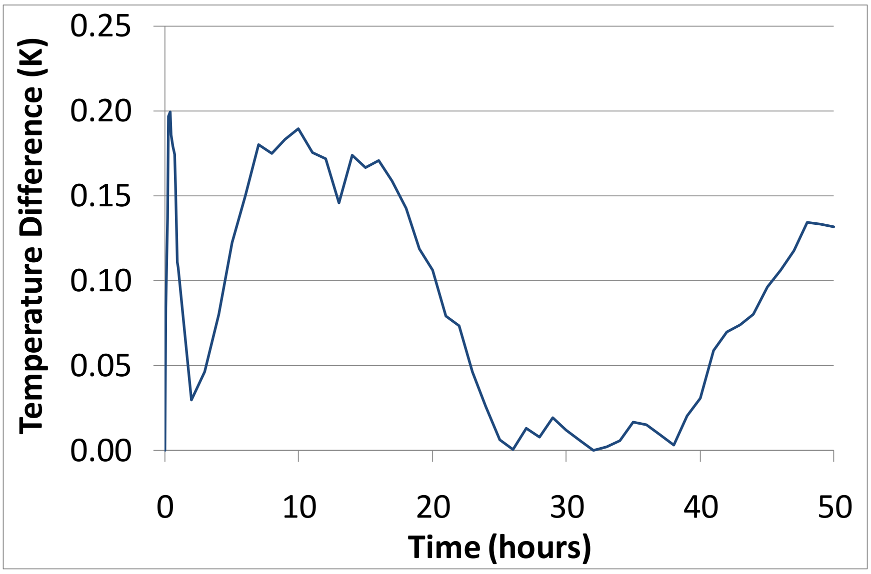


**Figure 4.11** Difference in fluid temperature from the new solutions and the experimental data.

## 4.5 Conclusions

New analytical and numerical solutions were developed to address the shortcomings of the existing solutions. The new models were tested and validated using different approaches. The comparison of the two solutions showed that the results from the new solutions agree to an accuracy of higher than 0.01 K. The results from the new solutions were also consistent with the results from a state-of-the art semi-analytical method adjusted for pipe and fluid resistances. Finally, the fluid temperature predicted by the new solutions also agreed with experimental results. A maximum difference of 0.2 K was observed between the simulated and the experimental results.

# 5 New ground source heat pump test facility

A new heating, ventilation and air-conditioning laboratory[25] has been established at Building Services Engineering at Chalmers University of Technology, Sweden. The new laboratory provides test facilities for experimental studies of various heating, ventilation and air-conditioning systems including borehole thermal energy storage and heat pump systems. The test facility can be used to test the operation and control strategies, to develop and validate models for ground source heat pump systems and to conduct thermal response tests. This chapter reports on the design and development of the laboratory's ground storage and heat pump system and its planned operation.

## 5.1 Introduction

The new test facility was developed with an aim to conduct experimental studies on system solutions of various Heating, Ventilation and Air-Conditioning (HVAC) systems including space conditioning, integrated control-on-demand and optimized control of HVAC systems. An integral part of the laboratory's HVAC system is its Ground Source Heat Pump (GSHP) system, which was primarily developed to study the performance of a wide range of GSHP system configurations. The GSHP test facility consists of a Borehole Thermal Energy Storage system (BTES), heat pumps, thermal storage tanks and multiple heat exchangers. The test facility can be used, among other things, to develop, test and optimize control strategies for different GSHP system configurations, to develop and validate component and system models and to perform Thermal Response Tests (TRTs) under different experimental conditions. The following sections describe the design and development and the planned operation of the test facility.

## 5.2 Design and development

The GSHP system consists of a BTES, made up of nine boreholes, connected to three water-to-water heat pumps. The boreholes are drilled in a 3x3 rectangular configuration. All the boreholes are groundwater filled and have single U-tubes as ground loop heat exchangers. The distance between adjacent boreholes is around 4 m and each borehole has an active depth of around 80 meters. The inclination of all nine boreholes in the ground has been measured and the horizontal deviation between the two ends of the boreholes varies between 1.7 to 7.2 meters. Additional details of the borehole field and its elements are given in Table 5.1. The layout and the geometry of the borehole system are further illustrated in Figures 5.1 and 5.2.

All nine boreholes have dedicated variable speed pumps and flow control valves to monitor and control the flow of process cooling agent (i.e. brine) in individual boreholes. Process cooling agent exiting the borehole system is stored and distributed through the accumulator tank AT1 (Figure 5.3). From AT1, process cooling agent can either be supplied to the evaporator of heat pump HP1 or directly pumped to the heat exchanger HX1 to provide free cooling. The effects of long-term heat injections or heat extractions on the boreholes can be minimized by balancing borehole loads or by recharging the boreholes using direct heat transfer between the process cooling agent and the ambient air by means of dry cooler DC1.

**Table 5.1** Details of the borehole system.

| Element | Specification |
|---|---|
| Borehole field | |
| Configuration | 3 x 3, Rectangular |
| Total borehole depth | ~ 80 m |
| Sand layer depth | ~ 18 m |
| Borehole spacing | ~ 4 m |
| Borehole diameter | 110 mm |
| Borehole filling material | Ground water |
| U-tube | |
| Pipe type | PEM PN8 DN40 |
| Outer diameter | 40 mm |
| Thickness | 2.3 mm |
| Thermal conductivity | 0.42 W/(m·K) |
| Shank spacing | Not controlled |
| Circulating fluid | |
| Type | Ethanol (29.5 %) |
| Thermal conductivity | 0.401 W/(m·K) |
| Freezing point | -20 °C |
| Specific heat capacity | 4180 J/(kg·K) |

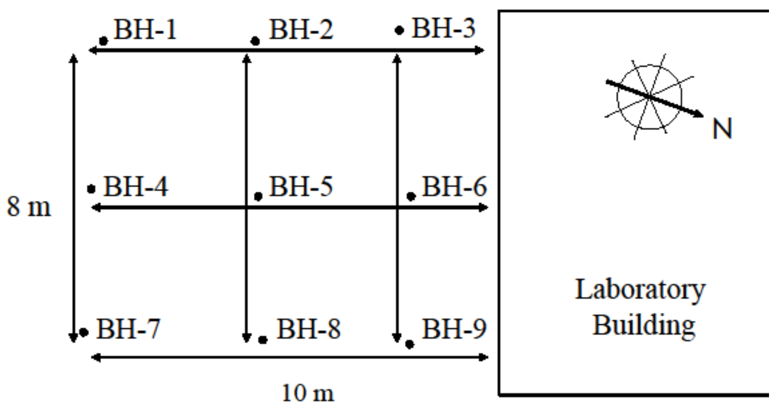


**Figure 5.1** Layout of the borehole system.

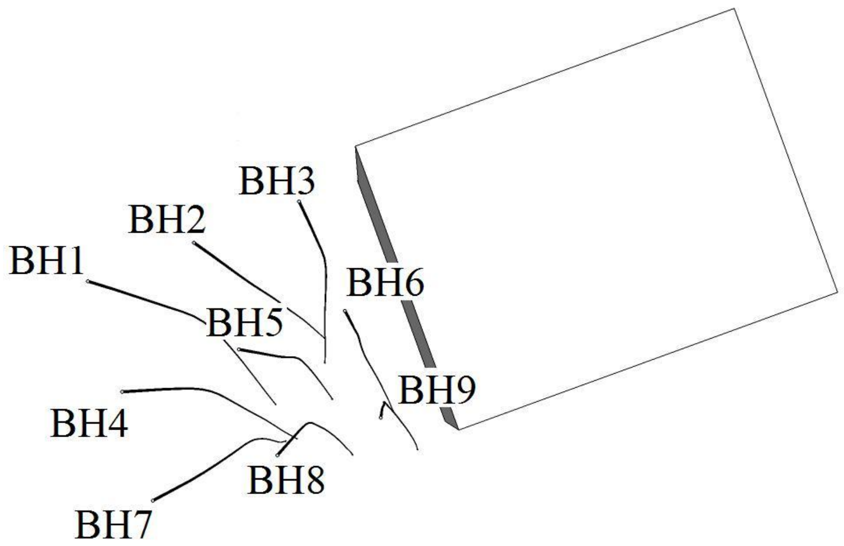


**(a)**

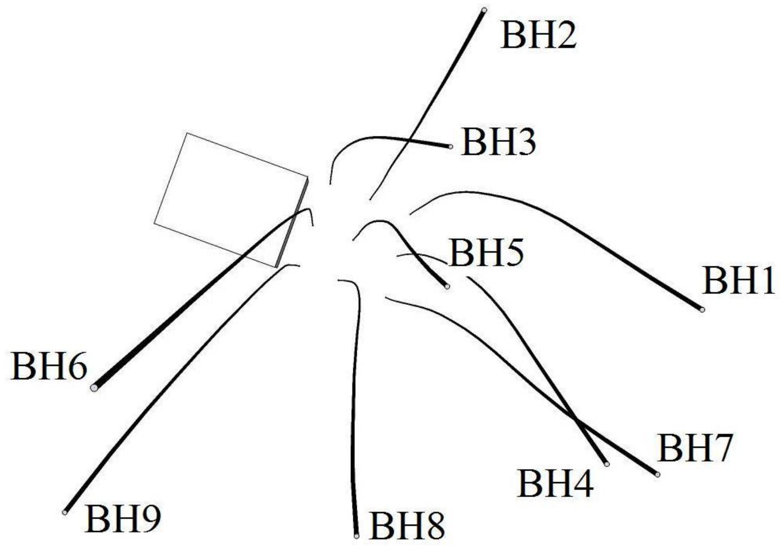


**(b)**

**Figure 5.2** The geometry of the borehole system: a) Top view b) Bottom view

(Note: The views show substantial deviation from the vertical of individual boreholes.)

The accumulator tank AT2 stores low temperature water (5-15 °C). This water may be cooled directly by heat pumps HP2 and HP3 (Figure 5.4) or indirectly by the ground storage or by outdoor air (DC1) via heat exchanger HX1. AT2 is also used to cool the condenser of heat pump HP1. The low temperature water is used for various laboratory operations. It is supplied to the air handling unit to produce cooling in summer, it is pumped to heat pump HP2 and HP3 evaporators as a low temperature heat source to produce heating and it is used in other laboratory operations requiring process cooling. The HW1 hot water (20-55 °C) produced by HP2 and HP3 can either be directly supplied for heating and process heating applications or can be stored in accumulator tanks AT3 and AT4 (Figure 5.5) and used when required. In case of additional heating requirements or high-temperature water demand, HW2 hot water (20-80 °C) produced by the EP1 electric storage water heater (Figure 5.5) and stored in accumulator tank AT5 can be utilized. Any excess heat in the hot water storage system can be rejected to ambient air using heat exchanger HX2 and dry cooler DC2.

A state-of-the-art building management system has been installed to monitor and control the test facility and for data acquisition and storage. Temperature measurements in the system are made at the inlet and outlet of all the installed components using electronic immersion temperature transmitters. Flow measurements in the system are taken for all the flow circuits using vortex flow meters. Electric power measurements in the system are made for all major components by means of meters that also provide the possibility of waveform analysis. Ambient air temperature and indoor air temperature are measured at multiple locations using electronic temperature transmitters.

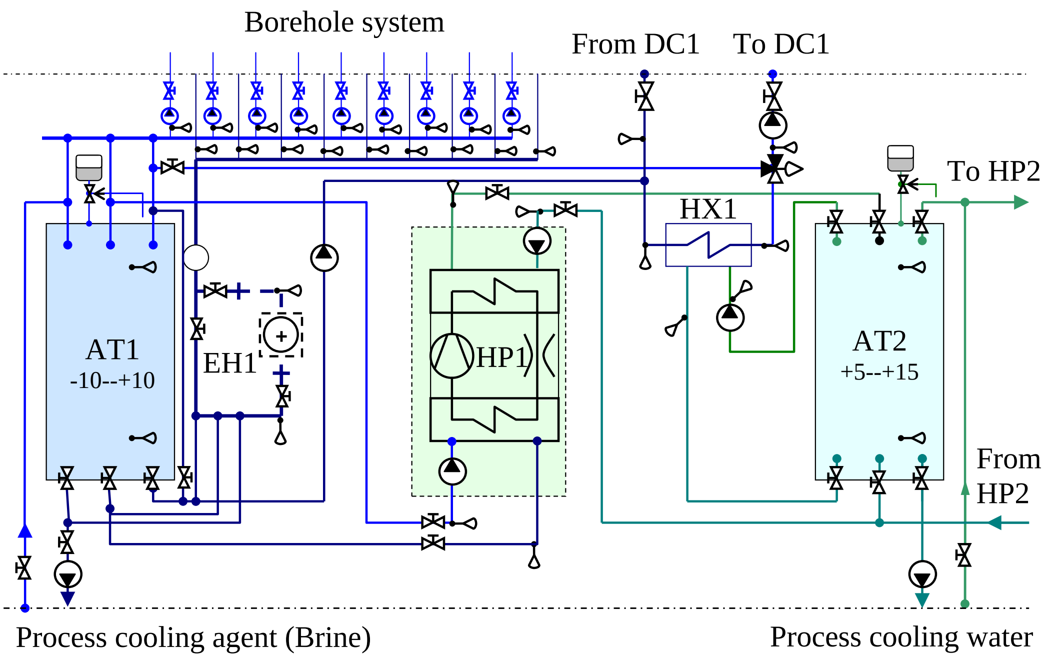


**Figure 5.3** Process cooling agent and process cooling water system (Fahlén[25]).

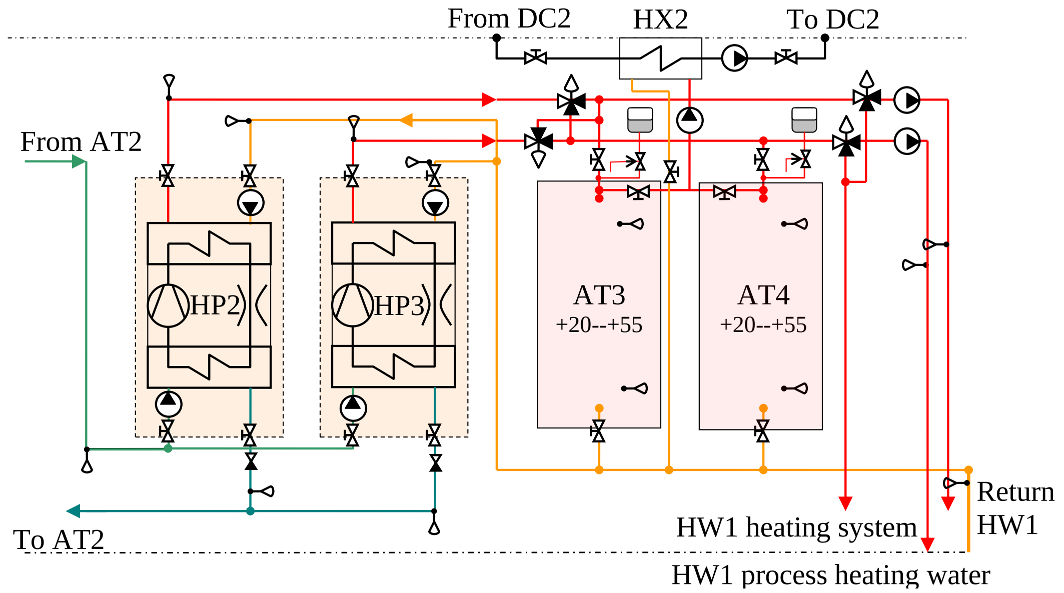


**Figure 5.4** The HW1 heating and process heating system (Fahlén[25]).

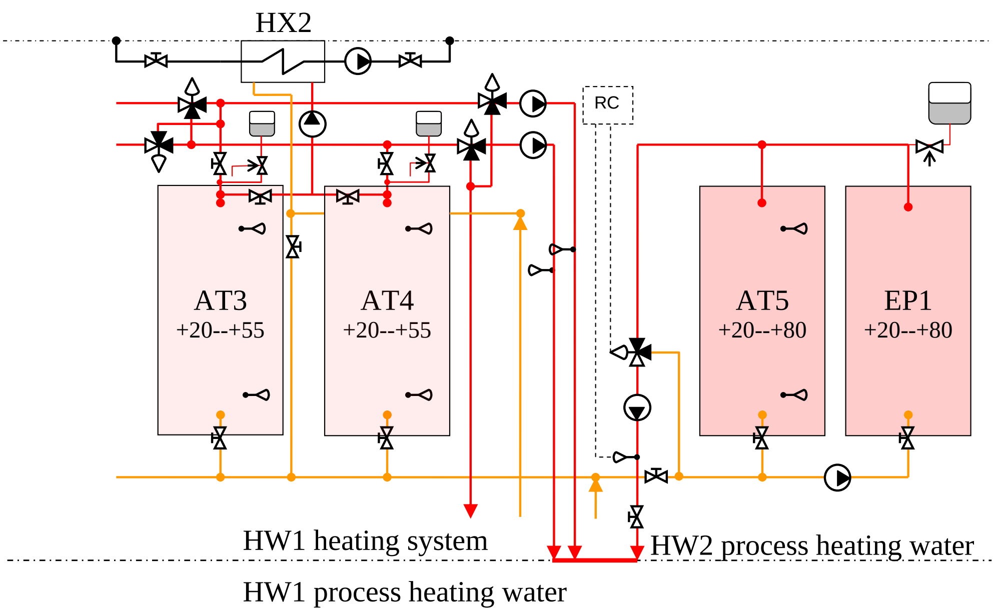


**Figure 5.5** The HW1 and HW2 process heating system (Fahlén[25]).

## 5.3 Planned operation

The test facility can be used to investigate the effects of various control strategies on the operation and performance of GSHP systems. Traditionally, controlling the heat pump entering fluid temperature has been the most common control strategy as a higher condenser inlet fluid temperature in winter and a lower evaporator inlet fluid temperature in summer increase the heat transfer and positively influences the performance of the heat pump. However, as discussed earlier, requirements for heating and cooling in buildings have changed considerably in recent years. The changes in the heating and cooling demands require new control strategies that need to be investigated and adapted to optimize the performance and operation of GSHP systems. Such strategies may be based on actual and predicted system loads, forecasted and historical energy use etc.

The new test facility will be used to study existing and new control strategies for different configurations of GSHP systems. The flexible design of the test facility permits components to be included or excluded from the system as per test requirements. The GSHP system to be investigated can be designed using various configurations of the borehole system, heat pumps, accumulator tanks and supplementary heat exchangers. Depending on the application, the borehole system can be used in heat storage or heat dissipation modes. When used in the rectangular configuration, the borehole system acts as a heat storage system to store thermal energy in the ground at a time of energy surplus for extraction later. When used in a line, a U or an open rectangular configuration, the borehole system acts as a heat dissipation system. Any number or configurations of boreholes can be chosen for a particular test. Dry cooler DC1 can be used to moderate borehole system temperature but it can also be used as a stand-alone alternative for free cooling during periods of low outdoor temperature.

The size and the thermal capacity of the system can be altered as it is possible to use either of heat pumps HP2 and HP3 with either of the accumulator tanks AT3 and AT4. Alternatively, it is also possible to operate HP2 and HP3 together with either or both of AT3 and AT4. Dry cooler DC2 can be used to reject any excess heat present in the hot water storage systems. Electric resistance heaters installed in all the accumulator tanks and electric storage water heater EP1 can be utilized to provide additional heating or to meet high-temperature water requirements. All of these possibilities allow a wide range of GSHP system configurations with flexible levels of temperature, thermal loads and thermal mass in the system. The test facility will be used to investigate control strategies for different GSHP system designs and to study the effects of system design on the operation and the performance of the GSHP system.

The test facility will also be used to develop new component and system models, to experimentally validate existing and new models and to conduct experimental studies. At a component level, models for the borehole system, heat pumps, storage tanks and auxiliary equipment can be developed, tested and validated. At the system level, investigations regarding operation, control and optimization of simple and hybrid GSHP systems can be carried out. The test facility can be used to test borehole system models both for heat storage and heat dissipation modes. Investigations regarding short-term borehole response, long-term borehole performance deterioration and thermal interaction between boreholes are of particular interest.

Other examples of possible experimental investigations, which can be conducted using the test facility, include studying the differences between the thermal response of peripheral and central boreholes, attainable free cooling in relation to ground heat injection and the trade-off between heat pump and the circulation pump energy consumption in free cooling modes. The laboratory system makes possible the testing of both brine-to-water and the water-to-water heat pump systems. Simultaneous testing of heat pumps at similar or different temperature levels is also possible using the test facility.

Another feature of the test facility is its flexibility in conducting TRTs. The laboratory borehole system provides a unique opportunity to study ground thermal properties such as undisturbed ground temperature, ground thermal conductivity and borehole thermal resistance of nine boreholes in close proximity. Such investigations have rarely been conducted on an academic level in controlled laboratory conditions. Issues like repeatability and reproducibility of TRTs can be comprehensively studied using various alternative approaches. The installed electric resistance heater EH1 (Figure 5.3) can be used to conduct the thermal response testing in the heat injection mode. It is also possible to conduct TRTs in heat extraction mode using heat pump HP1. Another possibility is to conduct TRTs using process cooling agent at constant input temperature to the boreholes.

When conducting a TRT, the process cooling agent accumulator tank, AT1, can either be included or excluded from the flow circuit. The storage tank is bypassed if the conventional constant heating flux approach is used for the thermal response testing. Alternatively, the storage tank is included in the flow circuit and is used to provide process cooling agent at a constant input temperature to the borehole for a constant heating temperature approach. The installation of nine variable speed pumps, one for each borehole, and an adjustable electric heater for heat input allow investigations regarding effects of different flow and heat injection rates when conducting TRTs. The results from TRTs of the laboratory borehole field can be used to simulate the long-term response of the individual boreholes. The differences between the long-term responses of the different boreholes can then be used to underline the uncertainties related to the borehole system design process.

## 5.4 Additional testing facilities

In addition to the GSHP system, the laboratory building houses a conference room and two test rooms for specific test applications. The first test room is designed as a ‘clean room’ with stainless steel interior and a dedicated air conditioning system. This test room is used to perform experiments which require precisely controlled temperature and air quality. It can also be used to test components like sensors and air cleaners and to study emissions from different materials. The second test room is made of clear glass and has a dedicated ventilation system. Special filming equipment has been installed to study the room-air and ventilation-air movement under specific conditions, e.g. that of an operating theatre etc.

The conference room was purpose built to investigate issues related to thermal climate and indoor air quality, lighting and noise, the control and positioning of room sensors and the operation and control of decentralized pumps and fans etc. The temperature in the room can be maintained using supply air from the centralized air handling unit or by using radiators, fan coil units, or under-floor heating and cooling as alternate systems. Supply and exhaust air flow rates, indoor air quality and noise levels in the conference room can all be precisely monitored and controlled. The use of four sets of supply and return ducts to the conference room also permits the division of the room into four cell-type offices to study the effects of indoor climate on the performance and behaviour of people.

## 5.5 Conclusions

The division of Building Services Engineering has designed and commissioned a ground source heat pump laboratory. The laboratory setup includes a nine borehole thermal energy storage system, three heat pumps, five accumulator and storage tanks, two dry coolers and several additional auxiliary components. The laboratory offers facilities to test different ground source heat pump system configurations in controlled laboratory conditions. The laboratory will be used to test operation and control strategies for ground source heat pump systems, to develop and validate system and component models and to conduct thermal response tests.

# 6 Thermal response tests

Accurate knowledge of ground thermal properties including undisturbed ground temperature, ground thermal conductivity and the borehole thermal resistance is required to design ground source heat pump and underground heat storage systems. These properties directly influence the required size of the borehole field and the depth of the individual boreholes, and consequently affect the economic feasibility of the applications using borehole heat exchangers. The ground thermal properties are often determined from an in-situ thermal response test of a pilot borehole. Although conducting such a test for a single pilot borehole has become a standard practice, both among academic researchers and practitioners, the issue of test accuracy has received little attention. Some researchers have looked at uncertainty analyses and comparisons to laboratory-scale studies. Another approach, examined in this chapter, is to examine the reproducibility of results for a group of nearby test boreholes at different times of the year.

This chapter first report on the results of thermal response tests conducted in controlled laboratory conditions for the borehole system of the newly built laboratory described in Chapter 5. The borehole system consists of nine groundwater filled boreholes, each about 80 m deep. The ground thermal properties including the undisturbed ground temperature, the ground thermal conductivity and the borehole thermal resistance are determined for all nine boreholes using standard evaluation methods. Comparison of the results of the ground thermal properties of the nine boreholes provides meaningful insight to the reproducibility issue of the thermal response tests.

## 6.1 Introduction

The general procedure of conducting a Thermal Response Test (TRT) is to first determine the undisturbed temperature of the ground. Next, a known amount of heat is extracted or injected into the borehole over a certain period of time. It is common to conduct thermal response tests in heat injection mode as it is easier to minimize the influence of external factors affecting the measurements in heat injection mode[51]. Electric resistance heaters are commonly used to inject heat into the ground by heating the circulating fluid. However, a heat pump can also be used to inject or to extract heat from the borehole. The heated fluid is circulated through the borehole for a minimum of 50 hours. The response of the ground is calculated by measuring the inlet and outlet fluid temperatures as a function of time. The readings are generally taken at regular intervals of 1-10 minutes. Other measurements include flow rate of the fluid, power input to electric heaters and circulation pump and the ambient temperature. The measurements are then analyzed using a mathematical heat transfer model to evaluate ground thermal conductivity and borehole thermal resistance.

## 6.2 Undisturbed ground temperature

Various approaches to determine the undisturbed ground temperature have been described in literature. The approaches most used in practice are discussed in the following.

**Approach 1:** The undisturbed ground temperature can be determined by inserting a thermocouple into the U-tube of an undisturbed borehole. Temperature measurements taken at several points along the borehole are then used to determine an average undisturbed ground temperature. This approach cannot be used to determine the undisturbed ground temperature of the laboratory boreholes as no sensors have been installed along the boreholes.

**Approach 2:** The undisturbed ground temperature can also be determined by circulating the fluid through the undisturbed borehole for about 20-30 minutes. The inlet and outlet fluid temperatures are recorded for short time intervals (10 sec). The recorded temperature profile of the 20-30 minutes is then used to determine the undisturbed ground temperature. This method has been used to determine the undisturbed temperature of the laboratory boreholes.

**Approach 3:** Another approach to determine the undisturbed ground temperature is to monitor the start-up exit fluid temperature from the U-tube. If the fluid is kept long enough in the U-tube it tends to reach equilibrium with the surrounding ground. ASHRAE[3] recommends using the temperature profile of the fluid in equilibrium with the surrounding ground to estimate the undisturbed ground temperature. Martin and Kavanaugh[45] have suggested using the minimum fluid temperature leaving the borehole as an approximation of the undisturbed ground temperature. Alternatively an average of the exit temperature of the fluid present in the U-tube can also be used. The undisturbed ground temperature of the laboratory boreholes has also been determined using the method recommended by ASHRAE.

## 6.3 Reduction and evaluation of TRT data

The ground thermal conductivity and the borehole thermal resistance can be evaluated using both direct and parameter estimation methods. The most commonly used methods are discussed in the following.

### 6.3.1 Line source approximation

The line source[36] solution, discussed in Chapter 2, is one of the most used direct methods to interpret ground thermal properties from the TRT measurements. It has undergone quite a few changes since it was first used by Mogensen[46]. Gehlin[27] and Witte et al.[63] have made significant contributions. The approach used by Gehlin and described in the following, has gained most acceptance because of its simpliciy and ease of use. Gehlin recommends approximating the integral in Equation 2.1 using the following approximation.

$$E_1\left(\frac{r_b^2}{4a_s\tau}\right) = \ln\left(\frac{4a_s \cdot \tau}{\gamma \cdot r_b^2}\right) \tag{6.1}$$

This line source approximation is mostly recommended to use for times larger than $20\ r_b^2/a_s$, which typically accounts to 10-20 hours for a normal borehole. The fluid temperature can be calculated using the relation:

$$T_f = T_b + q \cdot R_b. \tag{6.2}$$

Substituting the borehole wall temperature $(T_b)$ as calculated by the line source approximation in the Equation 6.2 gives:

$$T_f = \frac{q}{4\pi \cdot \lambda_s} \cdot \left( \ln \left( \frac{4a_s \cdot \tau}{\gamma \cdot r_b^2} \right) \right) + T_0 + q \cdot R_b. \tag{6.3}$$

Equation 6.3 is now comparable to Equation 6.4, which is the equation for a straight line.

$$T_f = k \cdot \ln(\tau) + m, \qquad k = \frac{q}{4\pi \cdot \lambda_s}. \tag{6.4}$$

The ground (soil) thermal conductivity ($\lambda_s$) can now be calculated using the slope ($k$) of the fluid temperature line when plotted against logarithmic time $ln(\tau)$.

$$\lambda_s = \frac{q}{4\pi \cdot k}. \tag{6.5}$$

Beier and Smith[8] extended the line source approximation to also obtain an estimate of borehole thermal resistance. They calculated an overall borehole thermal resistance value using Equations 6.3 and 6.5. The overall borehole resistance represents the sum of resistances of the fluid film, the piping, the grouting and any contact resistances as a single value.

$$R_b = \frac{1}{4\pi \cdot \lambda_s} \left[ \frac{T_f - T_0}{k} - \ln \left( \frac{4a \cdot \tau}{\gamma \cdot r_b^2} \right) \right]. \tag{6.6}$$

For any time $\tau_n$, the borehole resistance is determined by Equation 6.7, using the already estimated thermal conductivity, the slope of the late-time (i.e. 15 hours onwards) fluid temperature line, the undisturbed ground temperature (°C) and the fluid temperature (°C) at time $\tau_n$.

$$R_b = \frac{1}{4\pi \cdot \lambda_s} \left[ \frac{t_{f,n} - t_0}{k} - \ln \left( \frac{4a \cdot \tau_n}{\gamma \cdot r_b^2} \right) \right]. \tag{6.7}$$

### 6.3.2 Cylindrical source approximation

The cylindrical source[36] solution is another direct method used to interpret and evaluate TRTs. Carslaw and Jaeger[18] developed the so called 'probe method' to determine the thermal conductivity from a cylindrical source approximation. The probe method calculates the fluid temperature $T_f$ by approximating the value of the *G-factor* in Equation 2.3. For large values of the Fourier number the fluid temperature can be approximated using Equation 6.8.

$$T_f = T_0 + \frac{q}{4\pi \cdot \lambda_s}\left(ln\left(\frac{4a_s \cdot \tau}{\gamma \cdot r_b^2}\right) - \frac{4\pi \cdot \lambda_s \cdot R_b - (\rho_s c_s/\rho_b c_b)}{(2\rho_s c_s/\rho_b c_b) \cdot\ (a_s \cdot \tau/\gamma \cdot r_b^2)} \frac{(\rho_s c_s/\rho_b c_b) - 1}{(2\rho_s c_s/\rho_b c_b) \cdot\ (a_s \cdot \tau/\gamma \cdot r_b^2)} \cdot ln\left(\frac{4a_s \cdot \tau}{\gamma \cdot r_b^2}\right) +\ \ldots.\right) + q \cdot R_b \qquad (6.7)$$

Plotting $T_f$ against logarithmic time results in a curve which has a linear asymptote of slope $q/\lambda_s$. Measuring the slope of the linear asymptote and dividing it by the heat injection rate $q$ provides an estimate of the ground thermal conductivity.

### 6.3.3 Parameter estimation methods

The line source and the cylindrical source approximations assume constant input power to the circulating fluid loop. However, the fact that the injected power to the fluid loop can fluctuate in reality has prompted researchers to develop and use numerical methods to evaluate ground thermal properties. The numerical modelling of borehole heat transfer allows the use of time varying heat inputs in contrast to the constant heat input required by direct evaluation methods. This facilitates the use of the actual field-measured power instead of assuming an average value. Among others, Shonder and Beck[55] and Austin[4] have developed numerical methods which determine the ground thermal properties using parameter estimation techniques.

Shonder and Beck solved the 1-D radial heat transfer problem using a finite difference approach and used Gauss minimization technique to calculate parameter values which minimize the sum of squared errors between predicted and measured fluid temperatures. Austin instead used a two dimensional finite-volume numerical approach to estimate ground and grout thermal conductivities.

## 6.4 TRT setup in the laboratory

A general layout of equipment to conduct TRT typically consists of an electric heater, a circulation pump and measuring devices as shown in Figure 6.1. In a typical TRT setup the electric heater provides heat inputs of 50-80 W/m, the connection between the borehole and the test equipment is kept short and properly insulated, the temperature measurements are made close to the inlet and the outlet points to avoid influences from the surroundings, the power supply to the electric heaters is kept as stable as possible and the data is recorded at maximum 10 minutes intervals.

The laboratory setup includes a variable capacity electric heater, variable speed circulation pumps and temperature and flow sensors as shown in Figure 6.2. The circulating fluid temperatures are measured at two instances, firstly when entering or leaving the laboratory building and secondly before and after the electric heater. The flow rate is also measured twice, first using an installed Vortex flow meter and second over the individual borehole valves. The data can be recorded for any interval over 10 seconds.

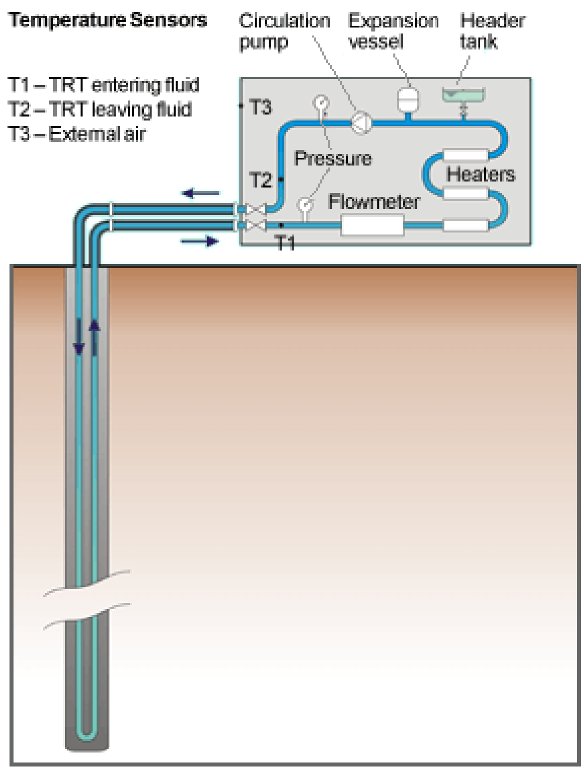


**Figure 6.1** Typical thermal response test setup (WJ Groundwater Limited[64]).

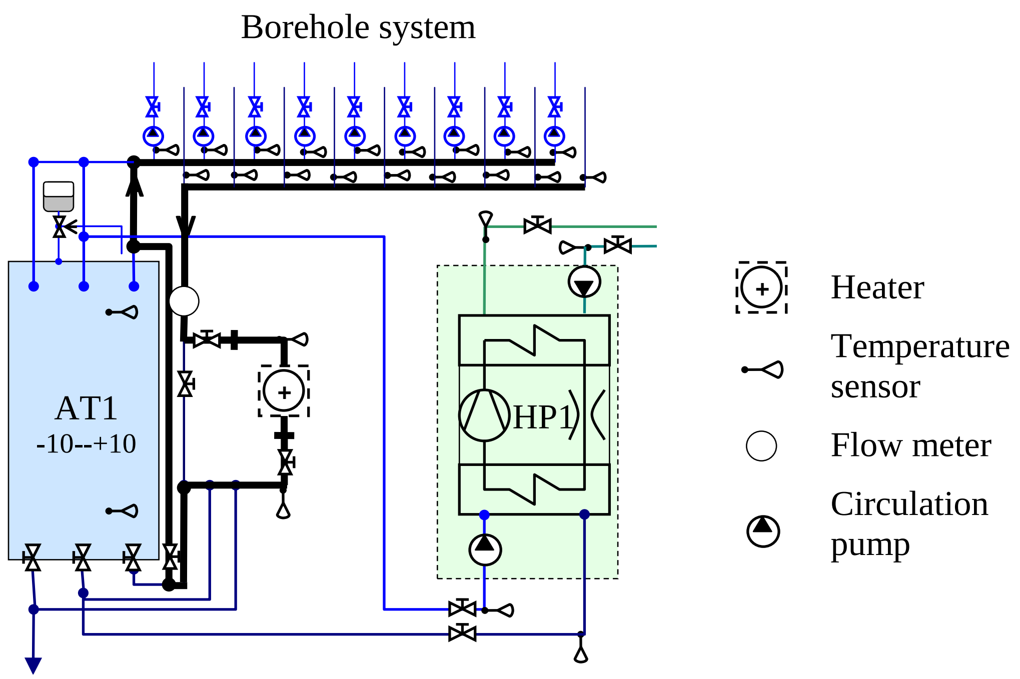


**Figure 6.2** Laboratory's TRT setup.

The only significant difference between the laboratory's TRT setup and a typical TRT setup is that in the laboratory setup the piping between the borehole and the test equipment is quite long. Though the piping is well insulated and has negligible heat losses yet the amount of additional fluid present in the piping increases the thermal capacity of the system. This additional thermal capacity can initially dampen the temperature increase of the circulating fluid.

## 6.5 Test procedure

The following procedure was carried out when conducting thermal response tests of laboratory boreholes.

1. The flow and the power input were set. The chosen power input of around 55 W/m matched the expected peak loads on the boreholes. The flow from the variable circulation pump was maintained in excess of 1.4 $m^3/h$ to ensure turbulent regime (Re > 4500) in the ground loop.

2. The fluid was circulated through the undisturbed borehole for a minimum of 30 minutes. During the circulation the inlet and outlet fluid temperatures were recorded for short time intervals (10 sec).

3. The heater was switched on. The power input was monitored and kept steady.

4. The inlet fluid, the outlet fluid and the ambient temperatures were recorded together with the flow and power input for time intervals between 3-5 minutes.

5. The tests were conducted for a minimum of 48 hours.

6. The undisturbed ground temperature, the ground thermal conductivity and the borehole thermal resistance were estimated from the measured data using an analytical method.

## 6.6 Test sequence

Thermal response tests were conducted for nine laboratory boreholes in the sequence shown in Table 6.1. Initially, unheated fluid was circulated through the undisturbed boreholes to measure the undisturbed ground temperature. The circulation time varied between 30 to 75 minutes for different boreholes.

Next, the thermal response tests were conducted for a minimum duration of 48 hours. The duration of most of the TRTs was between 68 to 98 hours but tests as short as 48 hours and as long as 267 hours were also conducted. The measurements were also taken for the recovery period which followed the actual test. Duration of the recovery period is indicated separately in addition to the test duration in Table 6.1. The ambient temperature during the test periods varied between the extremes of 8.2 and -17 °C.

**Table 6.1** Sequence and duration of the thermal response tests.

| No. | Undisturbed ground temperature | Thermal response test |
|---|---|---|
| BH1 | Date: 2009-12-03<br>Duration: 45 minutes | Date: 2009-12-03 – 2009-12-07<br>Duration: 75 + 20 hours |
| BH9 | Date: 2009-12-10<br>Duration: 35 minutes | Date: 2009-12-10 – 2009-12-15<br>Duration: 98 + 28 hours |
| BH2 | Date: 2009-12-18<br>Duration: 75 minutes | Date: 2009-12-18 – 2009-12-21<br>Duration: 54 + 24 hours |
| BH3 | Date: 2009-12-24<br>Duration: 30 minutes | Date: 2009-12-24 – 2010-01-07<br>Duration: 267 + 64 hours |
| BH6 | Date: 2010-01-14<br>Duration: 60 minutes | Date: 2010-01-14 – 2010-01-18<br>Duration: 91+ 24 hours |
| BH4 | Date: 2010-02-02<br>Duration: 60 minutes | Date: 2010-02-02 – 2010-02-04<br>Duration: 48 + 17 hours |
| BH8 | Date: 2010-02-05<br>Duration: 40 minutes | Date: 2010-02-05 – 2010-02-08<br>Duration: 69 + 25 hours |
| BH7 | Date: 2010-02-09<br>Duration: 30 minutes | Date: 2010-02-09 – 2010-02-11<br>Duration: 48 + 25 hours |
| BH5 | Date: 2010-02-12<br>Duration: 45 minutes | Date: 2010-02-12 – 2010-02-15<br>Duration: 68 + 26 hours |

## 6.7 Undisturbed ground temperature measurements

Undisturbed ground temperatures of all nine laboratory boreholes were determined using ‘fluid circulation’ and ‘start-up exiting fluid’ approaches described in Section 6.2. These two approaches respectively use the techniques of circulating the fluid through the undisturbed borehole and evaluating the outlet fluid temperature from a U-tube in equilibrium with the surrounding ground to determine the undisturbed ground temperature.

### 6.7.1 Fluid circulation method

To determine the undisturbed ground temperature using this approach, the fluid was circulated through the undisturbed ground while keeping the electric heaters off. One of the problems with this approach is that for times longer than 30 minutes the undisturbed ground temperature measurements get affected by the heat gains from the circulation pump[28]. However, the use of highly efficient custom made circulation pumps for borehole applications avoided this problem.

Figures 6.3 to 6.11 present the results of undisturbed ground temperature measurements using the ‘fluid circulation’ method. As seen from these figures, the heat gain from the circulating pumps is negligible and the circulating fluid temperature tends to stabilize after around 30 minutes of circulation. The stabilized fluid temperature provides an approximation of the undisturbed ground temperature for each borehole.

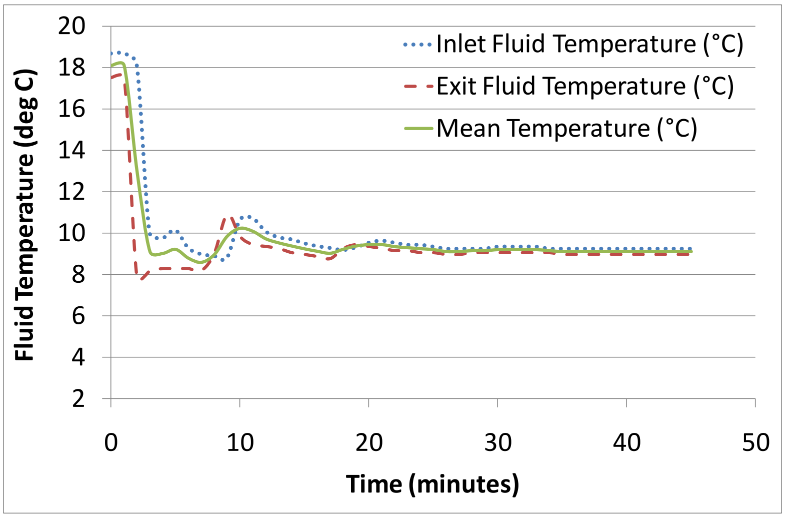


**Figure 6.3** Undisturbed ground temperature measurement for BH1.

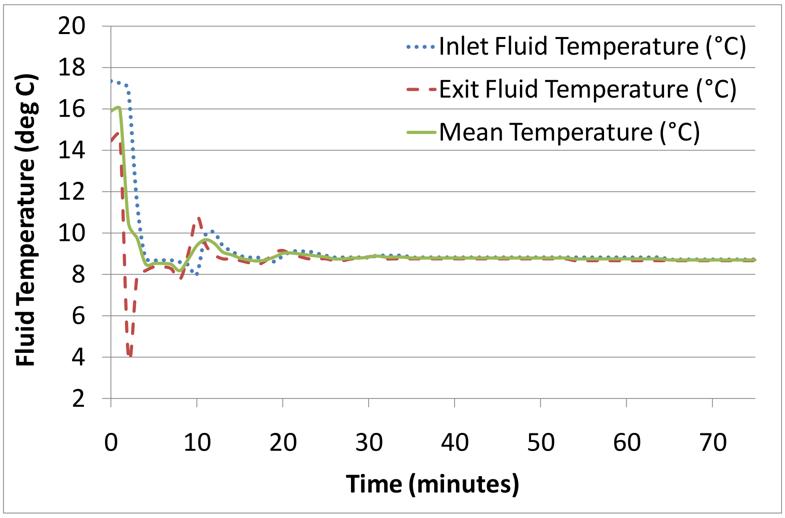


**Figure 6.4** Undisturbed ground temperature measurement for BH2.

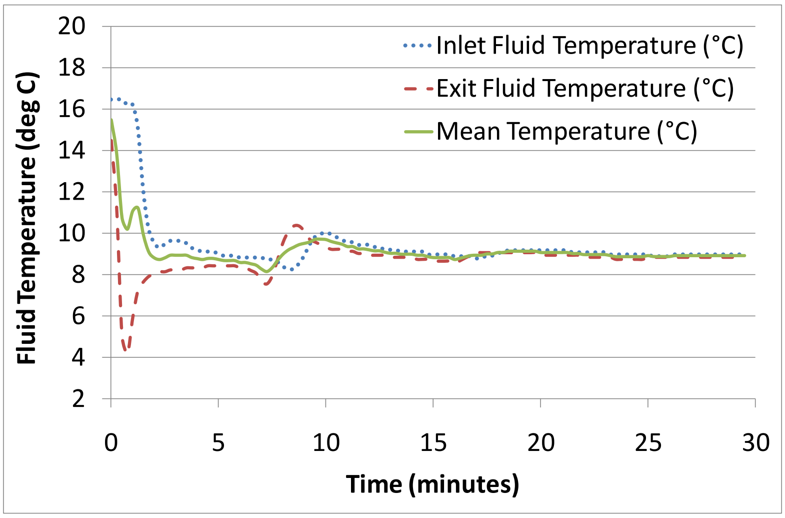


**Figure 6.5** Undisturbed ground temperature measurement for BH3.

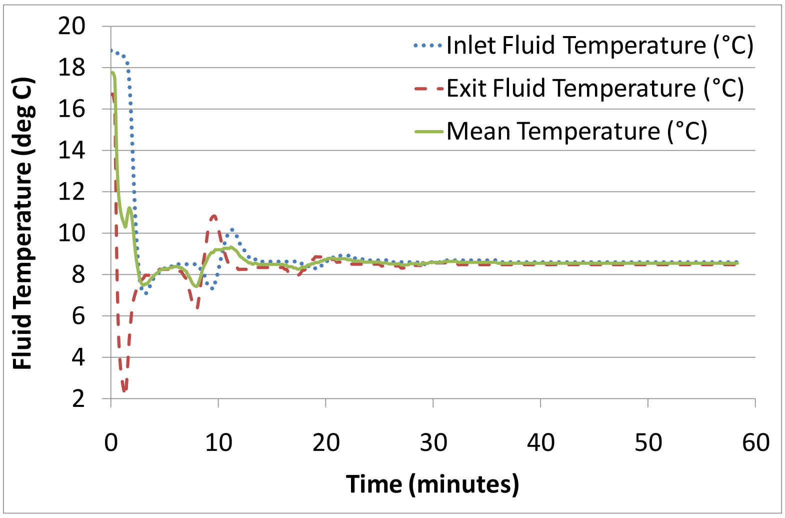


**Figure 6.6** Undisturbed ground temperature measurement for BH4.

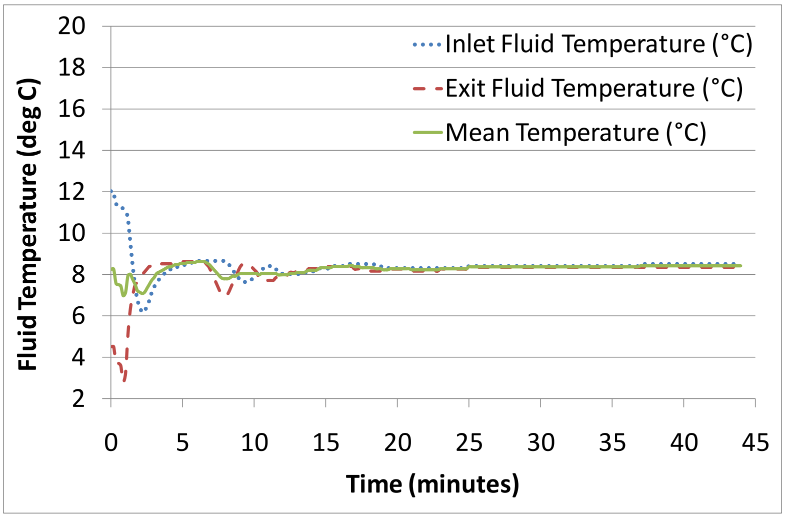


**Figure 6.7** Undisturbed ground temperature measurement for BH5.

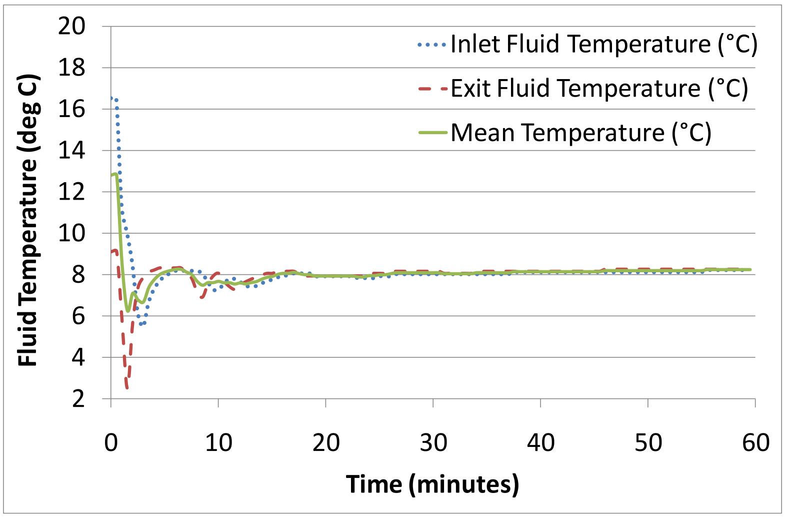


**Figure 6.8** Undisturbed ground temperature measurement for BH6.

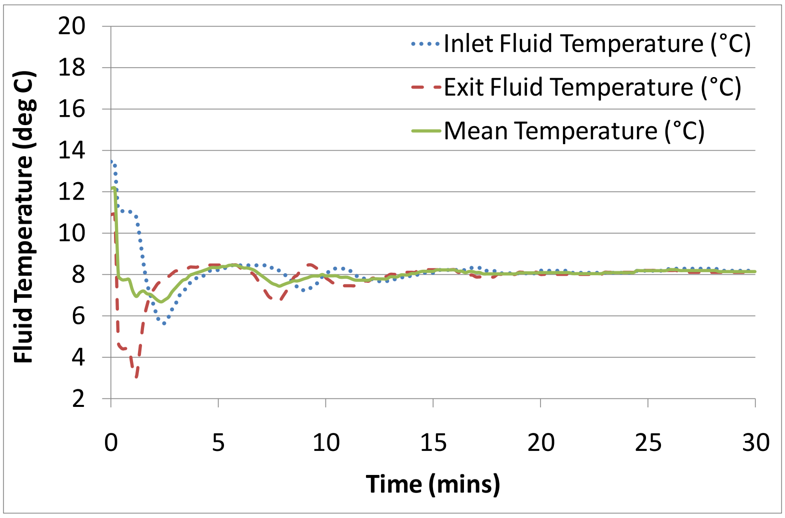


**Figure 6.9** Undisturbed ground temperature measurement for BH7.

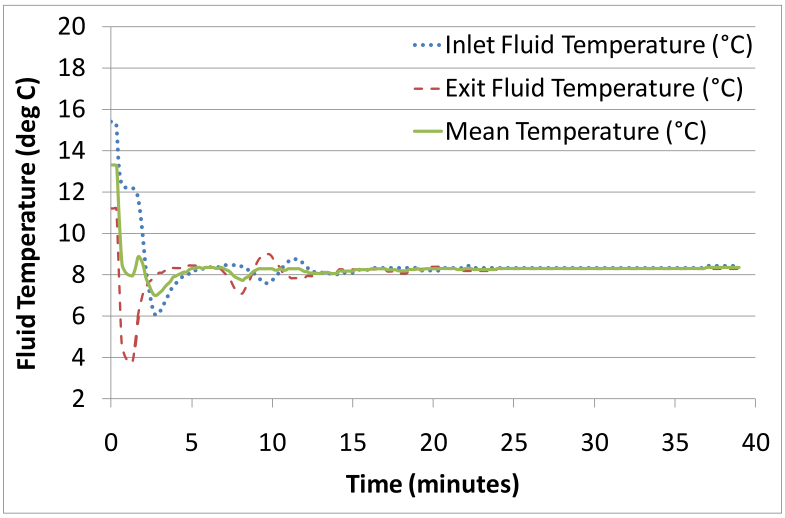


**Figure 6.10** Undisturbed ground temperature measurement for BH8.

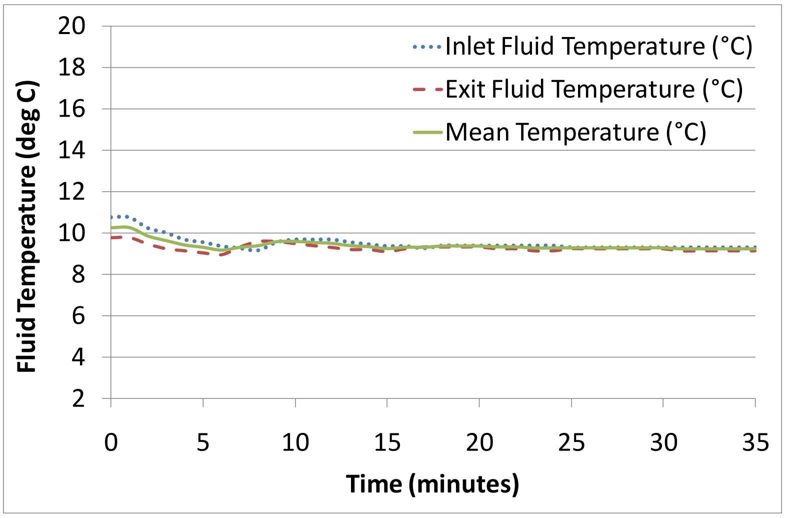


**Figure 6.11** Undisturbed ground temperature measurement for BH9.

Ideally, the undisturbed ground temperature measured for all nine boreholes should have been the same. But the measurements of the undisturbed ground temperature calculated by circulating the fluid in the undisturbed borehole vary between 8.1 to 9.2 °C. Table 6.2 summarizes the undisturbed ground temperature measurements for all nine boreholes.

**Table 6.2** Undisturbed ground temperature of laboratory boreholes.

| Borehole | Temperature (°C) | |
|---|---|---|
| | Ground | Ambient air |
| BH1 | 9.1 | 1.5 |
| BH2 | 8.7 | -3.0 |
| BH3 | 8.9 | 1.9 |
| BH4 | 8.5 | -0.7 |
| BH5 | 8.4 | -1.4 |
| BH6 | 8.2 | -0.1 |
| BH7 | 8.2 | -3.5 |
| BH8 | 8.3 | -2.4 |
| BH9 | 9.2 | 5.6 |

The reason behind different values of undisturbed ground temperature becomes clear when these values are studied together with the corresponding ambient temperatures. The top of the ground layer, surrounding the borehole, is slightly influenced by the ambient temperature changes. Moreover, with the water table for the laboratory borehole system at almost the ground level, the changes in the ambient temperature also affect the top of the water-filled boreholes. The effects of the variations in the ambient temperature, when measuring undisturbed ground temperature, become clear when the measured values of undisturbed ground temperatures are plotted together with the ambient temperatures. In Figures 6.12 and 6.13 the undisturbed ground temperatures are plotted together with the seasonal and instantaneous ambient temperatures respectively.

These figures indicate that the undisturbed ground temperature, measured using the ‘fluid circulation’ method, has a strong ambient coupling, at least for the laboratory borehole field of rather short boreholes.

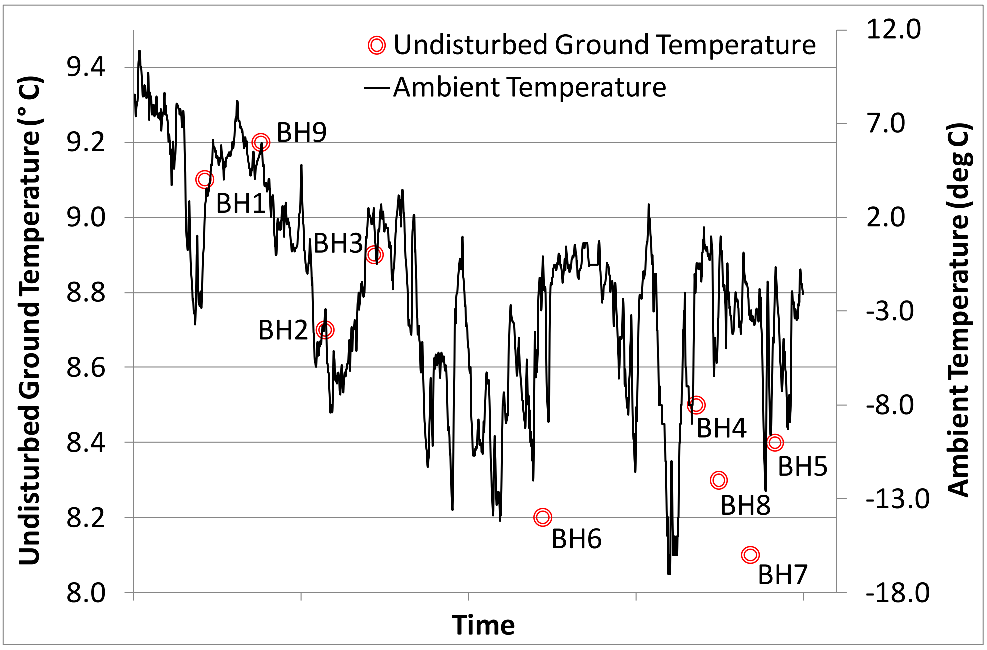


**Figure 6.12** Undisturbed ground temperature and the seasonal ambient air temperatures.

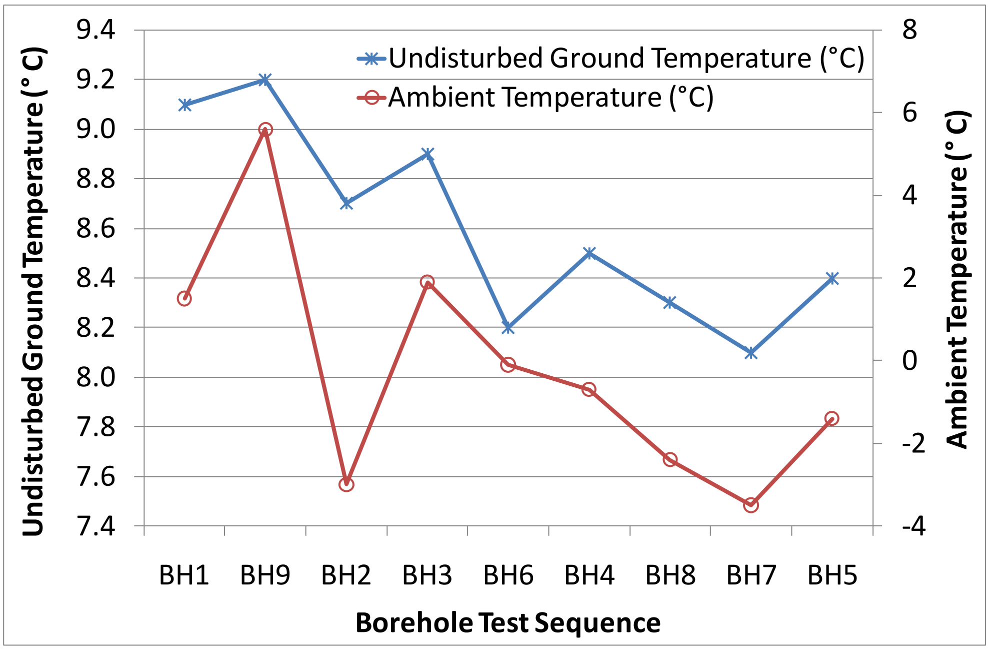


**Figure 6.13** Undisturbed ground temperature and the instantaneous ambient temperatures.

### 6.7.2 Undisturbed ground temperature from the fluid temperature exiting the U-tube

As the undisturbed ground temperature predicted by the ‘fluid circulation’ method for the nine laboratory boreholes varied in the rather wide range of 8.1 to 9.2 °C, the fluid temperatures exiting the borehole U-tube were further investigated to evaluate a more definite value of undisturbed ground temperature.

Figure 6.14 shows the temperature of the fluid entering the laboratory building from the nine boreholes after the circulation pump is switched on. The decline in temperatures from the start of the pumps to the first set of troughs in Figure 6.14 is because of the fluid present in the return horizontal piping from the boreholes to the building. The fluid remained in the horizontal piping for several weeks before the tests were performed and hence it was in equilibrium with the shallow ground temperatures. The fluid from the U-tube starts to enter the building around 3 minutes after switching on the circulation pump. The flow from the U-tube continues till 7 minutes. Fluid temperature between 3 and 7 minutes, highlighted in Figure 6.14, remains fairly constant at around 8.3 °C for all nine boreholes. This temperature presents a more consistent approximation of the undisturbed ground temperature.

After 7 minutes, the fluid present in the supply horizontal piping to the boreholes enters the building. This is represented by the second set of troughs in Figure 6.14. At this time, the fluid has completed the first round of circulation. During the next rounds, the variations peter out and the fluid temperature adjusts to the temperature profile of the surrounding ground. That is when the temperature of the top of the ground layer tends to influence the fluid temperature as discussed in the previous section.

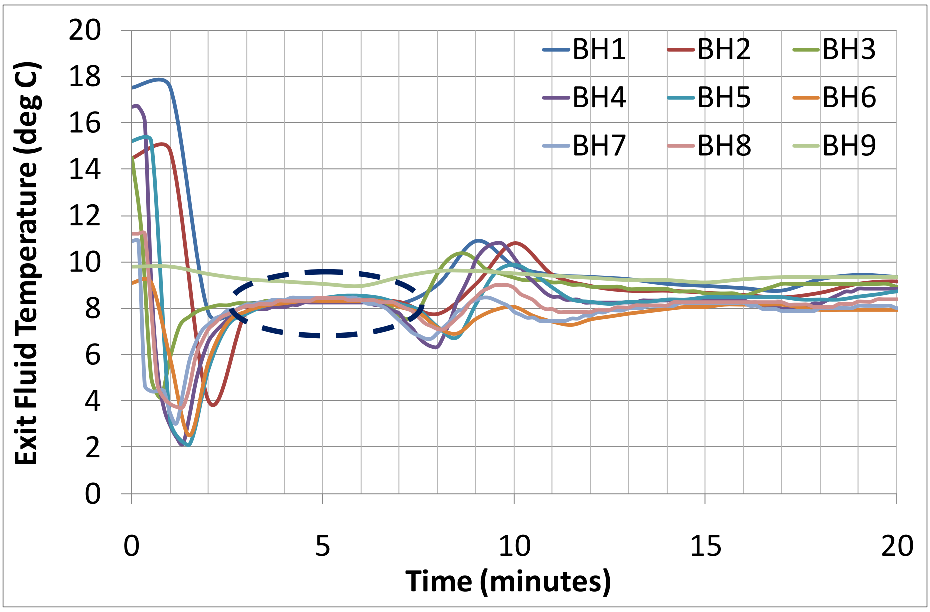


**Figure 6.14** Undisturbed ground temperature measurement from start-up exit fluid temperatures.

## 6.8 Ground thermal conductivity and borehole thermal resistance estimations

Several direct and numerical methods to calculate ground thermal conductivity and the borehole thermal resistance from the experimental data of TRTs were discussed in section 6.3. There are two significant issues when numerical methods are used to evaluate the TRTs of the laboratory boreholes. The first issue is that most numerical models estimate ground thermal conductivity and the borehole thermal resistance assuming only conductive heat transfer in the borehole. However, as the laboratory boreholes are filled with ground water, a heat injection to these boreholes will induce natural convection in the boreholes. For water-filled boreholes the convective heat transfer is typically 3-5 times higher than the conductive heat transfer of the boreholes[34]. As the numerical models are not developed to account for the convective heat transfer, the grout thermal conductivity estimated by these models is not very precise. This uncertainty also reflects in the borehole thermal resistance estimation which is generally determined using grout thermal conductivity estimation by the numerical methods. Using direct methods like the line source or the cylindrical source approximations solve this problem. Both these methods disregard the borehole geometry and only estimate the ground thermal conductivity. Consequently, the borehole thermal resistance is calculated using alternative approaches and not from the grout thermal conductivity.

The second issue, when using the numerical methods to estimate the TRTs of the laboratory boreholes, is the presence of additional thermal mass and capacity in the test system. The available numerical methods assume very short connections with the test rig and only consider the heat capacity of the fluid present in the borehole. For the laboratory system, the length of the horizontal piping outside the laboratory building varies between 13 and 29 meters. There is also significant length of piping inside the laboratory building. The fluid present in this piping adds to the thermal capacity and the transport time of the system. This thermal capacity initially dampens the temperature increase of the fluid when conducting a TRT. As the software implementation of most numerical methods cannot account for the additional heat capacity present in the system, the ground thermal conductivity and the borehole thermal resistance estimations from some of these methods can be inaccurate. On the other hand, it is common practise to disregard data for times smaller than 10-15 hours and to focus more on the late-time data when using direct methods to evaluate TRTs. This ensures that the effects of the additional thermal capacity present in the system become less significant.

Using direct methods to evaluate TRTs of the laboratory boreholes provides some distinctive advantages. For this particular case of groundwater filled boreholes, the use of a direct method to evaluate TRTs ensures more consistent estimates of borehole thermal resistance values for the nine boreholes. It can also evade the problems caused by the additional thermal capacity present in the system. For these reasons, the line source approximation together with the method proposed by Beier and Smith[8] to evaluate borehole thermal resistance has been used to evaluate the TRTs of the nine laboratory boreholes.

### 6.8.1 Borehole 1

Borehole 1 was tested between Dec 3, 2009 and Dec 7, 2009 for 75 hours. The inlet, exit and the mean fluid temperatures of borehole 1 are shown in Figure 6.15. Other details including power input and the ambient temperature are shown in Figure 6.16. The trend of the late-time (i.e. 15 hours onwards) mean fluid temperature data for borehole 1 is shown as a dotted line in Figure 6.17. The slope of the trend line (i.e. 1.508) is used in Equation 6.5 to determine the ground thermal conductivity value of 2.88 W/(m·K) for borehole 1 in Table 6.3. The estimated ground thermal conductivity value is then used in Equation 6.7 to determine the borehole thermal resistance value of 0.059 (m·K)/W.

As seen from Equation 6.7, the estimated value of borehole thermal resistance is linearly related to the value ($t_{f,1hr}$ - $t_0$). The temperature $t_{f,1hr}$, is the extrapolated temperature at hour 1 from the late-time mean fluid temperature trend. Its numerical value is equal to the intercept value of the trend line shown in Figure 6.17. The temperature $t_0$ is the undisturbed ground temperature for which a consistent value of 8.3 °C is used for all the nine boreholes. Using the undisturbed ground temperature value of 9.1 °C from the 'fluid circulation' method instead of 8.3 °C estimates the borehole thermal resistance value as 0.044 (m·K)/W.

**Table 6.3** Ground thermal conductivity and borehole thermal resistance calculations for BH1.

| **Ground thermal conductivity ($\lambda_s$) and borehole thermal resistance ($R_b$) of BH1** | |
|---|---|
| **Ground thermal conductivity** | |
| Average power (W): | 4373 |
| Borehole depth (m): | 80 |
| Injected heat flux, q (W/m): | 54.7 |
| Slope of the trend line, k: | 1.508 |
| $\lambda_s$ (W/(m·K)) = q/(4·pi·k): | 2.88 |
| **Borehole thermal resistance** | |
| Intercept value of the trend line, m = $t_{f,\,1\,hr}$ (°C): | 13.403 |
| Undisturbed ground temperature, $t_0$ (°C): | 8.3 |
| $t_{f,\,1\,hr} - t_0$ (K): | 5.1 |
| Thermal diffusivity, $a_s$ ($m^2$/h): | 0.0047 |
| Borehole radius, $r_b$ (m): | 0.055 |
| Constant, $\gamma$: | 1.78 |
| $R_b$ ((m·K)/W) = $[1/(4\cdot pi\cdot\lambda_s)]\cdot[\{(t_{f,\,1\,hr} - t_0)/k\} - \ln\{(4\cdot a_s)/(\gamma\cdot r_b^2)\}]$: | 0.059 |

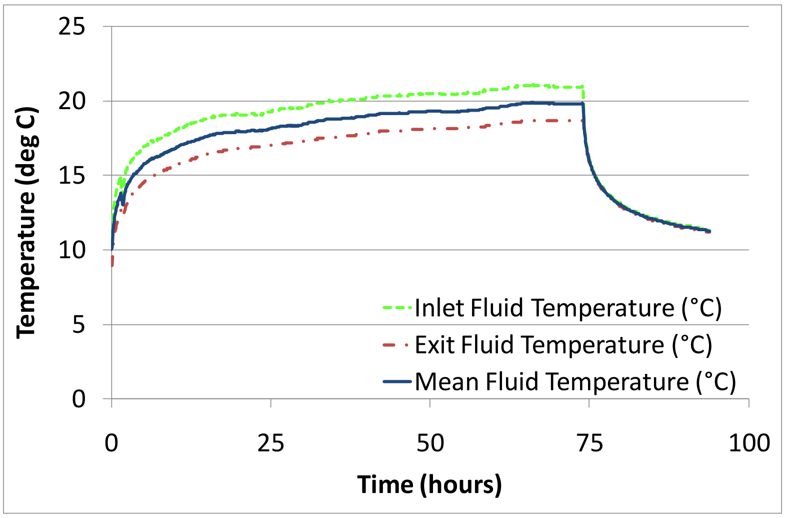


**Figure 6.15** Inlet, exit and mean fluid temperatures for the TRT of BH1.

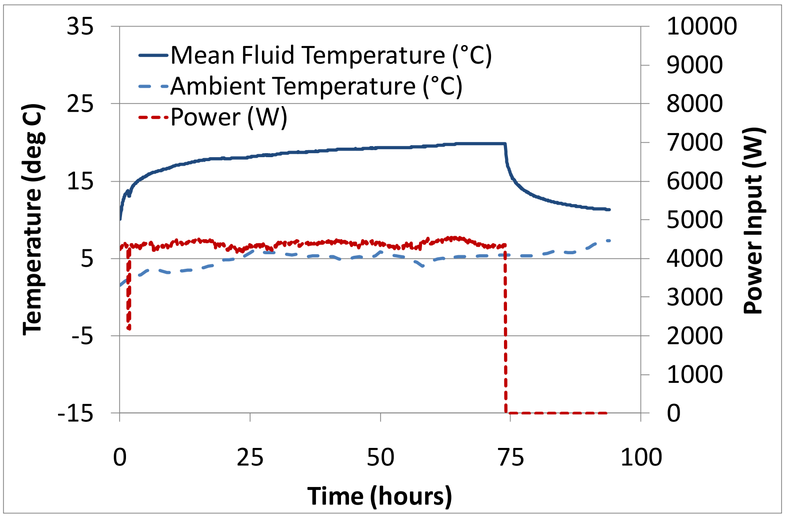


**Figure 6.16** Power input and ambient temperature for the TRT of BH1.

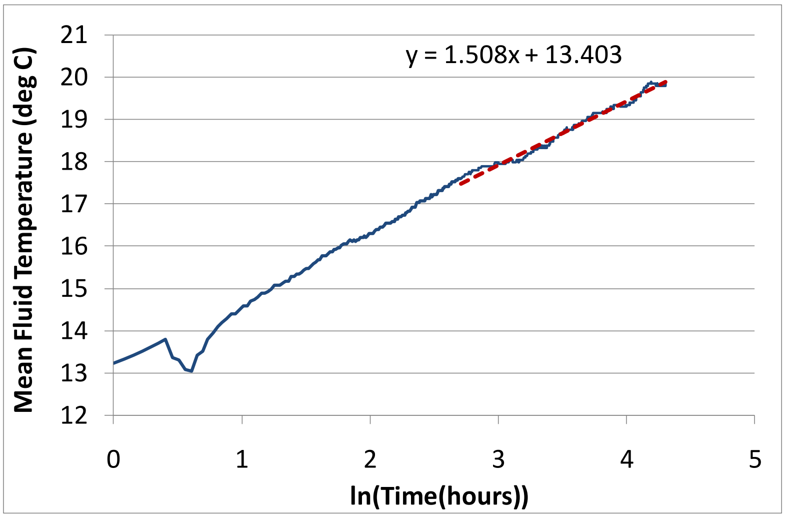


**Figure 6.17** Mean fluid temperature and its late-time trend for TRT of BH1.

### 6.8.2 Borehole 2

Borehole 2 was tested between Dec 18, 2009 and Dec 21, 2009 for 54 hours. The inlet, exit and the mean fluid temperatures of borehole 2 are shown in Figure 6.18. Other test details including power input and the ambient temperature are shown in Figure 6.19.

The trend of the late-time (i.e. 15 hours onwards) mean fluid temperature data for borehole 2 is shown as a dotted line in Figure 6.20. The slope of the trend line (i.e. 1.427) is used in Equation 6.5 to determine the effective ground thermal conductivity value of 3.06 W/(m·K) for borehole 2 in Table 6.4. The estimated ground thermal conductivity value is then used in Equation 6.7 to determine the borehole thermal resistance value of 0.064 (m·K)/W.

Using the undisturbed ground temperature value of 8.7 °C from the fluid circulation method instead of 8.3 °C estimates the borehole thermal resistance value as 0.057 (m·K)/W.

**Table 6.4** Ground thermal conductivity and borehole thermal resistance calculations for BH2.

| **Ground thermal conductivity ($\lambda_s$) and borehole thermal resistance ($R_b$) of BH2** | |
|---|---|
| **Ground thermal conductivity** | |
| Average power (W): | 4392 |
| Borehole depth (m): | 80 |
| Injected heat flux, q (W/m): | 54.9 |
| Slope of the trend line, k: | 1.427 |
| $\lambda_s$ (W/(m·K)) = q/(4·pi·k): | 3.06 |
| **Borehole thermal resistance** | |
| Intercept value of the trend line, m = $t_{f,\ 1\ hr}$ (°C): | 13.685 |
| Undisturbed ground temperature, $t_0$ (°C): | 8.3 |
| $t_{f,\ 1\ hr} - t_0$ (K): | 5.4 |
| Thermal diffusivity, $a_s$ ($m^2$/h): | 0.0050 |
| Borehole radius, $r_b$ (m): | 0.055 |
| Constant, $\gamma$: | 1.78 |
| $R_b$ ((m·K)/W) = $[1/(4\cdot pi\cdot\lambda_s)]\cdot[\{(t_{f,\ 1\ hr} - t_0)/k\} - \ln\{(4\cdot a_s)/(\gamma\cdot r_b^2)\}]$: | 0.064 |

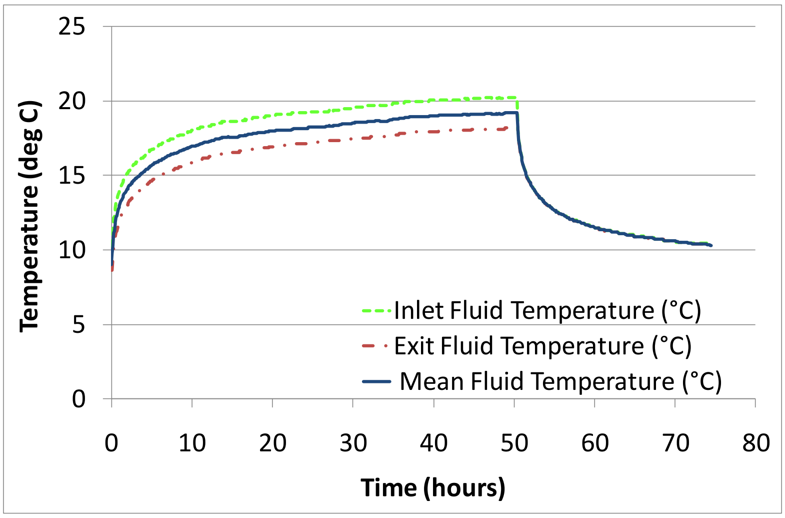


**Figure 6.18** Inlet, exit and mean fluid temperatures for the TRT of BH2.

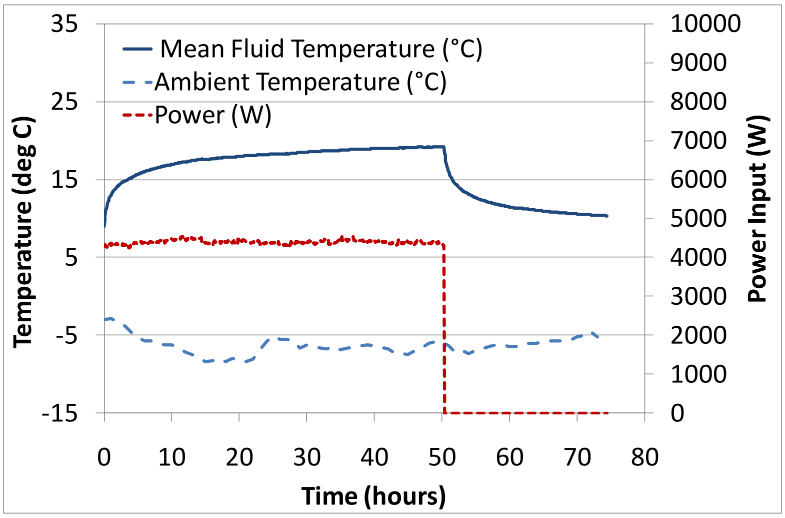


**Figure 6.19** Power input and ambient temperature for the TRT of BH2.

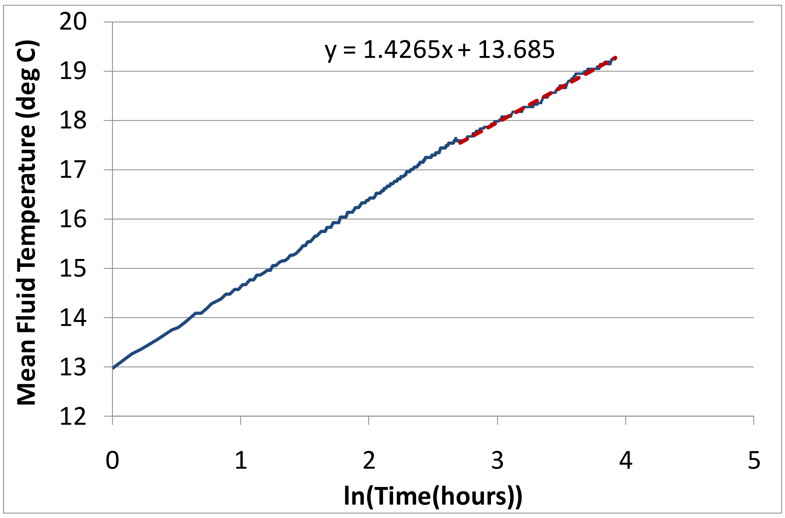


**Figure 6.20** Mean fluid temperature and its late-time trend for TRT of BH2.

### 6.8.3 Borehole 3

Borehole 3 was tested between Dec 24, 2009 and Jan 07, 2010 for 267 hours. The inlet, exit and the mean fluid temperatures of borehole 3 are shown in Figure 6.21. Other test details including power input and the ambient temperature are shown in Figure 6.22.

The trend of the late-time (i.e. 15 hours onwards) mean fluid temperature data for borehole 3 is shown as a dotted line in Figure 6.23. The slope of the trend line (i.e. 1.470) is used in Equation 6.5 to determine the effective ground thermal conductivity value of 3.04 W/(m·K) for borehole 3 in Table 6.5. The estimated ground thermal conductivity value is then used in Equation 6.7 to determine the borehole thermal resistance value of 0.074 (m·K)/W.

Using the discrete undisturbed ground temperature of 8.9 °C from the fluid circulation method, instead of 8.3 °C, estimates the borehole thermal resistance value as 0.063 (m·K)/W.

**Table 6.5** Ground thermal conductivity and borehole thermal resistance calculations for BH3.

| **Ground thermal conductivity ($\lambda_s$) and borehole thermal resistance ($R_b$) of BH3** | |
|---|---|
| **Ground thermal conductivity** | |
| Average power (W): | 4385 |
| Borehole depth (m): | 78 |
| Injected heat flux, q (W/m): | 56.2 |
| Slope of the trend line, k: | 1.470 |
| $\lambda_s$ (W/(m·K)) = q/(4·pi·k): | 3.04 |
| **Borehole thermal resistance** | |
| Intercept value of the trend line, m = $t_{f,\,1\,hr}$ (°C): | 14.361 |
| Undisturbed ground temperature, $t_0$ (°C): | 8.3 |
| $t_{f,\,1\,hr} - t_0$ (K): | 6.1 |
| Thermal diffusivity, $a_s$ ($m^2$/h): | 0.0050 |
| Borehole radius, $r_b$ (m): | 0.055 |
| Constant, $\gamma$: | 1.78 |
| $R_b$ ((m·K)/W) = $[1/(4\cdot pi\cdot\lambda_s)]\cdot[\{(t_{f,\,1\,hr} - t_0)/k\} - \ln\{(4\cdot a_s)/(\gamma\cdot r_b^2)\}]$: | 0.074 |

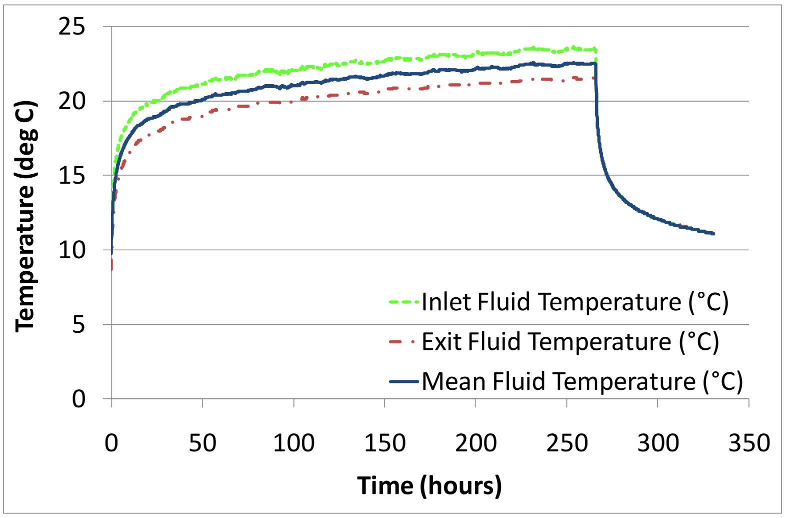


**Figure 6.21** Inlet, exit and mean fluid temperatures for the TRT of BH3.

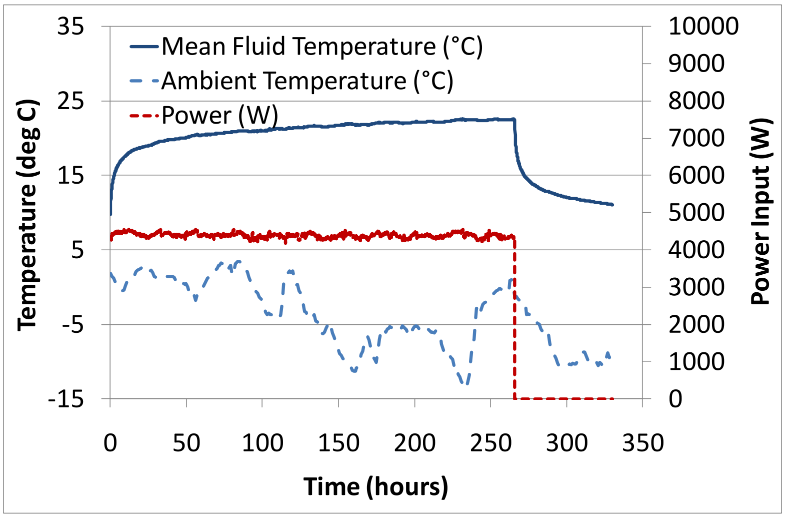


**Figure 6.22** Power input and ambient temperature for the TRT of BH3.

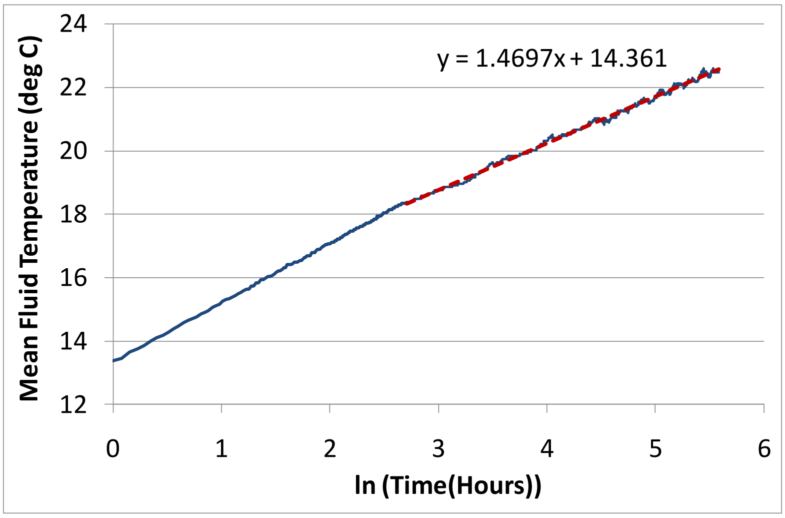


**Figure 6.23** Mean fluid temperature and its late-time trend for TRT of BH3.

### 6.8.4 Borehole 4

Borehole 4 was tested between Feb 02, 2010 and Feb 04, 2010 for 48 hours. The inlet, exit and the mean fluid temperatures of borehole 4 are shown in Figure 6.24. Other test details including power input and the ambient temperature are shown in Figure 6.25.

The trend of the late-time (i.e. 15 hours onwards) mean fluid temperature data for borehole 4 is shown as a dotted line in Figure 6.26. The slope of the trend line (i.e. 1.546) is used in Equation 6.5 to determine the effective ground thermal conductivity value of 2.81 W/(m·K) for borehole 4 in Table 6.6. The estimated ground thermal conductivity is then used in Equation 6.7 to determine the borehole thermal resistance value of 0.049 (m·K)/W.

Using the discrete undisturbed ground temperature of 8.5 °C from the fluid circulation method, instead of 8.3 °C, estimates the borehole thermal resistance value as 0.045 (m·K)/W.

**Table 6.6** Ground thermal conductivity and borehole thermal resistance calculations for BH4.

| Ground thermal conductivity ($\lambda_s$) and borehole thermal resistance ($R_b$) of BH4 | |
|---|---|
| **Ground thermal conductivity** | |
| Average power (W): | 4365 |
| Borehole depth (m): | 80 |
| Injected heat flux, q (W/m): | 54.6 |
| Slope of the trend line, k: | 1.546 |
| $\lambda_s$ (W/(m·K)) = q/(4·pi·k): | 2.81 |
| **Borehole thermal resistance** | |
| Intercept value of the trend line, m = $t_{f,\ 1\ hr}$ (°C): | 12.863 |
| Undisturbed ground temperature, $t_0$ (°C): | 8.3 |
| $t_{f,\ 1\ hr} - t_0$ (K): | 4.6 |
| Thermal diffusivity, $a_s$ ($m^2$/h): | 0.0046 |
| Borehole radius, $r_b$ (m): | 0.055 |
| Constant, $\gamma$: | 1.78 |
| $R_b$ ((m·K)/W) = $[1/(4 \cdot pi \cdot \lambda_s)] \cdot [\{(t_{f,\ 1\ hr} - t_0)/k\} - \ln\{(4 \cdot a_s)/(\gamma \cdot r_b^2)\}]$: | 0.049 |

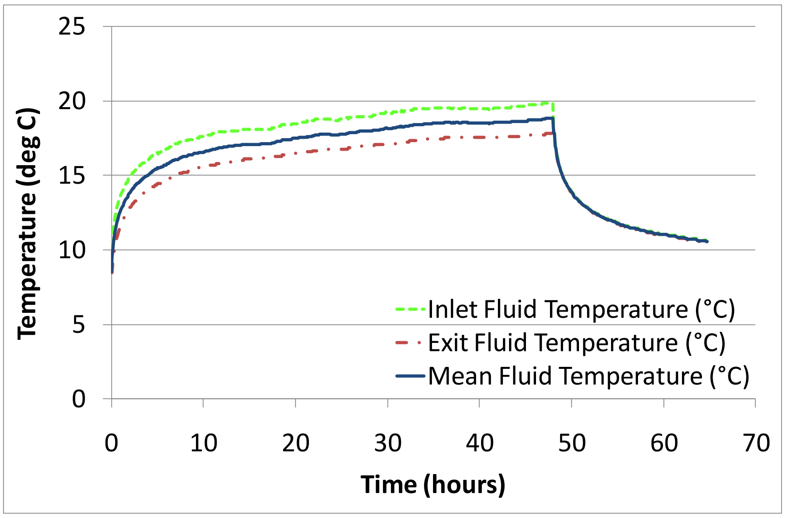


**Figure 6.24** Inlet, exit and mean fluid temperatures for the TRT of BH4.

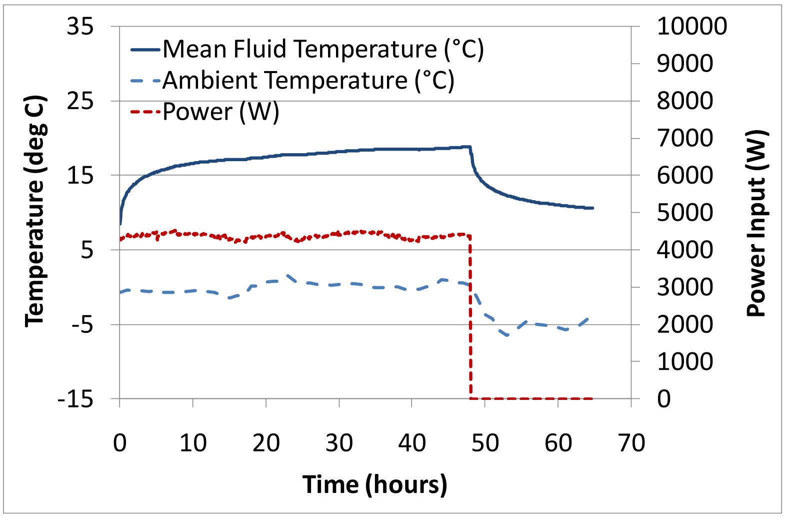


**Figure 6.25** Power input and ambient temperature for the TRT of BH4.

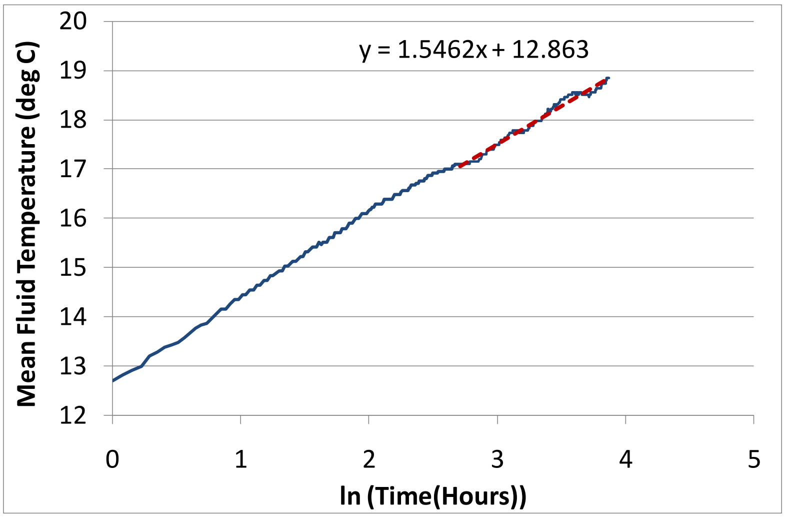


**Figure 6.26** Mean fluid temperature and its late-time trend for TRT of BH4.

### 6.8.5 Borehole 5

Borehole 5 was tested between Feb 12, 2010 and Feb 15, 2010 for 68 hours. The inlet, exit and the mean fluid temperatures of borehole 5 are shown in Figure 6.27. Other test details including power input and the ambient temperature are shown in Figure 6.28.

The trend of the late-time (i.e. 15 hours onwards) mean fluid temperature data for borehole 5 is shown as a dotted line in Figure 6.29. The slope of the trend line (i.e. 1.463) is used in Equation 6.5 to determine the effective ground thermal conductivity value of 2.98 W/(m·K) for borehole 5 in Table 6.7. The estimated ground thermal conductivity value is then used in Equation 6.7 to determine the borehole thermal resistance of value 0.064 (m·K)/W.

Using the discrete undisturbed ground temperature of 8.4 °C from the fluid circulation method, instead of 8.3 °C, estimates the borehole thermal resistance value as 0.062 (m·K)/W.

**Table 6.7** Ground thermal conductivity and borehole thermal resistance calculations for BH5.

| **Ground thermal conductivity ($\lambda_s$) and borehole thermal resistance ($R_b$) of BH5** | |
|---|---|
| **Ground thermal conductivity** | |
| Average power (W): | 4388 |
| Borehole depth (m): | 80 |
| Injected heat flux, q (W/m): | 54.85 |
| Slope of the trend line, k: | 1.463 |
| $\lambda_s$ (W/(m·K)) = q/(4·pi·k): | 2.98 |
| **Borehole thermal resistance** | |
| Intercept value of the trend line, m = $t_{f,\,1\,hr}$ (°C): | 13.674 |
| Undisturbed ground temperature, $t_0$ (°C): | 8.3 |
| $t_{f,\,1\,hr} - t_0$ (K): | 5.4 |
| Thermal diffusivity, $a_s$ ($m^2$/h): | 0.0049 |
| Borehole radius, $r_b$ (m): | 0.055 |
| Constant, $\gamma$: | 1.78 |
| $R_b$ ((m·K)/W) = $[1/(4\cdot pi\cdot\lambda_s)]\cdot[\{(t_{f,\,1\,hr} - t_0)/k\} - \ln\{(4\cdot a_s)/(\gamma\cdot r_b^2)\}]$: | 0.064 |

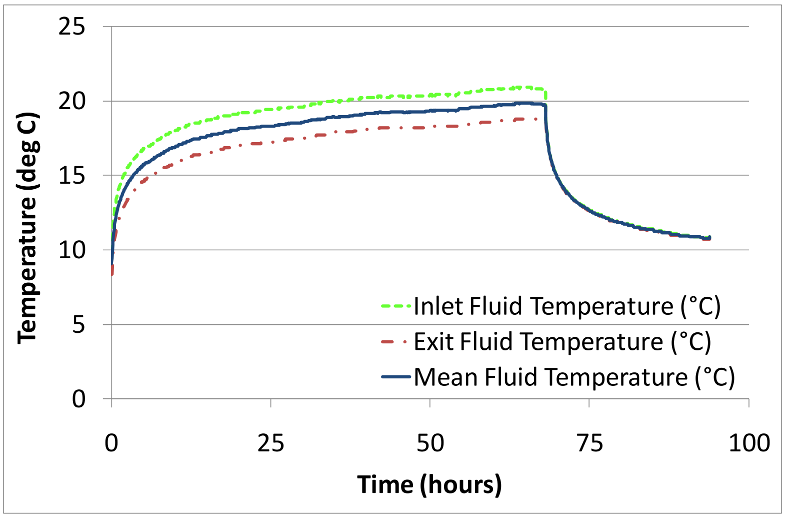


**Figure 6.27** Inlet, exit and mean fluid temperatures for the TRT of BH5.

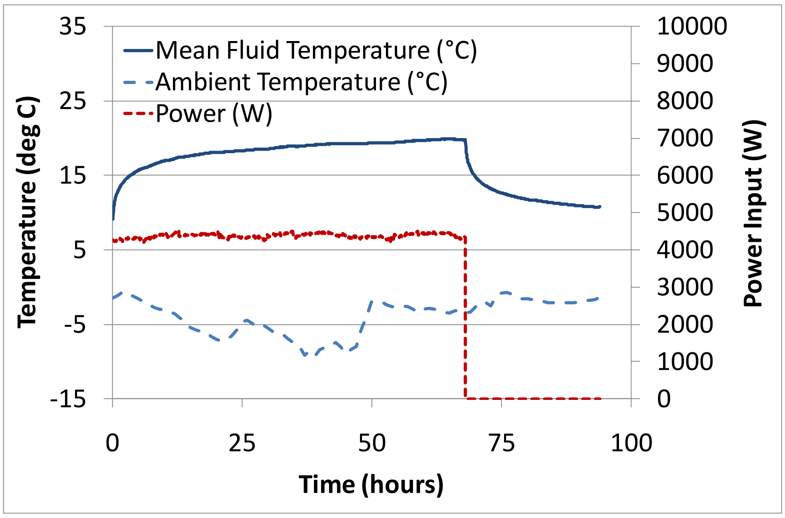


**Figure 6.28** Power input and ambient temperature for the TRT of BH5.

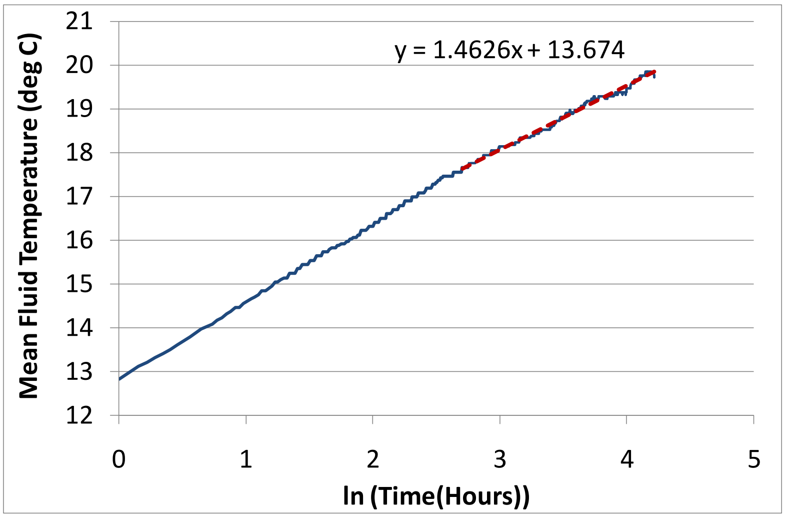


**Figure 6.29** Mean fluid temperature and its late-time trend for TRT of BH5.

### 6.8.6 Borehole 6

Borehole 6 was tested between Jan 14, 2010 and Jan 18, 2010 for 91 hours. The inlet, exit and the mean fluid temperatures of borehole 6 are shown in Figure 6.30. Other test details including power input and the ambient temperature are shown in Figure 6.31.

The trend of the late-time (i.e. 15 hours onwards) mean fluid temperature data for borehole 6 is shown as a dotted line in Figure 6.32. The slope of the trend line (i.e. 1.464) is used in Equation 6.5 to determine the effective ground thermal conductivity value of 2.89 W/(m·K) for borehole 6 in Table 6.8. The estimated ground thermal conductivity value is then used in Equation 6.7 to determine the borehole thermal resistance value of 0.063 (m·K)/W.

Using the discrete undisturbed ground temperature of 8.2 °C from the fluid circulation method, instead of 8.3 °C, estimates the borehole thermal resistance value as 0.065 (m·K)/W.

**Table 6.8** Ground thermal conductivity and borehole thermal resistance calculations for BH6.

| **Ground thermal conductivity ($\lambda_s$) and borehole thermal resistance ($R_b$) of BH6** | |
|---|---|
| **Ground thermal conductivity** | |
| Average power (W): | 4366 |
| Borehole depth (m): | 82 |
| Injected heat flux, q (W/m): | 53.2 |
| Slope of the trend line, k: | 1.464 |
| $\lambda_s$ (W/(m·K)) = q/(4·pi·k): | 2.89 |
| **Borehole thermal resistance** | |
| Intercept value of the trend line, m = $t_{f,\,1\,hr}$ (°C): | 13.513 |
| Undisturbed ground temperature, $t_0$ (°C): | 8.3 |
| $t_{f,\,1\,hr} - t_0$ (K): | 5.2 |
| Thermal diffusivity, $a_s$ ($m^2$/h): | 0.0047 |
| Borehole radius, $r_b$ (m): | 0.055 |
| Constant, $\gamma$: | 1.78 |
| $R_b$ ((m·K)/W) = $[1/(4 \cdot pi \cdot \lambda_s)] \cdot [\{(t_{f,\,1\,hr} - t_0)/k\} - \ln\{(4 \cdot a_s)/(\gamma \cdot r_b^2)\}]$: | 0.063 |

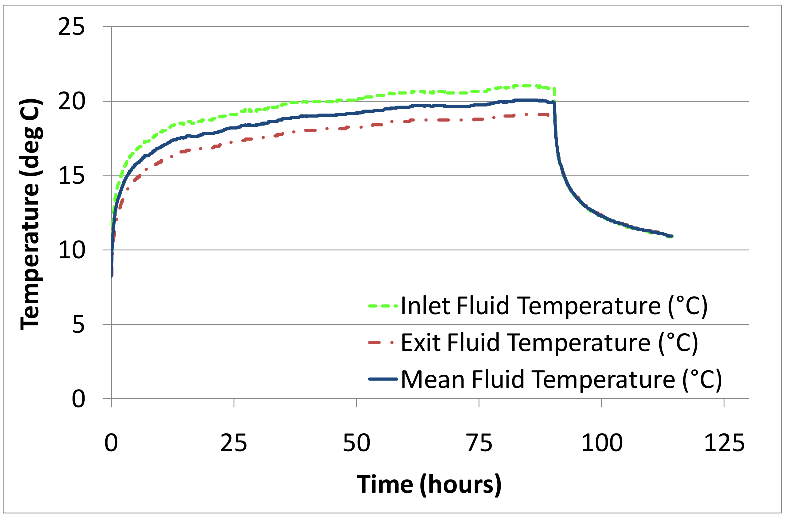


**Figure 6.30** Inlet, exit and mean fluid temperatures for the TRT of BH6.

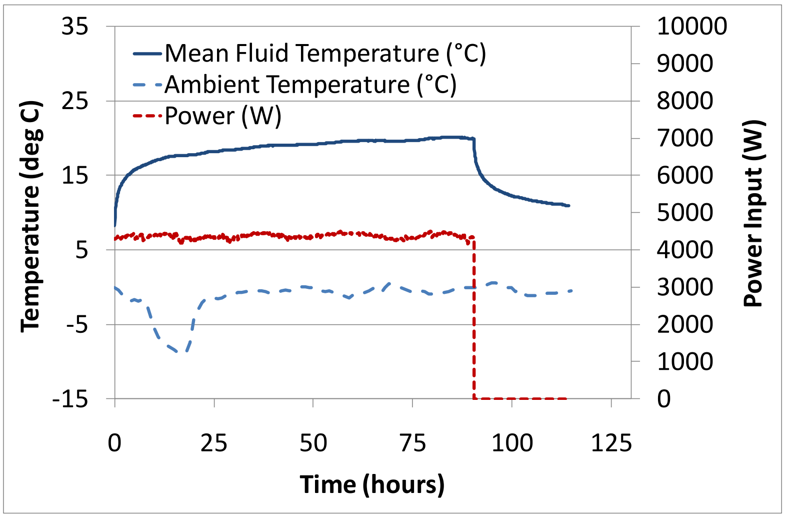


**Figure 6.31** Power input and ambient temperature for the TRT of BH6.

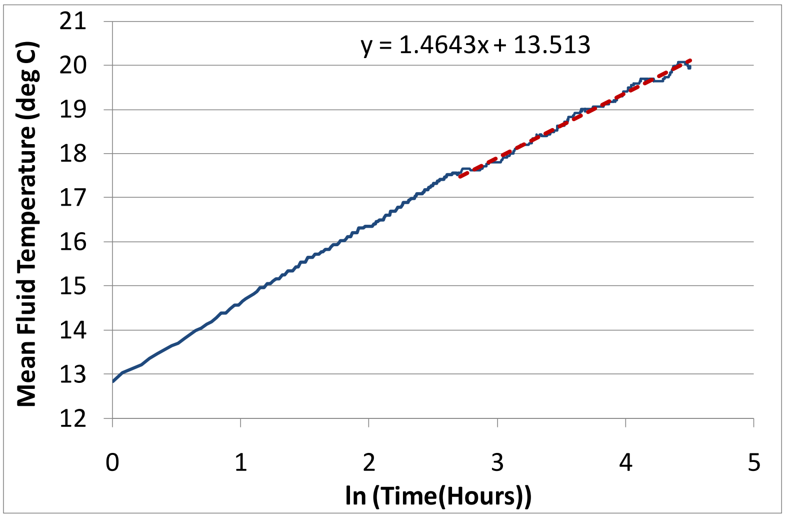


**Figure 6.32** Mean fluid temperature and its late-time trend for TRT of BH6.

### 6.8.7 Borehole 7

Borehole 7 was tested between Feb 9, 2010 and Feb 11, 2010 for 48 hours. The inlet, exit and the mean fluid temperatures of borehole 7 are shown in Figure 6.33. Other test details including power input and the ambient temperature are shown in Figure 6.34.

The trend of the late-time (i.e. 15 hours onwards) mean fluid temperature data for borehole 7 is shown as a dotted line in Figure 6.35. The slope of the trend line (i.e. 1.360) is used in Equation 6.5 to determine the effective ground thermal conductivity value of 3.19 W/(m·K) for borehole 7 in Table 6.9. The estimated ground thermal conductivity value is then used in Equation 6.7 to determine the borehole thermal resistance of 0.064 (m·K)/W.

Using the discrete undisturbed ground temperature of 8.2 °C from the fluid circulation method, instead of 8.3 °C, estimates the borehole thermal resistance value as 0.068 (m·K)/W.

**Table 6.9** Ground thermal conductivity and borehole thermal resistance calculations for BH7.

| **Ground thermal conductivity ($\lambda_s$) and borehole thermal resistance ($R_b$) of BH7** | |
|---|---|
| **Ground thermal conductivity** | |
| Average power (W): | 4361 |
| Borehole depth (m): | 80 |
| Injected heat flux, q (W/m): | 54.5 |
| Slope of the trend line, k: | 1.360 |
| $\lambda_s$ (W/(m·K)) = q/(4·pi·k): | 3.19 |
| **Borehole thermal resistance** | |
| Intercept value of the trend line, m = $t_{f,\,1\,hr}$ (°C): | 13.65 |
| Undisturbed ground temperature, $t_0$ (°C): | 8.3 |
| $t_{f,\,1\,hr} - t_0$ (K): | 5.4 |
| Thermal diffusivity, $a_s$ ($m^2$/h): | 0.0052 |
| Borehole radius, $r_b$ (m): | 0.055 |
| Constant, $\gamma$: | 1.78 |
| $R_b$ ((m·K)/W) = $[1/(4 \cdot pi \cdot \lambda_s)] \cdot [\{(t_{f,\,1\,hr} - t_0)/k\} - \ln\{(4 \cdot a_s)/(\gamma \cdot r_b^2)\}]$: | 0.064 |

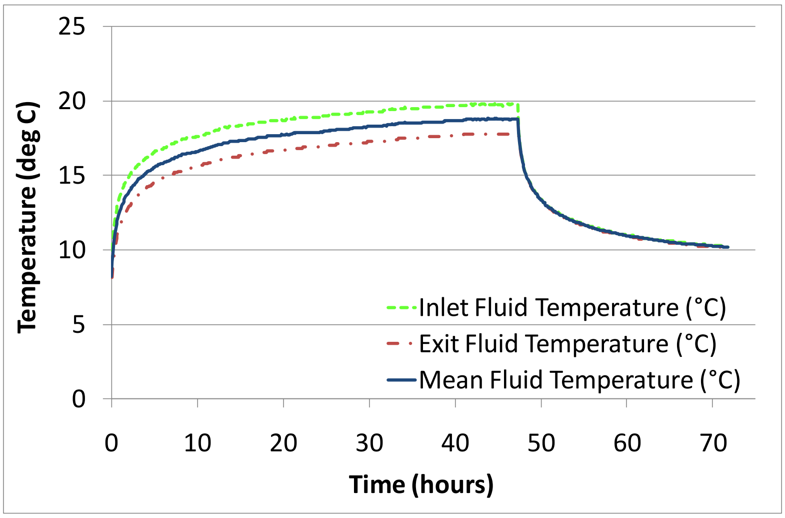


**Figure 6.33** Inlet, exit and mean fluid temperatures for the TRT of BH7.

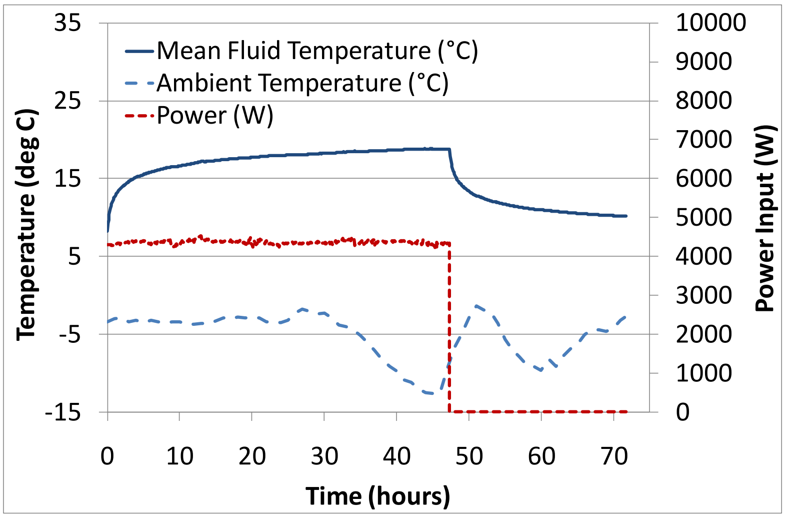


**Figure 6.34** Power input and ambient temperature for the TRT of BH7.

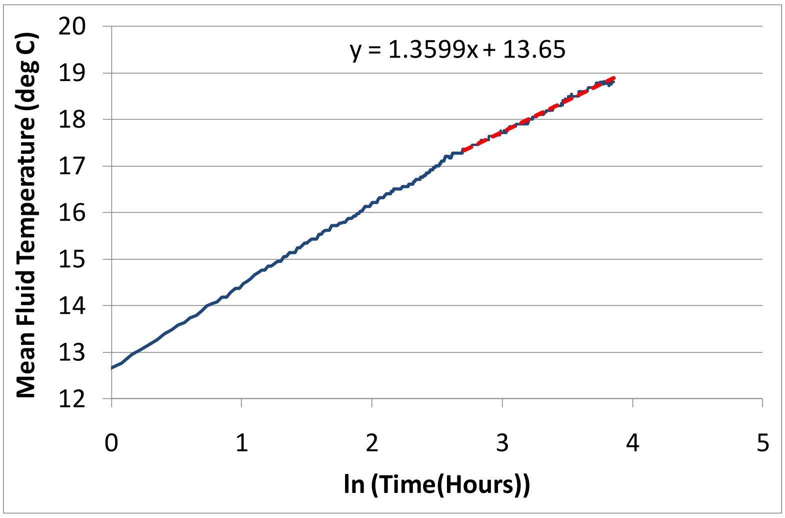


**Figure 6.35** Mean fluid temperature and its late-time trend for TRT of BH7.

### 6.8.8 Borehole 8

Borehole 8 was tested between Feb 5, 2010 and Feb 8, 2010 for 69 hours. The inlet, exit and the mean fluid temperatures of borehole 8 are shown in Figure 6.36. Other test details including power input and the ambient temperature are shown in Figure 6.37.

The trend of the late-time (i.e. 15 hours onwards) mean fluid temperature data for borehole 8 is shown as a dotted line in Figure 6.38. The slope of the trend line (i.e. 1.367) is used in Equation 6.5 to determine the effective ground thermal conductivity value of 3.2 W/(m·K) for borehole 8 in Table 6.10. The estimated ground thermal conductivity value is then used in Equation 6.7 to determine the borehole thermal resistance value of 0.065 (m·K)/W.

Using the discrete undisturbed ground temperature of 8.3 °C from the fluid circulation method also results in the borehole thermal resistance estimation of 0.065 (m·K)/W.

**Table 6.10** Ground thermal conductivity and borehole thermal resistance calculations for BH8.

| **Ground thermal conductivity ($\lambda_s$) and borehole thermal resistance ($R_b$) of BH8** | |
|---|---|
| **Ground thermal conductivity** | |
| Average power (W): | 4400 |
| Borehole depth (m): | 80 |
| Injected heat flux, q (W/m): | 55 |
| Slope of the trend line, k: | 1.367 |
| $\lambda_s$ (W/(m·K)) = q/(4·pi·k): | 3.2 |
| **Borehole thermal resistance** | |
| Intercept value of the trend line, m = $t_{f,\,1\,hr}$ (°C): | 13.738 |
| Undisturbed ground temperature, $t_0$ (°C): | 8.3 |
| $t_{f,\,1\,hr} - t_0$ (K): | 5.4 |
| Thermal diffusivity, $a_s$ ($m^2$/h): | 0.0052 |
| Borehole radius, $r_b$ (m): | 0.055 |
| Constant, $\gamma$: | 1.78 |
| $R_b$ ((m·K)/W) = $[1/(4\cdot pi\cdot\lambda_s)]\cdot[\{(t_{f,\,1\,hr} - t_0)/k\} - \ln\{(4\cdot a_s)/(\gamma\cdot r_b^2)\}]$: | 0.065 |

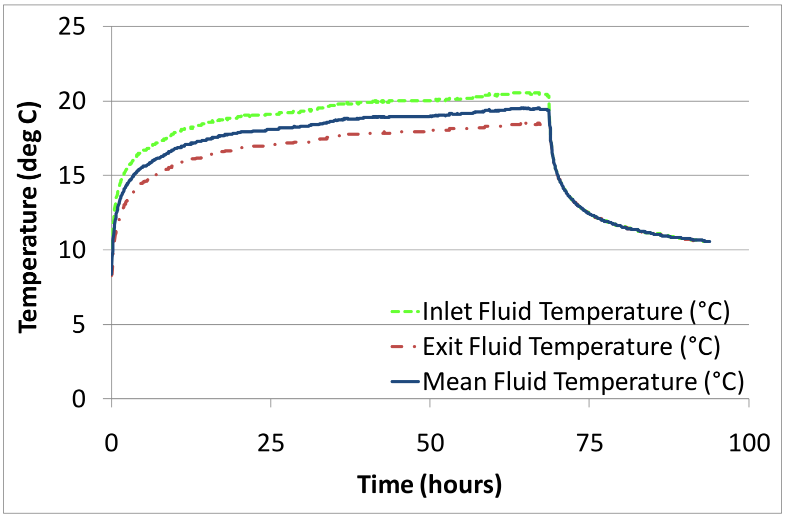


**Figure 6.36** Inlet, exit and mean fluid temperatures for the TRT of BH8.

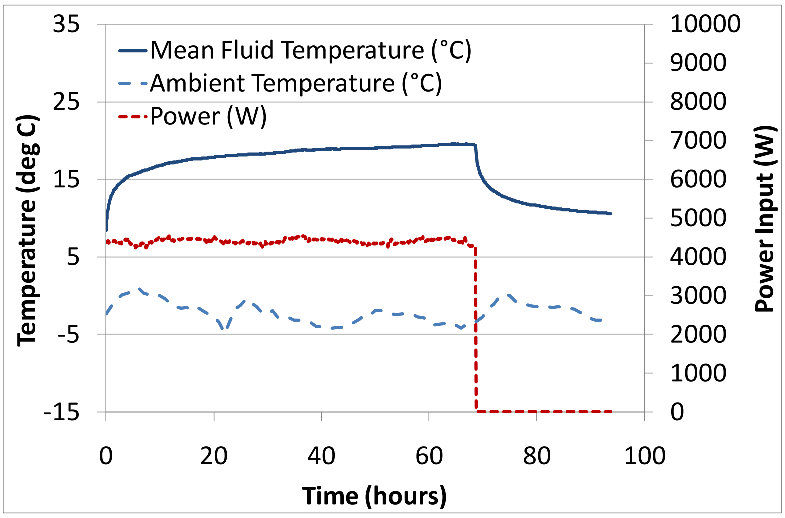


**Figure 6.37** Power input and ambient temperature for the TRT of BH8.

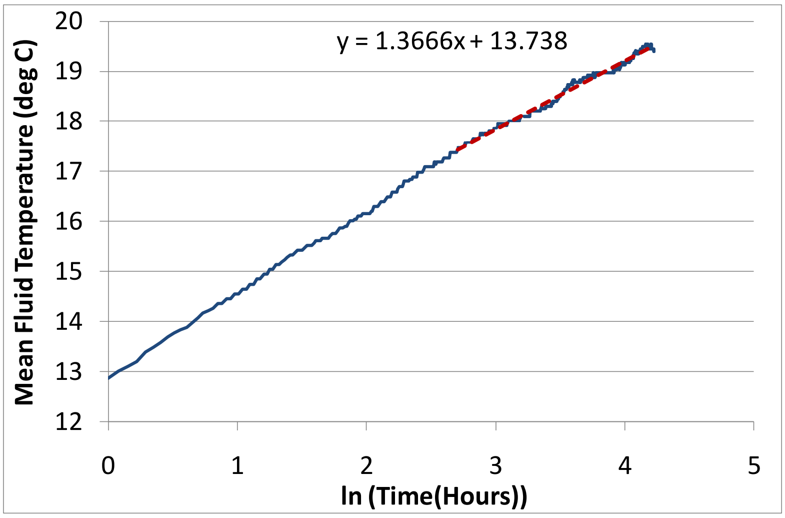


**Figure 6.38** Mean fluid temperature and its late-time trend for TRT of BH8.

### 6.8.9 Borehole 9

Borehole 9 was tested between Dec 10, 2009 and Dec 15, 2009 for 98 hours. The inlet, exit and the mean fluid temperatures of borehole 9 are shown in Figure 6.39. Other test details including power input and the ambient temperature are shown in Figure 6.40.

The trend of the late-time (i.e. 15 hours onwards) mean fluid temperature data for borehole 9 is shown as a dotted line in Figure 6.41. The slope of the trend line (i.e. 1.406) is used in Equation 6.5 to determine the effective ground thermal conductivity value of 3.12 W/(m·K) for borehole 9 in Table 6.11. The estimated ground thermal conductivity value is then used in Equation 6.7 to determine the borehole thermal resistance of 0.069 (m·K)/W.

Using the discrete undisturbed ground temperature of 9.2 °C from the fluid circulation method, instead of 8.3 °C, estimates the borehole thermal resistance value as 0.053 (m·K)/W.

**Table 6.11** Ground thermal conductivity and borehole thermal resistance calculations for BH9.

| **Ground thermal conductivity ($\lambda_s$) and borehole thermal resistance ($R_b$) of BH9** | |
|---|---|
| **Ground thermal conductivity** | |
| Average power (W): | 4403 |
| Borehole depth (m): | 80 |
| Injected heat flux, q (W/m): | 55 |
| Slope of the trend line, k: | 1.406 |
| $\lambda_s$ (W/(m·K)) = q/(4·pi·k): | 3.12 |
| **Borehole thermal resistance** | |
| Intercept value of the trend line, m = $t_{f,\,1\,hr}$ (°C): | 14.001 |
| Undisturbed ground temperature, $t_0$ (°C): | 8.3 |
| $t_{f,\,1\,hr} - t_0$ (K): | 5.7 |
| Thermal diffusivity, $a_s$ ($m^2$/h): | 0.0051 |
| Borehole radius, $r_b$ (m): | 0.055 |
| Constant, $\gamma$: | 1.78 |
| $R_b$ ((m·K)/W) = $[1/(4 \cdot pi \cdot \lambda_s)] \cdot [\{(t_{f,\,1\,hr} - t_0)/k\} - \ln\{(4 \cdot a_s)/(\gamma \cdot r_b^2)\}]$: | 0.069 |

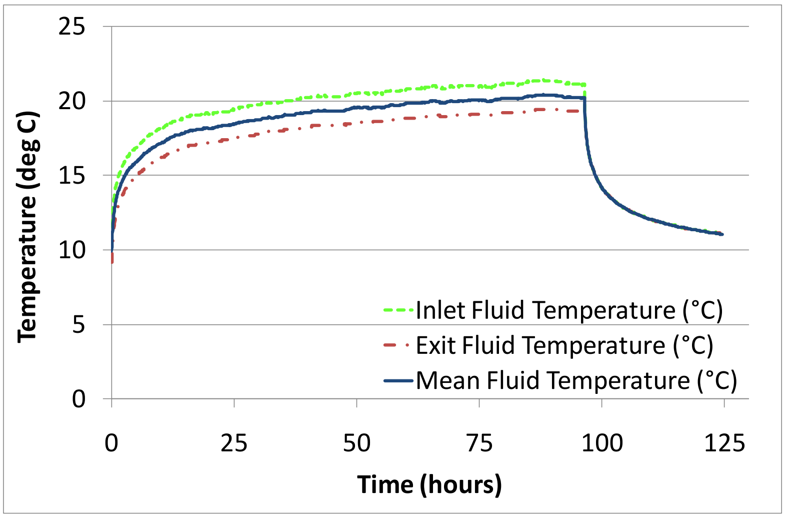


**Figure 6.39** Inlet, exit and mean fluid temperatures for the TRT of BH9.

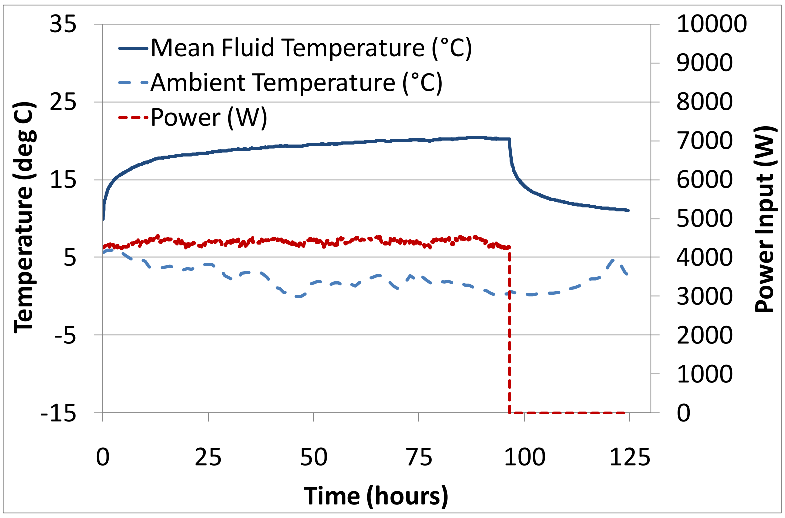


**Figure 6.40** Power input and ambient temperature for the TRT of BH9.

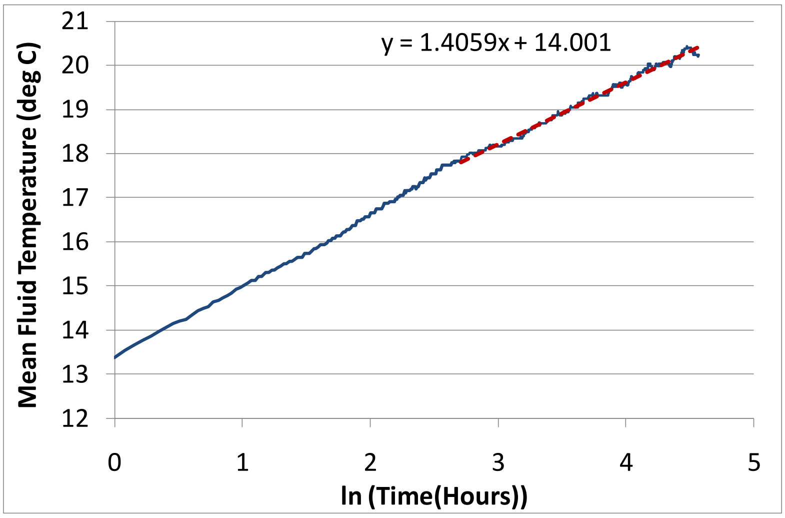


**Figure 6.41** Mean fluid temperature and its late-time trend for TRT of BH9.

## 6.9 Conclusions

The results of ground thermal conductivity and borehole thermal resistance estimations are summarized in Table 6.12. The ground thermal conductivity estimations for the nine boreholes vary between the extreme values of 2.81 and 3.2 W/(m·K). The mean value of the estimated ground thermal conductivities is 3.01 W/(m·K) and the ground thermal conductivity estimations for all nine boreholes lie within ±7 % of this mean value.

The estimated values of borehole thermal resistance vary between the extreme values of 0.049 and 0.074 (m·K)/W if a consistent undisturbed ground temperature value of 8.3 °C is considered. In this case, the estimated borehole thermal resistance values for all nine boreholes can be expressed as 0.0615 ± 0.012 (m·K)/W. If the individual undisturbed ground temperatures, calculated using 'fluid circulation method' and given in Table 6.2, are used to evaluate the borehole thermal resistance, then the estimation of borehole thermal resistance values vary between the extreme values of 0.044 and 0.068 (m·K)/W. In this case, the estimated borehole thermal resistance values for all nine boreholes can be expressed as 0.056 ± 0.012 (m·K)/W.

**Table 6.12** Summary of ground thermal conductivity and borehole thermal resistance estimations for laboratory boreholes.

| **No.** | **Test + recovery duration (Hours)** | **$\lambda_s$ (W/(m·K))** | **$R_b$ ((m·K)/W)** | |
|---|---|---|---|---|
| | | | **Fixed $t_0$ of 8.3 °C** | **Individually determined $t_0$** |
| BH1 | 75 + 20 | 2.88 | 0.059 | 0.044 |
| BH2 | 54 + 24 | 3.06 | 0.064 | 0.057 |
| BH3 | 267 + 64 | 3.04 | 0.074 | 0.063 |
| BH4 | 48 + 17 | 2.81 | 0.049 | 0.045 |
| BH5 | 68 + 26 | 2.98 | 0.064 | 0.062 |
| BH6 | 91 + 24 | 2.89 | 0.063 | 0.065 |
| BH7 | 48 + 25 | 3.19 | 0.064 | 0.068 |
| BH8 | 69 + 25 | 3.20 | 0.065 | 0.065 |
| BH9 | 98 + 28 | 3.12 | 0.069 | 0.053 |

# 7 Analysis of results of thermal response tests

Several factors can influence the results of a Thermal Response Test (TRT) and can hence cause uncertainties in the ground thermal conductivity and the borehole thermal resistance estimations. In this chapter, first the accuracy of the estimated ground thermal conductivity and the borehole thermal resistance values is checked. This is done by comparing the fluid temperatures simulated using the estimated ground thermal conductivity and the borehole thermal resistance values to the experimentally measured fluid temperatures. Accuracy is used in this discussion as a measure of the deviation between modelling and measurement and not in its true metrological sense (e.g. GUM[13] approach). A sensitivity analysis is then performed to see how uncertainties of input variables affect the output. This provides an indicator of the confidence that can be given to the estimated ground thermal conductivity and borehole thermal resistance values.

## 7.1 Introduction

In the previous chapter, the undisturbed ground temperatures for nine boreholes were estimated using two different approaches. The undisturbed ground temperatures were estimated by circulating the fluid for several minutes through the undisturbed borehole and by monitoring the start-up exiting fluid temperatures. The undisturbed ground temperatures estimated by these two approaches were then used to provide estimations of borehole thermal resistance values. The two sets of undisturbed ground temperature and borehole thermal resistance data are used together with the ground thermal conductivity estimations to predict the mean fluid temperatures which are then compared to the experimentally measured fluid temperatures. Next, the sensitivity of the estimated ground thermal conductivity and the borehole thermal resistance to various factors including test duration, power fluctuations and temperature measurements, among others, is investigated.

## 7.2 Comparison of simulated and measured mean fluid temperatures

The mean fluid temperatures are simulated using Equation 6.3 with estimated values of undisturbed ground temperature, ground thermal conductivity and borehole thermal resistance as inputs. The simulated fluid temperatures are then checked for accuracy and are compared to the experimentally measured mean fluid temperatures. As the line source approximation is invalid for times shorter than $20\ r_b^2/a_s$ (i.e. approximately 12 hours for the laboratory boreholes case), the comparisons are therefore made only for times larger than 15 hours. The results of the comparisons are shown in Figures 7.1 to 7.9. In these figures, the mean fluid temperature estimated using undisturbed ground temperature from the ‘start-up exiting fluid’ approach and the resulting borehole thermal resistance value is referred to as Method 1. Method 2 refers to the mean fluid temperature estimation using the undisturbed ground temperature from the ‘fluid circulation’ approach and the corresponding borehole thermal resistance estimation. The results indicate that both methods simulate the mean fluid temperatures reasonably well.

However, in some cases the mean fluid temperatures predicted using Method 1 match the experimental results marginally better than those simulated using Method 2. The overall variations in the simulated fluid temperatures from Method 1 and the experimentally measured fluid temperatures are almost negligible.

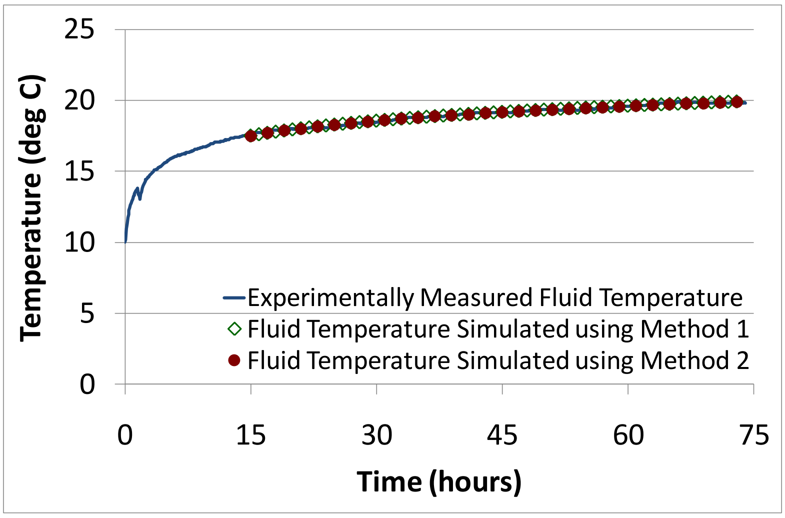


**Figure 7.1** Measured and simulated mean fluid temperatures for BH1.

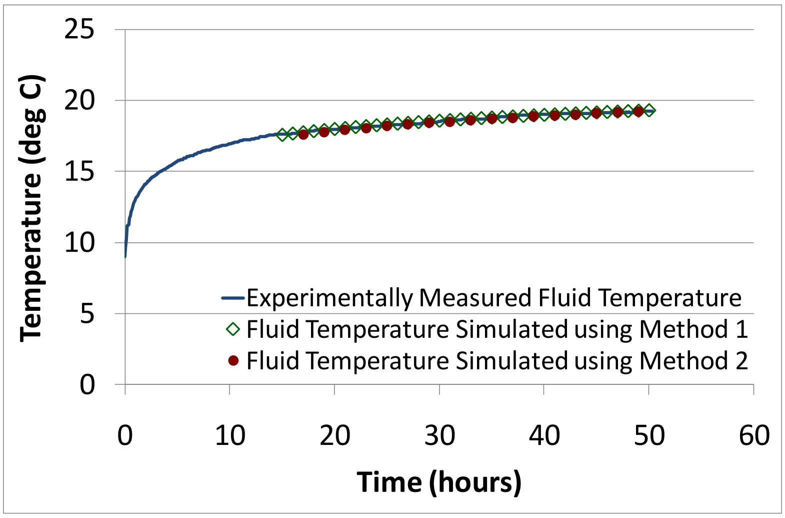


**Figure 7.2** Measured and simulated mean fluid temperatures for BH2.

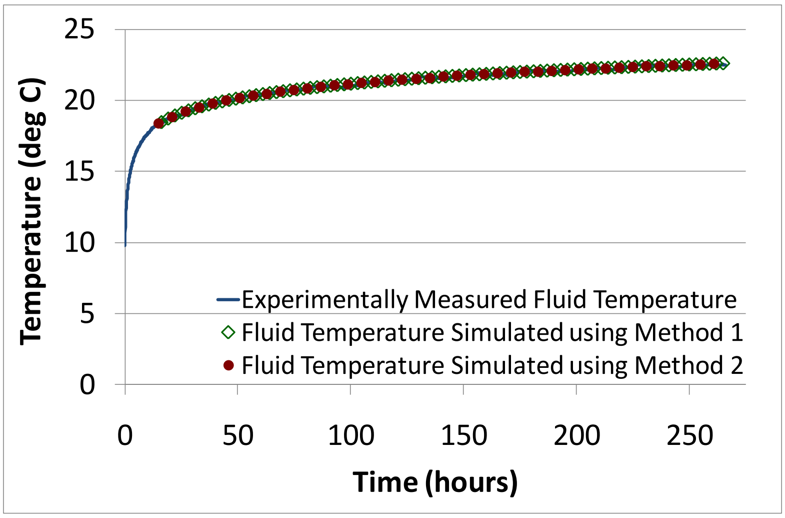


**Figure 7.3** Measured and simulated mean fluid temperatures for BH3.

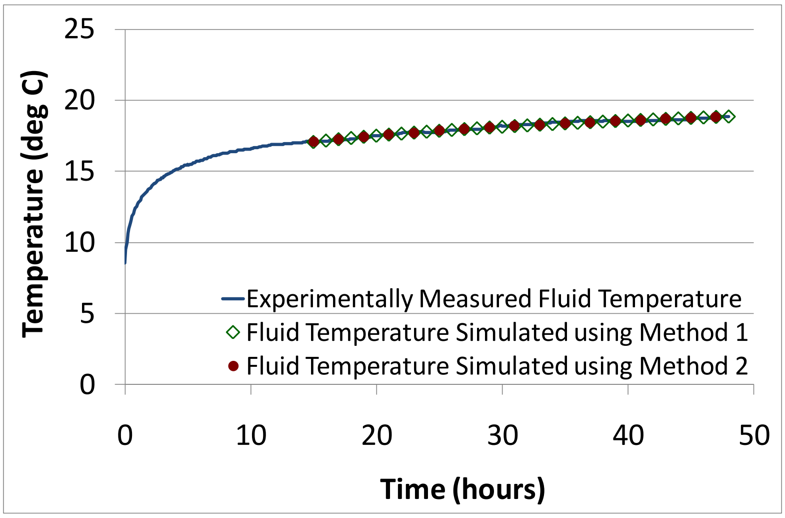


**Figure 7.4** Measured and simulated mean fluid temperatures for BH4.

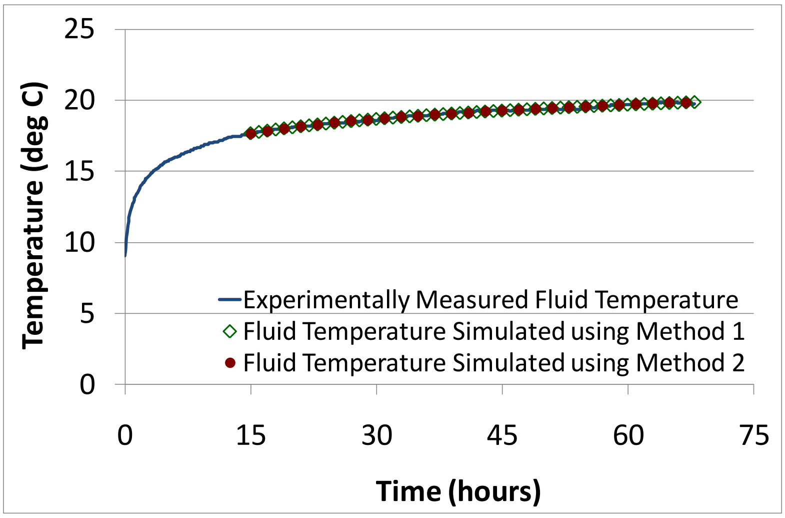


**Figure 7.5** Measured and simulated mean fluid temperatures for BH5.

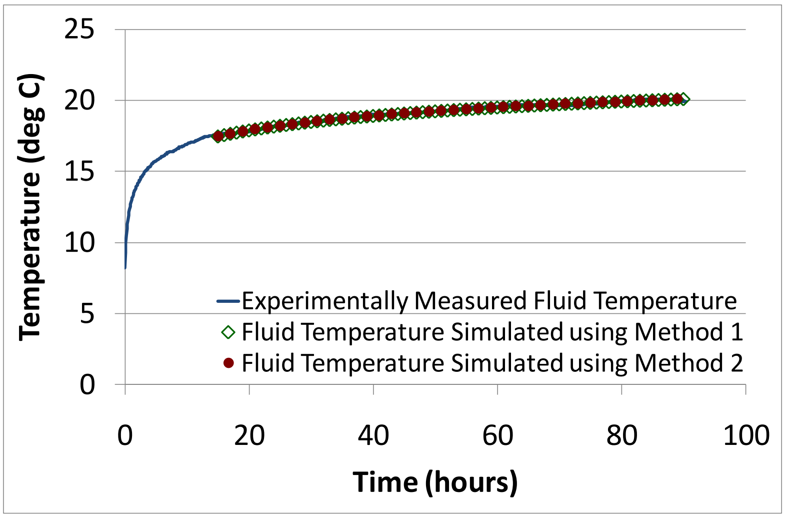


**Figure 7.6** Measured and simulated mean fluid temperatures for BH6.

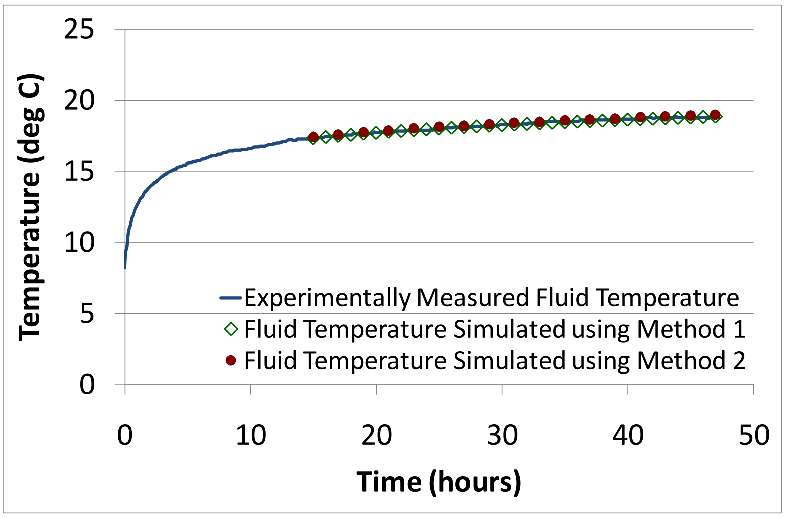


**Figure 7.7** Measured and simulated mean fluid temperatures for BH7.

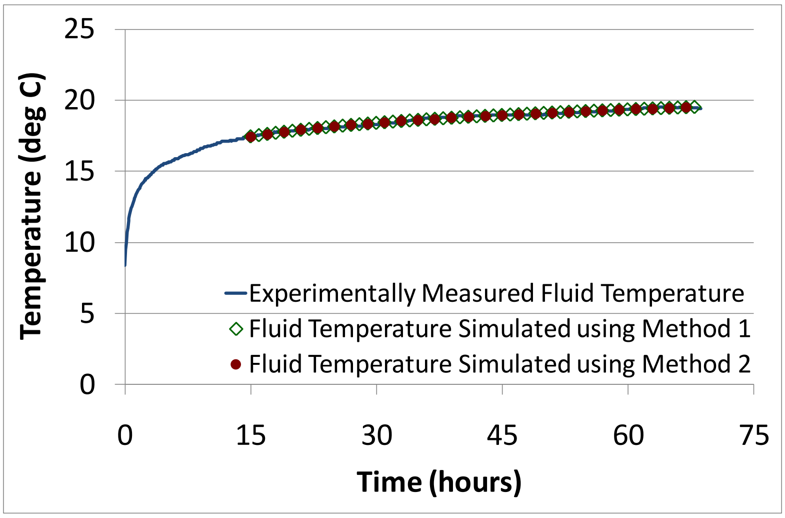


**Figure 7.8** Measured and simulated mean fluid temperatures for BH8.

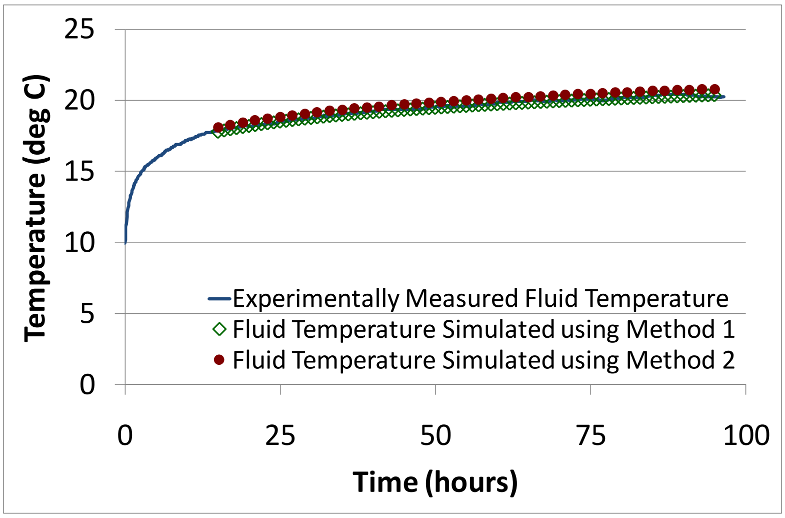


**Figure 7.9** Measured and simulated mean fluid temperatures for BH9.

## 7.3 Sensitivity analysis

The uncertainties in the estimated ground thermal conductivity and borehole thermal resistance values include those induced from the experimental setup, the evaluation method, and the input parameters to the evaluation method. These uncertainties have been identified and studied by Austin[4], Austin et al.[5], Witte et al.[63], Kavanaugh[38], Martin and Kavanaugh[45], Wagner and Clauser[62] and Sharqawy et al.[54], among others. In the following sections, a sensitivity analysis is carried out to determine the impact of the factors identified by these researchers on ground thermal conductivity and borehole thermal resistance estimations for laboratory boreholes. The undisturbed ground temperature determined from the 'start-up exiting fluid' approach and corresponding borehole thermal resistance values were used for the sensitivity analysis.

### 7.3.1 Test duration

The duration of the thermal response test has been often discussed as an uncertainty factor. Some researchers[56, 57] have suggested test durations shorter than 24 hours because of economic reasons. However, a balance must be struck between the test duration and the test accuracy as the ground thermal conductivity estimate converges only after 100 hours[5]. ASHRAE[3] recommends durations of 36-48 hours while Gehlin[27] suggests minimum testing of 60 hours.

In order to check the sensitivity of the ground thermal conductivity estimations to the length of the data used, borehole 3 was tested for over 260 hours. The ground thermal conductivity of borehole 3 has been estimated for various test durations between 30 and 250 hours using the line source approximation and the results are shown in Table 7.1. The estimated ground thermal conductivity converges after around 100 hours and subsequently no significant changes are seen in the estimated values. For test durations between 50 to 100 hours, a maximum absolute deviation of less than 4 % is observed. However, the deviation is significantly higher for test durations shorter than 50 hours and consequently test durations shorter than 50 hours are not recommended to evaluate thermal response tests when using the line source approximation for test evaluation.

**Table 7.1** Ground thermal conductivity estimations and absolute deviations for different test lengths of BH3 and BH9.

| Test duration (Hours) | BH3 | | BH9 | |
|---|---|---|---|---|
| | $\lambda_s$ (W/(m·K)) | Deviation (%) | $\lambda_s$ (W/(m·K)) | Deviation (%) |
| 30 | 3.47 | 13.77 | 3.55 | 15.26 |
| 40 | 2.87 | 5.90 | 3.15 | 2.27 |
| 50 | 2.99 | 1.97 | 3.11 | 0.97 |
| 60 | 2.93 | 3.93 | 3.12 | 1.30 |
| 70 | 2.95 | 3.28 | 3.05 | 0.97 |
| 80 | 2.98 | 2.30 | 3.09 | 0.32 |
| 90 | 2.96 | 2.95 | 3.07 | 0.32 |
| 100 | 3.05 | 0.00 | 3.12 | 1.30 |
| 125 | 3.08 | 0.98 | 3.12* | - |
| 150 | 3.08 | 0.98 | 3.09* | - |
| 175 | 3.07 | 0.66 | 3.08* | - |
| 200 | 3.05 | 0.00 | 3.08* | - |
| 250 | 3.05 | 0.00 | 3.08* | - |

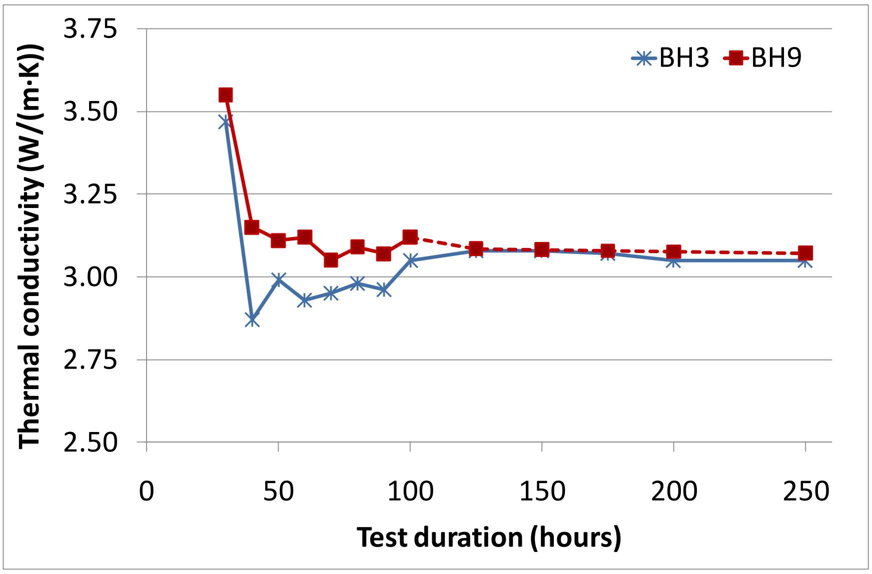


**Figure 7.10** Ground thermal conductivity estimations for different test durations.

The effects of the test duration on the ground thermal conductivity estimation are further investigated by logarithmically extrapolating ground thermal conductivity estimations of borehole 9 up till 250 hours. This is indicated by the dotted line in Figure 7.10. Upon comparison, trends similar to borehole 3 were observed. It was not possible to extrapolate ground thermal conductivity estimations for other boreholes as the estimation values for those boreholes had not converged because of shorter test durations.

The borehole thermal resistance estimation is not very sensitive to the duration of the thermal response test. The borehole thermal resistance estimations for boreholes 3 and 9 remain nearly constant for test durations larger than 50 hours as seen in Figure 7.11. A variation of less than 3 % is observed for any length of test duration between 50 and 250 hours.

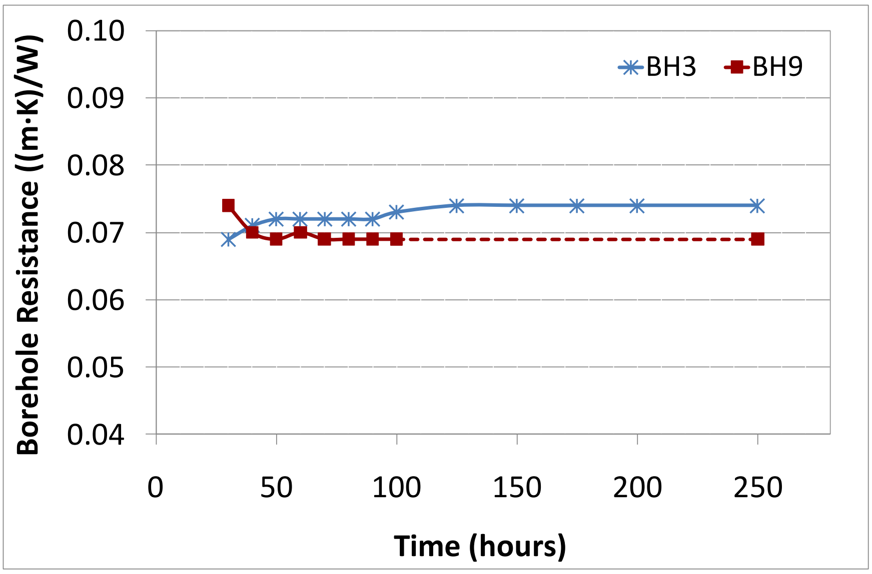


**Figure 7.11** Borehole thermal resistance estimations for different test durations.

### 7.3.2 Power fluctuations

When direct methods are used to evaluate TRTs, fluctuations in supply power can lead to inaccurate results. Both line source and cylindrical source approximations assume constant heat injection rates and hence ground thermal conductivity estimations are inevitably affected in case of excessive power fluctuations. In order to use direct methods to evaluate a thermal response test, ASHRAE[3] recommends that the standard deviation of the input power should be less than ±1.5 % of its mean value and the maximum variation in the input power should be less than ±10 % of its mean value. Moreover, it is also required that the power transducer and the recording device should be able to measure the supplied power within ±2 % of the actual reading.

The thermal conductivity estimations in Chapter 6 were determined using the mean value of the input power. The power inputs were examined and found within the acceptable range of power variations. As seen in Table 7.2, the standard deviation of the power input in most cases was less than or nearly equal to ±1.5 % of the mean input value. In the worst scenario (i.e. the case of BH1), the standard deviation of the input power is ±1.8 % of the mean value. The maximum variations were less than ±5 % of the mean power value for all TRTs. The power input was measured using a high-accuracy meter for all the tests. The uncertainty of the power meter was ±0.15 % of the reading and 0.025 % of the full scale, resulting in a total uncertainty below ±0.5 %.

**Table 7.2** Mean, standard deviation and maximum variation of the input power.

| No. | Mean input power (W) | ±1.5 % of mean power (W) | Standard deviation of input power (W) | Maximum variation of input power (%) |
|---|---|---|---|---|
| BH1 | 4373.36 | 65.60 | 75.29 | -4.92 |
| BH2 | 4391.82 | 65.88 | 41.35 | -3.50 |
| BH3 | 4385.07 | 65.78 | 60.25 | -4.65 |
| BH4 | 4364.92 | 65.47 | 70.87 | +3.97 |
| BH5 | 4388.16 | 65.82 | 53.71 | -4.24 |
| BH6 | 4365.55 | 65.48 | 63.01 | -4.46 |
| BH7 | 4360.52 | 65.41 | 39.77 | +3.93 |
| BH8 | 4400.31 | 66.00 | 58.32 | -3.87 |
| BH9 | 4403.01 | 66.05 | 67.46 | -4.47 |

The effects of changes in the power input on the ground thermal conductivity estimations were investigated and the results are shown in Table 7.3. Two cases of 2 and 5 % increase in power were considered and the corresponding ground thermal conductivity values were estimated. The results indicate that the increments of 2 and 5 % in the input power affect the thermal conductivity estimations by similar percentages. For the laboratory thermal response tests, an overall uncertainty of 1 % in the input power measurement was considered which would affect the ground thermal conductivity estimations by 1 %.

The effects of uncertainties in power input on borehole thermal resistance estimations were analyzed for boreholes 3 and 4. These two boreholes respectively have the maximum and minimum thermal resistance estimations and hence represent the complete range of the thermal resistance values for the nine laboratory boreholes.

Figure 7.12 shows that the increments of 2 and 5 % in the power input rates of boreholes 3 and 4 result in the borehole thermal resistance values falling respectively by around 2.5 and 6 %. Hence it can be concluded that the expected 1 % uncertainty in the input power would affect the borehole thermal resistance estimations by only 1 %.

**Table 7.3** Sensitivity of ground thermal conductivity estimations to power variations.

| No. | Base case | | 2 % power increase | | 5 % power increase | |
|---|---|---|---|---|---|---|
| | Power (W) | $\lambda_s$ (W/(m·K)) | $\lambda_s$ (W/(m·K)) | Change (%) | $\lambda_s$ (W/(m·K)) | Change (%) |
| BH1 | 4373.36 | 2.88 | 2.94 | 2.1 | 3.03 | 5.2 |
| BH2 | 4391.82 | 3.06 | 3.12 | 2.0 | 3.22 | 5.2 |
| BH3 | 4385.07 | 3.04 | 3.10 | 2.0 | 3.20 | 5.3 |
| BH4 | 4364.92 | 2.81 | 2.87 | 2.1 | 2.96 | 5.3 |
| BH5 | 4388.16 | 2.98 | 3.04 | 2.0 | 3.13 | 5.0 |
| BH6 | 4365.55 | 2.89 | 2.95 | 2.1 | 3.04 | 5.2 |
| BH7 | 4360.52 | 3.19 | 3.25 | 1.9 | 3.35 | 5.0 |
| BH8 | 4400.31 | 3.20 | 3.27 | 2.2 | 3.36 | 5.0 |
| BH9 | 4403.01 | 3.12 | 3.18 | 1.9 | 3.27 | 4.8 |

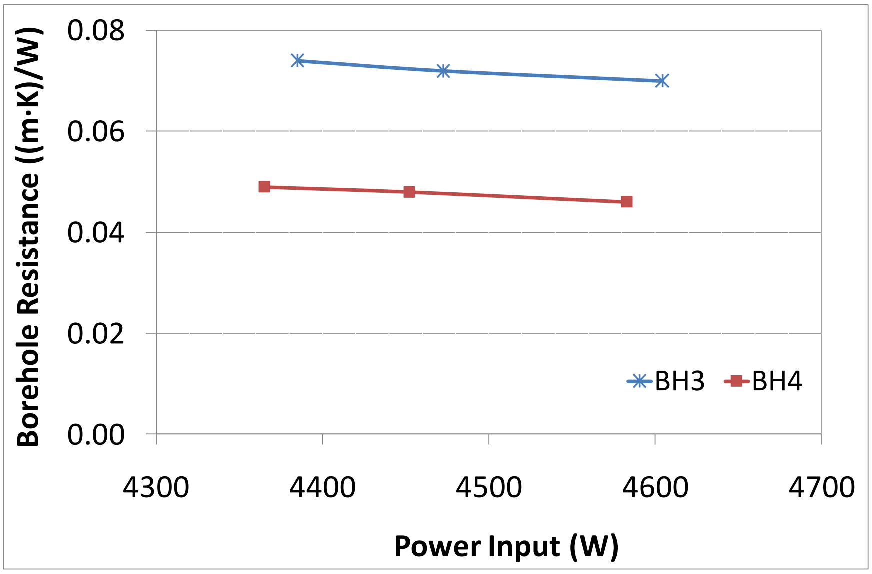


**Figure 7.12** Borehole thermal resistance estimations for different power inputs.

### 7.3.3 Temperature measurements

Ground thermal conductivity estimations are also affected by any uncertainty in the circulating fluid temperature. Improperly calibrated sensors, sensor installation effects and the ambient coupling phenomenon all introduce uncertainties in the measurement of circulating fluid temperature. In this particular case of the laboratory borehole system, the ambient coupling could severely affect the circulating fluid temperature as there is significant length of piping both inside the laboratory and from the laboratory building to the borehole field. All the piping has been insulated to reduce ambient coupling possibilities. Moreover, the temperature of the circulated fluid is measured twice, firstly when entering and leaving the laboratory building and secondly before and after the electric heater, to check for any temperature variations due to ambient coupling.

The variations measured in the mean fluid temperature by two different sets of temperature sensors are shown in Figure 7.13. All sensors were compared with a calibrated sensor before being installed. The resulting corrections were subsequently used in the calculations. The magnitude of variations in the measured temperatures is less than 0.2 K for TRTs of all nine boreholes. This shows that the temperature sensors are reasonably well calibrated and that the ambient coupling remains negligible during the tests. The effects of these slight temperature variations on the ground thermal conductivity and the borehole thermal resistance estimations are almost negligible. Unfortunately, in the existing laboratory setup it was not possible to investigate the effect of shallow ground temperature on the buried horizontal piping.

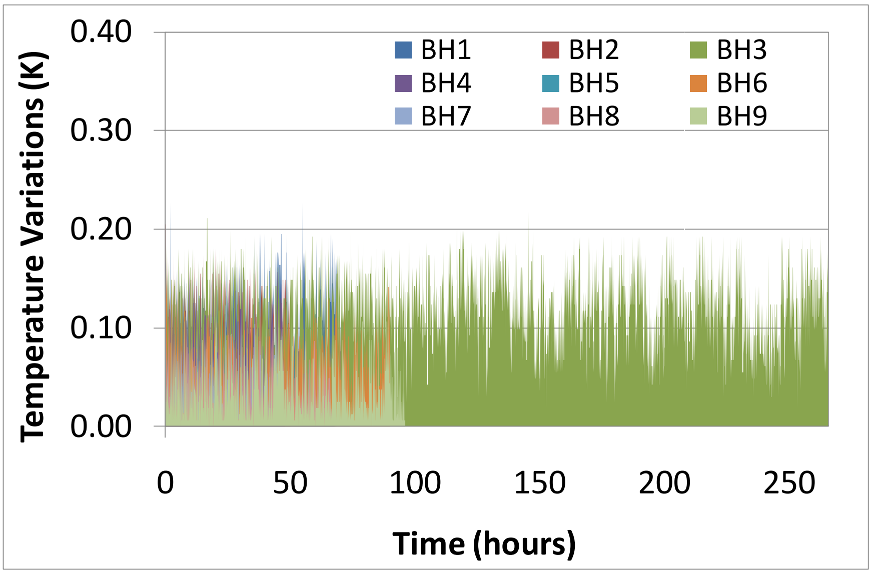


**Figure 7.13** Variations in fluid temperatures measured by two sets of temperature sensors.

### 7.3.4 Undisturbed ground temperature

The uncertainty in the undisturbed ground temperature value does not affect the ground thermal conductivity estimations when the line source approximation is used to evaluate the thermal response tests. However, the borehole thermal resistance estimations do get affected as they are linearly related to the increase in the circulating fluid temperature from the initial undisturbed value. The sensitivity of the borehole thermal resistance to two different values of the undisturbed ground temperature is shown in the Table 7.4. As seen, the difference in borehole thermal resistance estimations can be as high as 25 % when the undisturbed ground temperatures calculated by the ‘fluid circulation’ approach are used instead of temperatures from the ‘start-up exiting fluid’ approach. However, the difference in the two values of borehole thermal resistance does not reflect on the fluid temperature calculations as long as the corresponding value of the undisturbed ground temperature is also used.

**Table 7.4** Sensitivity of borehole thermal resistance estimations to the undisturbed ground temperature value.

| No. | Borehole resistance ((m·K)/W) | | Change (%) |
|---|---|---|---|
| | Fixed $t_0$ of 8.3 °C | Individually determined $t_0$ | |
| BH1 | 0.059 | 0.044 | 25.4 |
| BH2 | 0.064 | 0.057 | 11.0 |
| BH3 | 0.074 | 0.063 | 14.9 |
| BH4 | 0.049 | 0.045 | 8.2 |
| BH5 | 0.064 | 0.062 | 3.1 |
| BH6 | 0.063 | 0.065 | 3.1 |
| BH7 | 0.064 | 0.068 | 6.3 |
| BH8 | 0.065 | 0.065 | 0.1 |
| BH9 | 0.069 | 0.053 | 23.2 |

### 7.3.5 Volumetric heat capacity

When the line source approximation is used to evaluate thermal response tests, the ground thermal conductivity estimations are not sensitive to uncertainties in the ground volumetric heat capacity. This is despite the fact that there exists a strong correlation between the volumetric specific heat and the thermal conductivity of the ground.

The volumetric heat capacity is an indirect input when estimating borehole thermal resistance using the line source approach. It is used to determine the value of ground thermal diffusivity which is a direct input to the method suggested by Beier and Smith[8]. The borehole thermal resistance values for nine laboratory boreholes were originally simulated using volumetric heat capacity value of 2.2 MJ/($m^3$·K), which is typical for Swedish ground formation. However, the effects of uncertainty in the volumetric heat capacity were studied by simulating borehole thermal resistance values for 15 % variation in the volumetric heat capacity of the ground. The results of these simulations are shown in Figure 7.14 for boreholes 3 and 4. The changes in the borehole thermal resistance estimations for both boreholes are of similar numerical magnitude but BH4 has a higher percentage change of around 8 % compared to 5 % for BH3. The percentage change in the borehole thermal resistance estimations for all other boreholes are in between these two values for ±15 % uncertainties in the volumetric heat capacity.

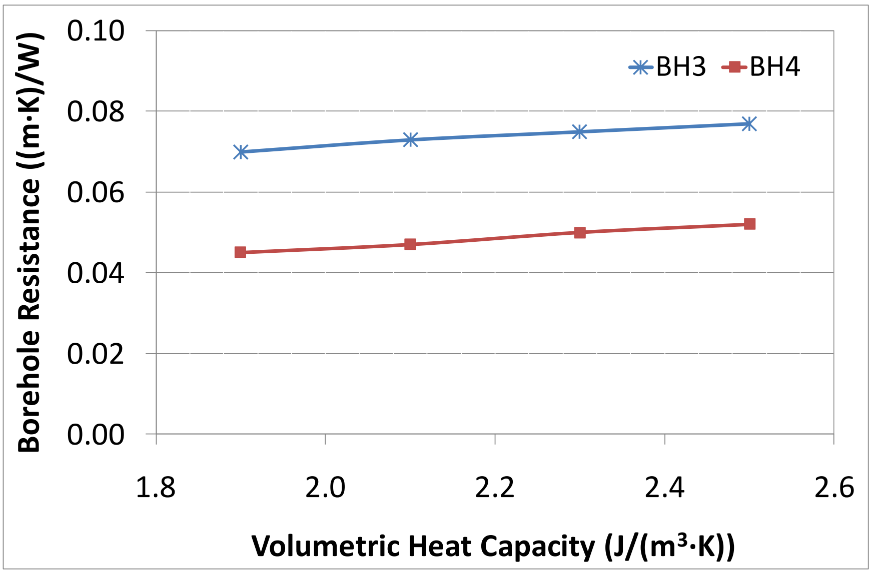


**Figure 7.14** Borehole thermal resistance estimations for different values of volumetric heat capacity.

### 7.3.6 Borehole geometry

The geometry of the borehole includes parameters like diameter and depth of the borehole and number and shank spacing of the U-tubes. Of these parameters, the borehole diameter and the number and the shank spacing of the U-tube have no effect on the ground thermal conductivity estimations by the line source approximation. This is because the line source approximation assumes the borehole as a line source of constant heat output surrounded by an infinite homogeneous medium and ignores the actual borehole geometry. However, the depth of the borehole is an indirect input to the line source approximation as it is used to determine the heat injection rate. The effects of uncertainty in the depth of the boreholes on the thermal conductivity estimations are shown in Table 7.5. As seen, 1 % (i.e. around 0.8 m) uncertainty in the depth of the borehole effects the thermal conductivity estimations by around 1 %.

**Table 7.5** Sensitivity of thermal conductivity estimations to uncertainties in the borehole depth.

| No. | Base case | | 1 % increase in depth | |
|---|---|---|---|---|
| | Depth (m) | $\lambda_s$ (W/(m·K)) | $\lambda_s$ (W/(m·K)) | Change (%) |
| BH1 | 80 | 2.88 | 2.86 | 0.7 |
| BH2 | 80 | 3.06 | 3.03 | 1.0 |
| BH3 | 78 | 3.04 | 3.01 | 1.0 |
| BH4 | 80 | 2.81 | 2.79 | 0.7 |
| BH5 | 80 | 2.98 | 2.95 | 1.0 |
| BH6 | 82 | 2.89 | 2.86 | 1.0 |
| BH7 | 80 | 3.19 | 3.16 | 1.0 |
| BH8 | 80 | 3.20 | 3.17 | 0.9 |
| BH9 | 80 | 3.12 | 3.08 | 1.3 |

On the other hand, the effects of 1 % uncertainty in the borehole depth on the borehole thermal resistance estimations are negligible and can be easily ignored. However, in contrast to the ground thermal conductivity estimation, the borehole thermal resistance estimation is sensitive to the uncertainties of the borehole radius. The effects of ±1 % uncertainties in the radii of boreholes 3 and 4 are shown in Figure 7.15. Once again, the changes in the borehole thermal resistance estimations for both boreholes are of similar numerical magnitude but BH4 has a higher percentage change of around 12 % when compared with 8 % for BH3. The percentage change in the borehole thermal resistance estimations for ±1 % uncertainties in the radii of the other boreholes lie between the two extremes of BH3 and BH4.

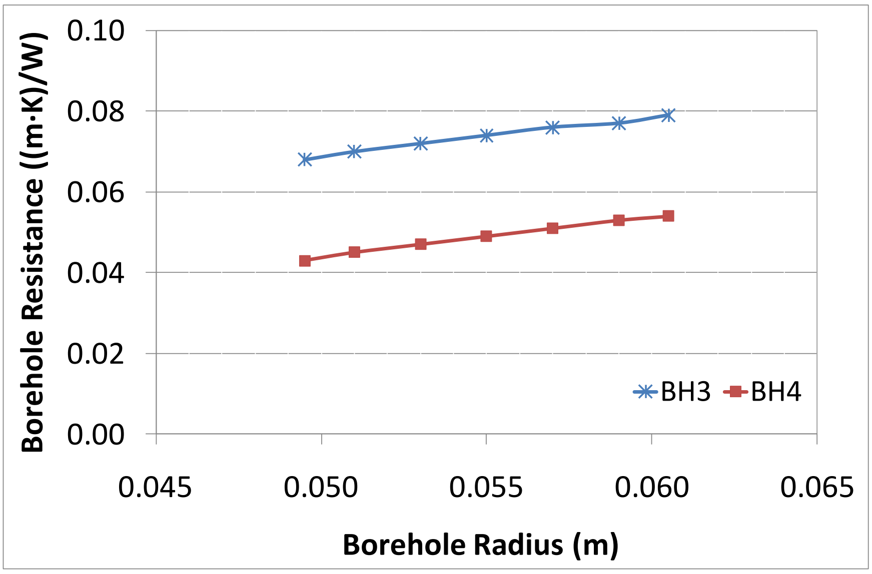


**Figure 7.15** Borehole thermal resistance estimations for different borehole radii.

### 7.3.7 Model Accuracy

As discussed earlier in Chapter 6, the line source approximation is valid for times larger than 20 $r_b^2/a_s$. This is because the accuracy of the Equation 6.1 to approximate the integral increases with time. The error for time 5 $r_b^2/ a_s$ is around 10 % which decreases to less than 2.5 % for times larger than 20 $r_b^2/a_s$[27]. For the laboratory boreholes system the value 20 $r_b^2/a_s$ translates to around 12.5 hours. Hence, the data of the first 15 hours was disregarded when evaluating thermal response tests. For comparison purposes, additional simulations disregarding initial data of 20 and 25 hours were also carried out. The results, shown in Table 7.6, indicate that the increased length of disregarded data has little effect on the estimates of thermal conductivity except for relatively short tests. For tests shorter than 60 hours, disregarding the initial data of 20 to 25 hours affects the slope of the late-time trend line which consequently influences ground thermal conductivity estimations.

The method used to estimate the borehole thermal resistance has been tested previously[8]. The method can estimate the borehole thermal resistance within 10 % of the actual value. The effects of disregarding 15 to 25 hours of test data on the thermal resistance estimations were simulated for boreholes 3 and 4. The results of these simulations are shown in Figure 7.16. No changes in thermal resistance were noticed for borehole 3 which has the longest test duration. In contrast, variations around 10 % in the thermal resistance estimations were recorded for borehole 4 if initial test data of 20-25 hours are disregarded. However, these variations in the borehole thermal resistance are more because of the changes in the estimated ground thermal conductivity values than anything else.

**Table 7.6** Sensitivity of thermal conductivity estimations to the length of disregarded data.

| No. | 15 hours of data disregarded | | 20 hours of data disregarded | | 25 hours of data disregarded | |
|---|---|---|---|---|---|---|
| | Duration (hours) | $\lambda_s$ (W/(m·K)) | $\lambda_s$ (W/(m·K)) | Change (%) | $\lambda_s$ (W/(m·K)) | Change (%) |
| BH1 | 74 | 2.88 | 2.81 | 2.4 | 2.81 | 2.4 |
| BH2 | 54 | 3.06 | 2.99 | 2.3 | 2.92 | 4.5 |
| BH3 | 267 | 3.04 | 3.04 | 0.1 | 3.05 | 0.3 |
| BH4 | 48 | 2.81 | 2.95 | 5.0 | 2.98 | 6.0 |
| BH5 | 68 | 2.98 | 2.95 | 1.0 | 2.93 | 1.7 |
| BH6 | 91 | 2.89 | 2.90 | 0.3 | 2.96 | 2.1 |
| BH7 | 48 | 3.19 | 3.15 | 1.2 | 3.19 | 0.1 |
| BH8 | 69 | 3.20 | 3.16 | 1.2 | 3.12 | 2.5 |
| BH9 | 96 | 3.12 | 3.07 | 1.6 | 3.13 | 0.3 |

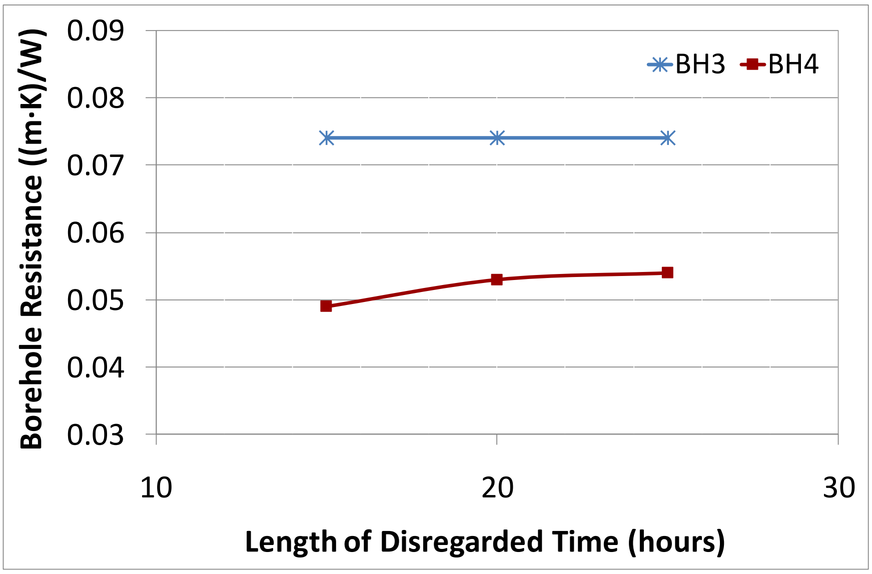


**Figure 7.16** Borehole thermal resistance estimations for different lengths of disregarded data.

## 7.4 Conclusions

As observed in Chapter 6, ground thermal conductivity and borehole thermal resistance estimations, for nine laboratory boreholes, vary up to ±7 and ±20 % of their respective mean values. In this chapter, first the estimated ground thermal conductivity and borehole thermal resistance values were used to simulate the mean fluid temperatures. The simulated temperatures were then compared to the experimentally measured fluid temperatures. Comparisons showed that the estimated values can be used to accurately simulate the mean fluid temperatures. A sensitivity analysis to determine the effects of uncertainties in various input parameters was then carried out. The results of the sensitivity analysis are summarized in Table 7.7.

**Table 7.7** Uncertainties in the estimated values of ground thermal conductivity and borehole thermal resistance.

| Factors | Uncertainty in estimated $\lambda_s$ | Uncertainty in estimated $R_b$ |
|---|---|---|
| Test duration between 50 and 100 hours | ± 4 % | ± 3 % |
| Power fluctuations of ± 1 % | ± 1 % | ± 1 % |
| Temperature measurement uncertainty of ± 0.15 K | < ±1 % | < ±1 % |
| Uncertainty of ± 0.9 K in undisturbed ground temperature measurement | - | ± 25 % |
| Uncertainty of ± 15 % in the volumetric heat capacity | - | ± 8 % |
| Borehole geometry | | |
| – ± 1 % uncertainty in borehole depth | ± 1 % | < ±1 % |
| – ± 1 % uncertainty in borehole radius | - | ± 8 % |
| Estimation method | ± 2.5 % | ± 10 % |

# 8 Discussion and conclusions

The design of a GSHP system is an intricate procedure. It is based on the load profile of the building, the operating characteristics of the heat pump and the thermal response of the borehole field. The design of the borehole field is of particular interest. The optimized design of the borehole field not only enhances the overall performance of the GSHP system but also provides environmental and economical benefits. This thesis presented several methods that can be used to optimize the design of a borehole field for GSHP system applications. The procedure of estimating properties using thermal response tests was investigated and major improvements in the modelling and simulation of borehole systems were suggested. The following sections provide a summarizing discussion of the research reported in this thesis.

## 8.1 Discussion

This thesis has looked into different aspects of improving the design procedure for borehole fields. Firstly, borehole modelling and simulation procedures were critically analyzed from a design perspective. It was noted that there is only a limited number of programs available to design a multiple borehole system. The available programs are not only costly but can also be complicated to use. To address these issues, different combinations of existing analytical single borehole solutions were tested to model multiple borehole systems. The suggested methods calculate the borehole wall temperature of individual boreholes and then account for the temperature penalty from surrounding boreholes by applying a superposition principle. The results, which were compared to an exact numerical solution, indicated that the suggested methods can be successfully used to simulate the multiple borehole system. One limitation to this approach is that the calculation time increases with the increasing number of boreholes. The computational efficiency decreases significantly for systems larger than 20 boreholes.

Secondly, it was noted that one of the major hurdles in optimizing the control and operation of GSHP systems is the unavailability of an accurate short-term response analytical solution. The existing analytical solutions are inaccurate and use ambiguous and inexplicit corrections which contradict the essence and purpose of analytical solutions. This lead to the development of an exact analytical solution which was later tested with remarkable accuracy against experimental data to determine the short-term borehole response. A flexible numerical solution was also developed. The implementation of the new solutions into building energy simulation software will enable optimized design of the whole GSHP system.

Finally, the effects of uncertainties of the input parameters on the borehole system design were investigated. In practice, the input parameters are either estimated for small systems or determined experimentally for large systems. Thermal response tests were conducted on nine laboratory boreholes which were drilled specifically for this work. The undisturbed ground temperature, ground thermal conductivity and borehole thermal resistance values were estimated for all nine boreholes. It was shown that the estimated parameters can accurately simulate the experimentally measured fluid temperatures. A sensitivity analysis of the undisturbed ground temperature, ground thermal conductivity and borehole thermal resistance estimations was also carried out to see the effects of various design uncertainties. The estimated values of undisturbed ground temperature, ground thermal conductivity and borehole thermal resistance for the nine boreholes had slight variations. The undisturbed ground temperature that was calculated by using the ‘fluid circulation’ approach varied between 8.2 and 9.2 °C for the nine boreholes but gave a consistent value of 8.3 °C using the “start-up exit fluid” approach. The ground thermal conductivity estimations varied between 2.81 and 3.20 W/(m·K). The variations in the estimated values of borehole thermal resistance were between 0.049 and 0.074 (m·K)/W, when calculated using the undisturbed ground temperature value of 8.3 °C. When the undisturbed ground temperatures estimated from the ‘fluid circulation’ approach were used to calculate the borehole thermal resistance then the calculated values varied between 0.044 and 0.068 (m·K)/W.

**Table 8.1** Two sets of estimated parameters for laboratory boreholes.

| No. | Set A | | | Set B | | |
|---|---|---|---|---|---|---|
| | $t_0$ (°C) | $\lambda_s$ (W/(m·K)) | $R_b$ ((m·K)/W) | $t_0$ (°C) | $\lambda_s$ (W/(m·K)) | $R_b$ ((m·K)/W) |
| BH1 | 8.3 | 2.88 | 0.059 | 9.1 | 2.88 | 0.044 |
| BH2 | 8.3 | 3.06 | 0.064 | 8.7 | 3.06 | 0.057 |
| BH3 | 8.3 | 3.04 | 0.074 | 8.9 | 3.04 | 0.063 |
| BH4 | 8.3 | 2.81 | 0.049 | 8.5 | 2.81 | 0.045 |
| BH5 | 8.3 | 2.98 | 0.064 | 8.4 | 2.98 | 0.062 |
| BH6 | 8.3 | 2.89 | 0.063 | 8.2 | 2.89 | 0.065 |
| BH7 | 8.3 | 3.19 | 0.064 | 8.2 | 3.19 | 0.068 |
| BH8 | 8.3 | 3.20 | 0.065 | 8.3 | 3.20 | 0.065 |
| BH9 | 8.3 | 3.12 | 0.069 | 9.2 | 3.12 | 0.053 |

One issue not addressed in Chapter 7 is the effects of variations in the estimated parameters on the design of the borehole system. This issue can be investigated by simulating the expected mean fluid temperature of a single borehole using the sets of parameters estimated for the nine laboratory boreholes. Studying the fluid temperature deterioration over time for different parameter sets will indicate the effect of the variations in estimated parameters on the performance of a single borehole. Figures 8.1 and 8.2 show the fluid temperatures simulated for a single borehole using the line source approximation. The fluid temperatures are simulated for 25 years of operation using a constant heat flux of 50 W/m and two data sets given in Table 8.1. The data sets are based on the estimated undisturbed ground temperature, ground thermal conductivity and borehole resistance values for the nine laboratory boreholes as calculated in Chapter 6. As observed earlier in Section 7.2, there is no significant variation between the predicted fluid temperatures of any particular borehole simulated using either of the two data sets. However, the fluid temperatures predicted for nine boreholes have variations despite using same input data. The largest variation is between the predicted fluid temperatures of borehole 6 and borehole 8. Both these boreholes have similar values of estimated boreholes thermal resistances but the ground thermal conductivity values vary slightly. The difference in the ground thermal conductivity values results in mean fluid temperatures of boreholes 6 and 8 varying by around 1 °C. The variation in the mean fluid temperatures of these two boreholes remains nearly constant throughout the simulated time of 25 years. Uncertainties like these in the estimated parameters are typically countered by adding a few additional meters to the required borehole length.

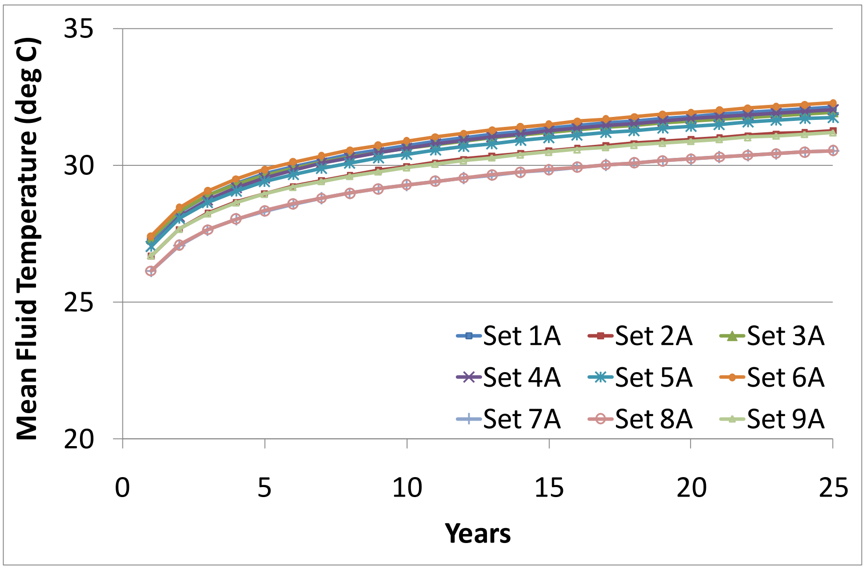


**Figure 8.1** Mean fluid temperatures of a single borehole using data set A.

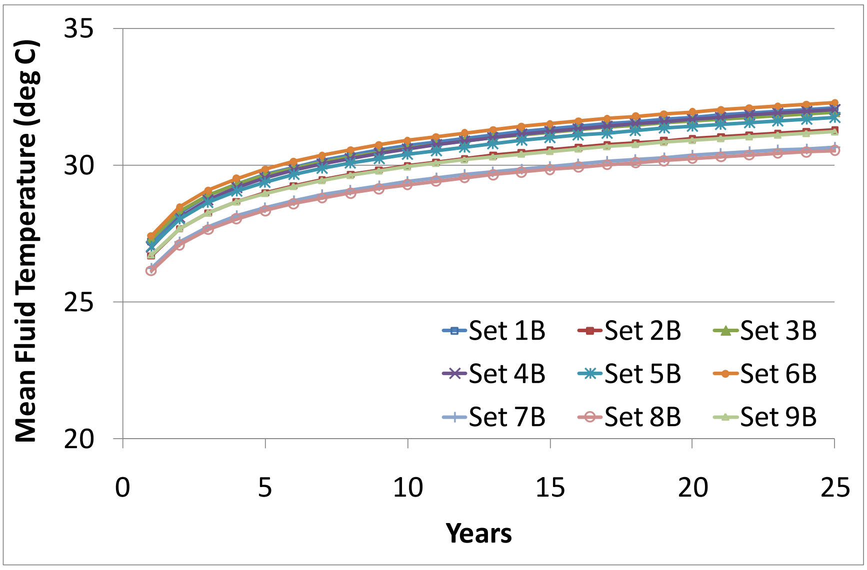


**Figure 8.2** Mean fluid temperatures of a single borehole using data set B.

The two extreme cases of borehole 6 and 8 were also tested for a multiple borehole configuration. The Astronomy-House case study from Chapter 3 was used to analyze the effects of ground thermal conductivity and borehole thermal resistance variations on the design of a multiple borehole system. As seen from Figure 8.3, the two apparently different data sets of estimated parameters for boreholes 6 and 8 result in similar maximum and minimum fluid temperatures for a 4x5 borehole system throughout 25 years of its operation. As the Astronomy-House building has both heating and cooling requirements the variations in predicted fluid temperatures are even smaller than those seen earlier for a single borehole.

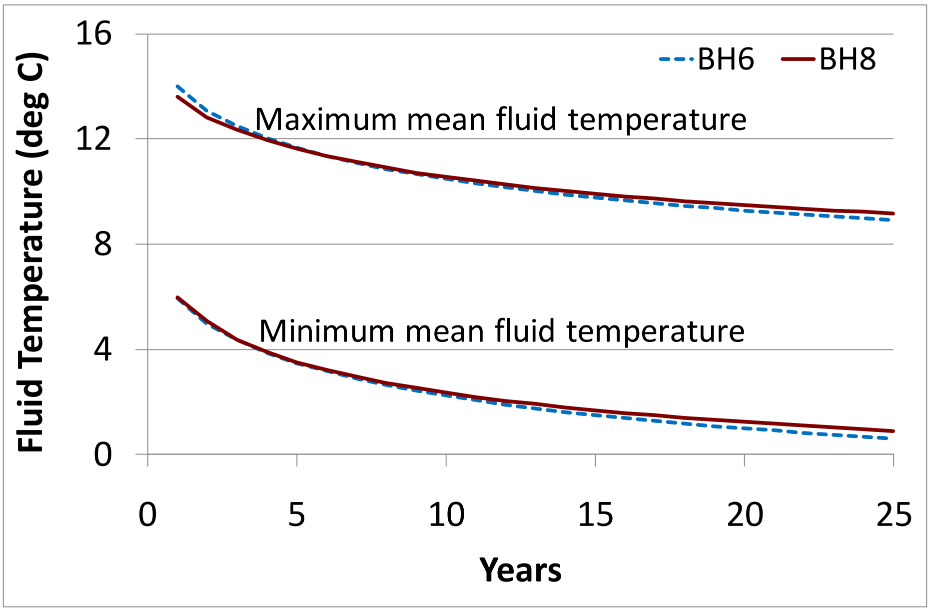


**Figure 8.3** Fluid temperatures of a 4x5 borehole system using thermal conductivity and borehole resistance estimations of boreholes 6 and 8.

The above discussion indicates that the variations among different sets of experimentally estimated thermal conductivity and borehole resistance values do not significantly affect the design of a borehole field. However, further investigations should be carried out to confirm this finding.

## 8.2 Conclusions

The research presented in this thesis can be concluded as:

- The simple analytical solutions, presented in the Chapter 2 of this thesis, can be used to model the long-term response of single and multiple boreholes. The results from all the noteworthy analytical solutions are rather close to each other but the finite length line source gives more accurate results than other solutions when compared to the state-of-the-art Superposition Borehole Model. On the other hand, the existing analytical solutions cannot accurately determine the short-term response of the borehole system. This is because the existing analytical solutions use simplifying assumptions regarding geometry and heat transfer of the borehole and hence distort the predicted short-term response of the borehole.

- The new analytical and numerical solutions presented in this thesis can accurately determine the short-term response of the borehole system. The developed solutions are validated using different approaches including inter-model comparison, comparison with a semi-analytical solution and comparison with experimental data. The new solutions are flexible and can be used as stand-alone applications or alternatively be implemented in building energy simulation software.

- A new GSHP laboratory has been developed. The laboratory has a borehole system consisting of 9 boreholes coupled with three heat pumps and five storage tanks. The laboratory can be used to conduct thermal response tests, to develop and validate system and component models and to test operation and control strategies.

- A battery of thermal response tests was conducted to estimate undisturbed ground temperature, ground thermal conductivity and borehole thermal resistance. It was shown that the "start-up exit fluid temperature" approach provides consistent undisturbed ground temperature estimations. If the fluid is allowed to circulate for 25-30 minutes then the temperature of the top ground layer affects the undisturbed ground temperature measurement. The estimated mean ground thermal conductivity value was 3.01 W/(m·K). The ground thermal conductivity estimations for all nine boreholes lie within ±7 % of the mean value. The estimated borehole thermal resistance values using the line source approximation depend on the value of the undisturbed ground temperature. If the undisturbed ground temperature of 8.3 °C, as estimated by the "start-up exit fluid temperature" approach, is used for all nine boreholes then the estimated mean borehole thermal resistance values are in the range 0.0615 ± 0.012 (m·K)/W. On the other hand, if the individual undisturbed ground temperatures estimated using the 'fluid circulation' approach are used, then the borehole thermal resistance values are in the range 0.056 ± 0.012 (m·K)/W.

- Despite having two estimated borehole thermal resistance values for any particular borehole, the mean fluid temperature of the boreholes can be accurately predicted if the corresponding value of undisturbed ground temperature is used. When using the line source approximation, the borehole thermal resistance estimations are more sensitive than the thermal conductivity estimations to the uncertainties of the input data. The uncertainties of the borehole radius, undisturbed ground temperature and volumetric heat capacity of the ground all affect the borehole thermal resistance estimations considerably. The largest uncertainty in the estimations of ground thermal conductivity using the line source approximation is caused by the short length of the test duration.

- The variations between the estimated ground thermal conductivity and borehole thermal resistance values for any two boreholes do not significantly affect the design of the borehole field.

## 8.3 Future work

In this thesis the foundation of a major work to improve the design process of GSHP system applications was reported. The work planned for next phase of the project is summarized in the following.

- The short-term response solutions presented in this thesis will be implemented in a building energy simulation software. The implementation will enable the dynamic modelling and operation and performance optimization of the GSHP system.

- A stand-alone program to determine both the long and short term response of the borehole system will be developed. The program will make use of load aggregation techniques to enable swift modelling and simulation of the borehole system.

- The new analytical solution will be adapted to evaluate thermal response tests and to estimate ground and borehole thermal properties. This will hopefully decrease the required duration of the thermal response test.

- More thermal response tests will be conducted to see the effects of heat input, flow rate and other parameters. The thermal response tests will also be conducted in a heat extraction mode and comparisons to tests in the heat injection mode will be made. Investigations regarding the required time before repeating a test will also be conducted.

- Experimental investigations regarding short-term borehole response, long-term borehole performance deterioration and the thermal interaction between boreholes will be carried out. The thermal response of peripheral and central boreholes and attainable free cooling in relation to heat injection will also be studied for different borehole field configurations.

- The existing and new control strategies for simple and hybrid GSHP system configurations will be tested to identify key optimization parameters.

# 9 References


1. Abramowitz, M, Stegun, I, 1964. Handbook of Mathematical Functions. (Dover Publications.) New York.

2. Andersson, O, 2009. Ground source heating and cooling in Sweden. IEA Heat Pump Newsletter, vol. 27, no. 2/2009, pp. 19-22.

3. ASHRAE, 2007. HVAC Applications. (American Society of Heating, Refrigerating and Air-Conditioning Engineers.) Atlanta.

4. Austin, W, 1998. Development of an In-situ System for Measuring Ground Thermal Properties. Mechanical And Aerospace Engineering, M.Sc. Thesis, (Oklahoma State University.) USA.

5. Austin, W, Yavuzturk, C, Spitler, J, 2000. Development of an in-situ system for measuring ground thermal properties. ASHRAE Transactions, vol. 106(1), pp. 365-379.

6. Bandos, T V, Montero, Á, Fernández, E, Santander, J, Isidro, J, Pérez, J, Córdoba, P, Urchueguía, J, 2009. Finite line-source model for borehole heat exchangers: effect of vertical temperature variations. Geothermics, vol. 38, no. 2, pp. 263-270.

7. Bandyopadhyay, G, Gosnold, W, Mann, M, 2008. Analytical and semi-analytical solutions for short-time transient response of ground heat exchangers. Energy and Buildings, vol. 40, no. 10, pp. 1816-1824.

8. Beier, R A, Smith, M D, 2002. Borehole thermal resistance from line-source model of in-situ tests. ASHRAE Transactions, vol. 108 PART 2, pp. 212-219.

9. Beier, R A, Smith, M D, 2003. Minimum duration of in-situ tests on vertical boreholes. ASHRAE Transactions, vol. 109 (2), pp. 475-486.

10. Bernier, M A, 2001. Ground-coupled heat pump system simulation. ASHRAE Transactions, vol. 106, no. 1, pp. 605-616.

11. Bernier, M A, Labib, R, Pinel, P, Paillot, R, 2004. A Multiple load aggregation algorithm for annual hourly simulations of GCHP systems. HVAC&R Research, vol. 10, no. 4, pp. 471-487.

12. Bernier, M A, Pinel, P, Labib, R, Paillot, R, 2004. A multiple load aggregation algorithm for annual hourly simulations of GCHP systems. Hvac&R Research, vol. 10, no. 4, pp. 471-487.

13. BIPM, IEC, IFCC, ISO, IUPAC, IUPAP, OIML, 1993. Guide to the Expression of Uncertainty in Measurement. (ISO: Geneva.).

14. Blackwell, J H, 1954. A Transient-Flow Method for Determination of Thermal Constants of Insulating Materials in Bulk (Part I-Theory). Journal of Applied Physics, vol. 25, no. 2, pp. 137-144.

15. Blomberg, T, Claesson, J, Eskilson, P, Hellström, G, Sanner, B, 2008. EED 3.0 - Earth Energy Designer, User Manual. (Blocon.) Sweden.

16. Bose, J E, Parker, J D, McQuiston, F C, 1985. Design/Data Manual for Closed-Loop Ground Coupled Heat Pump Systems. (American Society of Heating, Refrigerating and Air-Conditioning Engineers.) Atlanta.

17. Carslaw H S, J J C, 1959. Conduction of Heat in Solids.

18. Carslaw, H S, Jaeger, J C, 1959. Conduction of heat in solids. (Oxford University Press.) Oxford.

19. Claesson, J, In press. Radial heat flow for a pipe in a borehole in ground using Lapalce solutions - Mathematical Background Report. (Building Technology, Chalmers University of Technology.) Sweden.

20. Clark, D R, 1985. HVACSIM+ Building Systems and Equipment Simulation Program Reference Manual. (National Bureau of Standards.) USA.

21. Crawley, D B, Pedersen, C O, Lawrie, L K, Winkelmann, F C, 2000. Energy plus: Energy simulation program. ASHRAE Journal, vol. 42, no. 4, pp. 49-56.

22. Diao, N R, Zeng, H Y, Fang, Z H, 2004. Improvement in modeling of heat transfer in vertical ground heat exchangers. HVAC&R Research, vol. 10, no. 4, pp. 459-470.

23. Eckert, E, Drake, R, 1987. Analysis of heat and mass transfer. (McGraw-Hill Book Company.) New York.

24. Eskilson, P, 1987. Thermal analysis of heat extraction boreholes. Department of Mathematical Physics, PhD Thesis, (Lund University.) Sweden.

25. Fahlén, P, 2009. The laboratory facility of building services engineering - Supply systems for heating and cooling. R2009:03, (Building Services Engineering, Chalmers University of Technology.) Sweden.

26. Forsén, M, Lundqvist, P, 2005. A novel design tool for heat pump systems. Proceedings of the 8th IEA Heat Pump Conference, Las Vegas, USA.

27. Gehlin, S, 2002. Thermal response test - Method development and evaluation. PhD Thesis, (Luleå University of Technology.) Sweden.

28. Gehlin, S E A, Nordell, B, 2003. Determining undisturbed ground temperature for thermal response test. ASHRAE Transactions, vol. 109 (1), pp. 151-156.

29. Gu, Y, O'Neal, D L, 1995. Analytical solution to transient heat conduction in a composite region with a cylindrical heat source. Journal of Solar Energy Engineering, Transactions of the ASME, vol. 117, no. 3, pp. 242-248.

30. Gu, Y, O'Neal, D L, 1998. Development of an equivalent diameter expression for vertical U-tubes used in ground-coupled heat pumps. ASHRAE Transactions, vol. 104, pp. 347-355.

31. Gu, Y, O'Neal, D L, 1998. Modeling the effect of backfills on U-tube ground coil performance. ASHRAE Transactions, vol. 104, pp. 356-365.

32. Hart, D P, Couvillion, R, 1986. Earth coupled heat transfer. (National Water Well Association.) Dublin, OH.

33. Hellström, G, 1991. Ground Heat Storage Thermal Analyses of Duct Storage Systems. PhD Thesis, (University of Lund.) Sweden.

34. Hellström, G, 1998. Thermal Performance of Borehole Heat Exchangers. Proceedings of the Second Stockton International Geothermal Conference New Jersey, USA.

35. Ingersoll, L R, Plass, H J, 1948. Theory of the ground pipe heat source for the heat pump. Heating, Piping & Air Conditioning Journal, vol. 20, no. 7, pp. 119-122.

36. Ingersoll, L R, Zobel, O J, Ingersoll, A C, 1954. Heat conduction with engineering, geological and other applications. (McGraw-Hill.) New York.

37. Katsura, T, Nagano, K, Takeda, S, 2008. Method of calculation of the ground temperature for multiple ground heat exchangers. Applied Thermal Engineering, vol. 28, no. 14-15, pp. 1995-2004.

38. Kavanaugh, S, 2000. Investigation of methods for determining soil and rock formation thermal properties from short-term field tests. (American Society of Heating, Refrigerating and Air-Conditioning Engineers.) Atlanta.

39. Kavanaugh, S, Rafferty, K, 1997. Design of Geothermal Systems for Commercial and Institutional Buildings. (American Society of Heating, Refrigerating and Air Conditioning Engineers.) Atlanta.

40. Kavanaugh, S P, 1985. Simulation and experimental verification of vertical ground-coupled heat pump systems. PhD Thesis, (Oklahoma State University.) USA.

41. Kelvin, T W, 1882. Mathematical and physical papers. (Cambridge University Press.) London.

42. Lamarche, L, Beauchamp, B, 2007. A new contribution to the finite line-source model for geothermal boreholes. Energy and Buildings, vol. 39, no. 2, pp. 188-198.

43. Lamarche, L, Beauchamp, B, 2007. New solutions for the short-time analysis of geothermal vertical boreholes. International Journal of Heat and Mass Transfer, vol. 50, no. 7-8, pp. 1408-1419.

44. Lund, J W, Freeston, D H, Boyd, T L, 2005. Direct application of geothermal energy: 2005 Worldwide review. Geothermics, vol. 34, no. 6, pp. 691-727.

45. Martin, C A, Kavanaugh, S P, 2002. Ground thermal conductivity testing - Controlled site analysis. ASHRAE Transactions, vol. 108 (1), pp. 945-952.

46. Mogensen, P, 1983. Fluid to duct wall heat transfer in duct system heat storages. Proceedings of International Conference on Subsurface Heat Storage in Theory and Practice, Sweden.

47. Nagano, K, Katsura, T, Takeda, S, 2006. Development of a design and performance prediction tool for the ground source heat pump system. Applied Thermal Engineering, vol. 26, no. 14-15, pp. 1578-1592.

48. Naumov, J, 2005. Optimization of ground-coupled systems for heating and cooling of buildings. Building Services Engineering, Licentiate Thesis, (Chalmers University of Technology.) Sweden.

49. Paul, N D, 1996. The Effect of Grout Thermal Conductivity on Vertical Geothermal Heat Exchanger Design and Performance. M.Sc. Thesis, (South Dakota State University.) USA.

50. Pesl, M, Goricanec, D, Krope, J, 2008. Thermal influence between boreholes in the vertical geothermal heat exchangers and response functions. Proceedings of the 5th Wseas International Conference on Heat and Mass Transfer (Hmt '08), Mexico.

51. Sanner, B, Mands, E, Sauer, M, Grundmann, E, 2007. Technology, development status, and routine application of Thermal Response Test. Proceedings of the European Geothermal Congress, Germany.

52. SEL, TRANSSOLAR, CSTB, TESS, 2004. Trnsys 16: a transient system simulation programme. (University of Wisconsin.) USA.

53. Sharqawy, M H, Mokheimer, E M, Badr, H M, 2009. Effective pipe-to-borehole thermal resistance for vertical ground heat exchangers. Geothermics, vol. 38, no. 2, pp. 271-277.

54. Sharqawy, M H, Mokheimer, E M, Habib, M A, Badr, H M, Said, S A, Al-Shayea, N A, 2009. Energy, exergy and uncertainty analyses of the thermal response test for a ground heat exchanger. International Journal of Energy Research, vol. 33, no. 6, pp. 582-592.

55. Shonder, J A, Beck, J V, 1999. Determining effective soil formation properties from field data using a parameter estimations technique. ASHRAE Transactions vol. 105 (1), pp. 458–466.

56. Smith, M, 1999. Comments on in-situ borehole thermal conductivity testing. The Source, vol. 3-4/99.

57. Smith, M, Perry, R, 1999. In situ testing and thermal conductivity testing. Proceedings of the 1999 GeoExchange Technical Conference and Expo, Oklahoma, USA.

58. Spitler, J, 2010. Validation Data. Javed, S. (Personal Communication.).

59. Spitler, J D, 2000. GLHEPRO - A Design Tool For Commercial Building Ground Loop Heat Exchangers. Proceedings of the Fourth International Heat Pumps in Cold Climates Conference, Aylmer, Québec.

60. Stehfest, H, 1970. Remark on algorithm 368: Numerical inversion of Laplace transforms. Commun. ACM, vol. 13, no. 10, pp. 624.

61. Sutton, M G, Couvillion, R J, Nutter, R K, 2002. An algorithm for approximating the performance of vertical bore heat exchangers installed in a stratified geological regime. ASHRAE Transactions, vol. 108 (2), pp. 177-184.

62. Wagner, R, Clauser, C, 2005. Evaluating thermal response tests using parameter estimation for thermal conductivity and thermal capacity Journal of Geophysics and Engineering vol. 2, no. 4, pp. 349–356.

63. Witte, H J L, Van Gelder, G J, Spitler, J D, 2002. In situ measurement of ground thermal conductivity: A dutch perspective. ASHRAE Transactions, vol. 108 PART 1, pp. 263-272.

64. WJ.Groundwater.Limited, Thermal Response Testing (http://www.wjgl.com/thermaltest.php). Access Date: April 15, 2010.

65. Yavuzturk, C, 1999. Modelling of vertical ground loop heat exchangers for ground source heat pump systems. Building and Environmental Thermal Systems Research Group, PhD Thesis, (Oklahoma State University.) USA.

66. Yavuzturk, C, Spitler, J D, 1999. Short time step response factor model for vertical ground loop heat exchangers. ASHRAE Transactions, vol. 105 (2), pp. 475-485.

67. Young, T R, 2004. Development, verification, and design analysis of the Borehole Fluid Thermal Mass Model for approximating Short Term Borehole thermal response. Mechanical and Aerospace Engineering, M.Sc. Thesis, (Oklahoma State University.) USA.

68. Zeng, H Y, Diao, N R, Fang, Z H, 2002. A finite line-source model for boreholes in geothermal heat exchangers. Heat Transfer - Asian Research, vol. 31, no. 7, pp. 558-567.

69. Zeng, H Y, Diao, N R, Fang, Z H, 2003. Heat transfer analysis of boreholes in vertical ground heat exchangers. International Journal of Heat and Mass Transfer, vol. 46, no. 23, pp. 4467-4481.